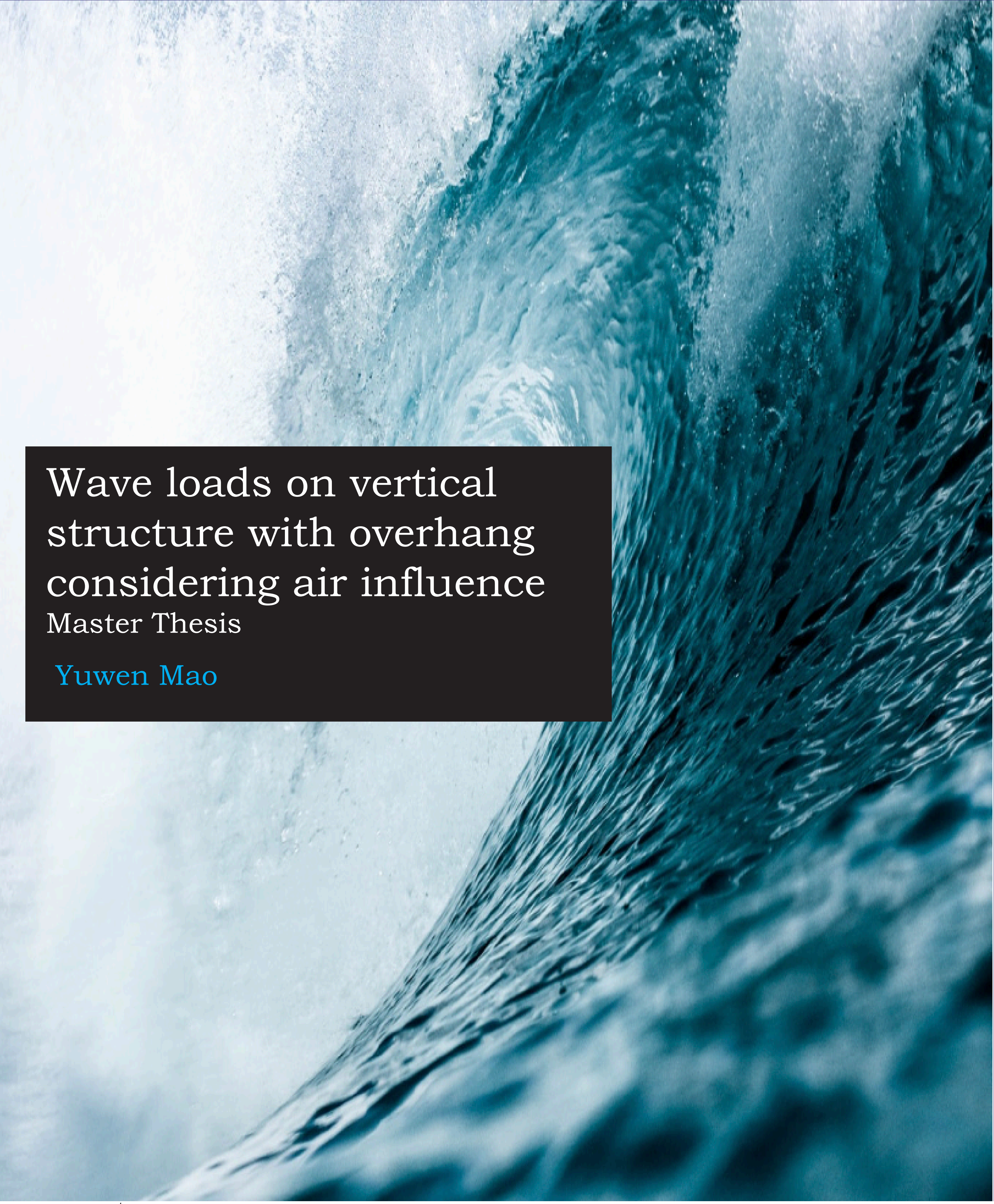

Wave loads on vertical structure with overhang considering air influence

Master Thesis

Yuwen Mao

TU Delft
Delft University of Technology

DynaHicS

Wave loads on vertical structure with overhang considering air influence

Master Thesis

by

Yuwen Mao

As a requirement to attend the degree of

Master of Science
in Civil Engineering

at Technische Universiteit Delft (TU Delft)
Delft, The Netherlands

to be defended publicly on Monday March 25, 2019 at 11:00 AM

Student number:	4540360	
Under supervision of:	Dr. ir. B. Hofland	TU Delft
	Ir. E. de Almeida (daily supervisor)	TU Delft
	Prof. dr. ir. S. N. Jonkman	TU Delft
	Dr. M. F. S. Tissier	TU Delft

An electronic version of this thesis is available at http://repository.tudelft.nl/.

Preface

This master thesis is submitted as the result of my final project to obtain the master degree in Hydraulic Structure and Flood Risk, in the track of Hydraulic Engineering, at Technical University of Delft. I would like express my gratitude to Bas Hofland and Ermano de Almeida Sousa for their supervision, patience and encouragement, which gives me directions in my research and makes it possible for me to learn continuously throughout the whole process of completing this thesis. Also, I would like thank Marion Tissier and Bas jonkman for being part of my committee. It is lucky to complete the master thesis study in Technical University of Delft and have the opportunity to learn from these respectable researchers.

Finally, special thanks to my parents for supporting me to complete master's degree in Technical University of Delft.

Yuwen Mao
Rotterdam, March 2019

Summary

The need to protect areas from sea wave actions is urgent in the Netherlands. To improve the designing performance of hydraulic structures under wave loads, project Dynamics of Hydraulic Structures (DynaHicS) is launched. DynaHicS aims to characterize loads on hydraulic structures considering fluid-structure interaction. Impulsive wave impacts, which are often the governing load on coastal structures, is one of the research focuses. Over the last decades, studies of impulsive wave impacts mainly focused on vertical structures like breakwaters or caissons. For wave impacts on vertical structures with overhangs, the research also has its practical value. Apart from structural complexity, air involvement also adds to the difficulty of wave impact study. As a part of DynaHicS, this master thesis combines 2 factors above to study impulsive wave loads on hydraulic structures with overhang under air influence.

Three challenges are dealt with in *Wave loads on vertical structure with overhang considering air influence*. Objectives of this thesis are summarized as follows:

- **1. Illustrate air development in wave impacts**: How does the entrapped air change during the process of wave impacts ?
- **2. Discuss structure influence on wave load**: How is the wave loading influenced by the presence of horizontal overhang ?
- **3. Study the relationship between air involvement and wave load**: How is the wave loading influenced by the presence of air pocket?

Research objectives are addressed by setting up a theoretical model and using one physical model result. First, a new theoretical model simulating wave impact with air influence under horizontal overhang is set up in combination of 2 previous models (Peregrine & Thais (1996)model with overhang and model with air influence Wood & Peregrine (2000)). Second, data from a physical test carried out in a flume with flat bottom is analysed.

Air development in wave impacts

The first research objective is addressed by describing air development under regular waves and irregular waves with pictures recorded in experiment test. Several wave impacts are selected to be analysed in detail. It is found that during one typical wave impact, air pocket is first entrapped by wave water and then splits into several parts with water wave movement. Small air pockets breaks into air bubbles under wave impacts and get mixed with water. Most air bubbles are washed away from the vertical structure by reflected waves, finally float up and escape into the atmosphere. Very few air bubbles may still hide under the overhang bottom.

Discuss structure influence on wave load

The second research objective is addressed by analyzing 2 cases in an experiment. Regular waves are generated and the only different in these two cases is the structure. One is a vertical wall and the other one is a vertical wall with horizontal overhang. Measurement data is processed and compared. For vertical structures without overhang, regular waves do not induce wave impacts. For structures with overhang loaded under non-breaking regular waves(regular waves rA60s), when the wave touches the bottom of the overhang, wave impulse occurs. Peak impulse on the vertical structure is observed, with a bending moment occurs on the vertical structure. Regular trigonometric function distribution of pressure changes to irregular distribution with two peak pressures during each wave impact. Also, pressure measurement shows that with the presence of overhang, both pressure and pressure impulse loaded on the vertical structure is increased.

Study the relationship between air involvement and wave load

The third research objective is addressed by combining results of the theoretical model and the physical model. Two physical quantities are analysed as wave loads.

The first load studied is wave pressure. 180 waves are recorded and analyzed. 6 wave impacts are selected for pressure-air involvement relationship analysis. Typical moments during each wave impact are selected, with comparison to pressure measured at this moment. It is found that during each wave impact, peak pressure occurs when least air is entrapped. For different wave impacts, the less the air is entrapped under the horizontal overhang, the larger the impulsive peak pressure would be. Also, pressure distribution along the vertical structure is calculated. It is observed that impact pressure decreases with the increase of water depth, which means influence of wave impact and air entrapment decreases away from the water surface.

The second load studied is impact impulse (pressure integration over impact peak period), which is a large load. Pressure impulse is selected to be the critical research variable because it is more constant for different wave impacts and it is the load that indeed has an effect on structures. Low-pass filtering is first launched and the value of of impact impulse is almost not changed. Impact impulse distribution along the vertical wall is calculated by both theoretical model and physical model.

In theoretical model, air is assumed to exist as air pocket when impact occurs and air influence is considered to be bounce back effect. Air pocket size and air pocket position are 2 variables. 7 situations are modelled and it can be concluded that with the increase of air pocket size and decrease of distance between air pocket and the structure, impact pressure-impulse loaded on hydraulic structure is increased. Presence of air (bounce back effect) increases wave impact pressure-impulse.

In physical experiment, structure is loaded under regular waves. Impact pressure distribution along the vertical structure is calculated and then non-dimensionalized. For de-dimensionalization of tested pressure impulse, overhang length is taken to be the length scale and peak velocity measured under regular waves with vertical structure is selected to be the impact velocity. Results of the physical model and theoretical model matches well with each other, which verifies the rationality of the theoretical model. Thus wave loads exerted on vertical structures with overhang, considering air influence, can be modelled theoretically and described quantitatively.

Contents

1 Introduction

A lot of hydraulic structures are exposed to wave loading conditions. Wave loading can be divided into two types: First, quasi-static loading conditions caused by reflecting non-breaking waves (e.g. Sainflou equation). Second, impulsive loading conditions caused by violent wave impacts on the structure due to wave breaking or the structure configuration.

The second type of loading is the research focus, which can lead to very high forces acting on the structure for a very short duration (e.g. 10-100ms). Response to such loads depends on structure characteristics (e.g. stiffness and natural frequency). Hydraulic structures with steel elements (i.e. low stiffness and high natural frequencies) can present a dynamic response under such loads. Due to the short duration of these peak loads, it is not clear whether the load on a large structure will be damped due to its mass, or it may be increased due to dynamic amplification (a sort of transient resonance).

This thesis is actually a part of Project Dynamics of Hydraulic Structure. Impulsive wave loads is the focus of study. In this MSc project, wave impacts on certain structures —- vertical structures with overhangs, will be studied. Throughout high tides or storms, coastal structures with overhanging horizontal cantilever slabs are exposed to violent wave impacts, including wave running up the vertical wall and slamming on the horizontal deck. Thus an uplifting force on the horizontal deck is introduced, which has the property of high magnitude and short duration. Meanwhile, extra force will be introduced on vertical wall. We need to know more about the process of how wave loads act on these structures and the response of the structures. The main load to be studied is violent wave impacts, which is often the governing load. The primary design variable in this thesis is the impulse of impacts because it is relatively constant. Impulsive wave impact loads will be characterized by the impulse of the separate impacts, instead of the peak forces. Knowledge of pressure impulse and wave theory will be combined to study the pressures acting on the structures. Also, wave impact forces are influenced by air involvement, model and scale effects.

To study impulsive wave impacts, the whole thesis is split into 6 chapters. Chapter 1 is the introduction of the whole thesis, including research motivation, research questions and approach. Chapter 2 is literature review, which summarizes important theories and concepts of wave impacts. Chapter 3 sets up a theoretical model simulating experimental conditions in chapter 4 and studies wave impacts against the bottom of overhang. Chapter 4 and chapter 5 is detailed physical experiment description and experimental data analysis. Impulsive wave loads on vertical structure are described both qualitatively and quantitatively. Chapter 6 compares results of theoretical model and physical model. Discussion is made about how wave load is influenced by different factors. Chapter 7 summarize the previous research results of air influence and proposes suggestions for future research.

1.1. Motivation

Demand for the research during this master thesis is explained. This is addressed in the two following sub-sections: a review of wave impact study (Background) and questions to be solved (Research questions).

1.1.1. Background

The need to protect areas from sea wave actions is urgent in the Netherlands. Protective structures should be strong enough to withstand violent wave impacts. Also, many hydraulic structures are approaching their design lifetime and in need of maintenance or reconstruction. Such hydraulic structures are usually slender featured, containing components like steel gates, which display complicated dynamic response under dynamic wave loads. Impulsive wave loads should be better understood to improve the designing performance of hydraulic structures under such wave loads. Project Dynamics of Hydraulic Structures (DynaHicS) is launched for such research requirement. DynaHicS aims to combine the study of structural response and impulsive wave loads, consider fluid-structure interaction and characterize loads on these structures. Then hydrodynamic loads on hydraulic structures can be better described. Also, hydraulic structures, such as Stevin Outlet Sluis of Afsluitdijk (Figure 1.1), can be reassessed and maintained more effectively, efficiently and economically. Thus the Netherlands can be better protected by the hydraulic structures. Studies about wave impacts have been carried for more than 50 years and air influence on hydrodynamic loads has always been inevitable in research.

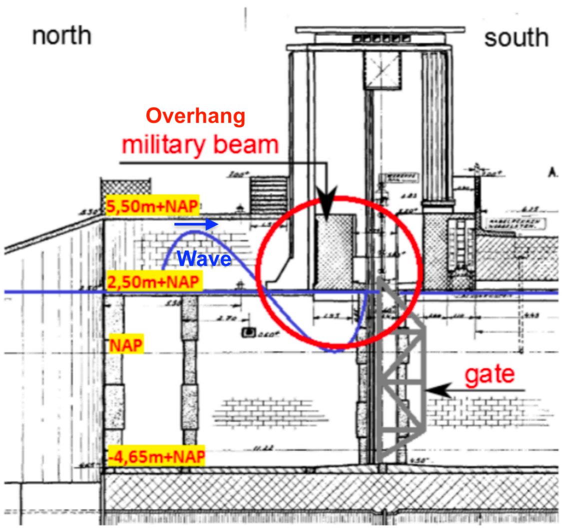

Figure 1.1: Detailed view of the wave impact problem (Rijkswaterstaat, 2012, https://www.deafsluitdijk.nl/documenten/)

Wave Impacts

Wave impacts on vertical structures have been studied a lot in the last decades. Since piezo-electric probs could be used in the 1930s, measurements of pressures in violent wave impacts became possible. Reliable pressure recordings by Rouville & Petry (1938) and Bagnold (1939) laid foundations for experimental wave impact study. Denny & Hewson (1951), Richert (1968) and Kirkgoz (1982) report a wider scatter (50%) in experimental measurements of peak pressures on vertical walls. Kortenhaus & Oumeraci (1998) classified wave loading on monolithic coastal structures and identified the conditions leading to wave impacts based on PROVERBS and MAST III program of the European Union.

There are several theories of wave impact pressure. Weggel & Maxwell (1970), and Partenscky & Tounsi (1989) modeled wave pressure distribution by solving the wave equation in a compressible fluid with pressure sources at the wall. Goda (1974) developed prediction formula for quasi-static force. Peregrine (2003) carried a systematic study on water-wave impact on walls over tens of years and described pressure-impulse theory for liquid impact problems mathematically.

Bagnold (1939) observed that the impulsive pressures exhibits a large variation because of turbulence and the sensitivity of the pressure to detail's of the wave's shape. The pressures were greatest when the amount of air trapped by wave is least. The pressure impulse, which is the time integral of pressure through impact, is approximately constant (e.g. Cooker & Peregrine (1995)). Impact due to violent peak is often considered:

$$P(\mathbf{x}) = \int_{before}^{after} p(\mathbf{x}, t)dt \tag{1.1}$$

in which,
P: impact impulse (Ns/m^2);
p: pressure (Pa).

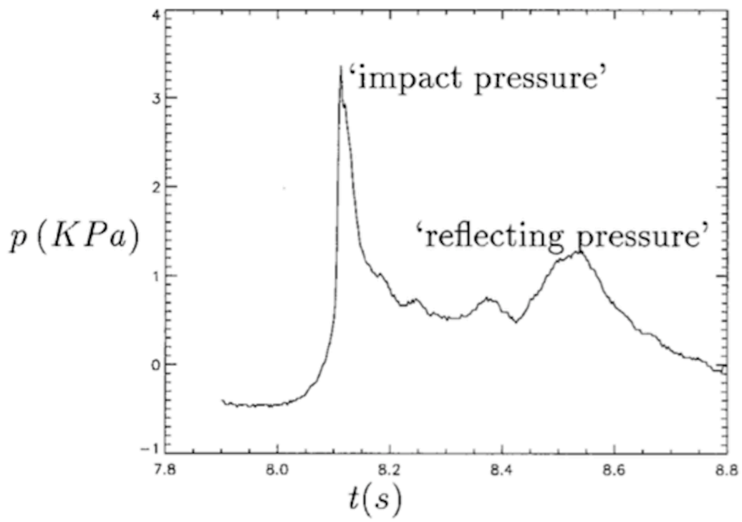

FIG. 1. Typical Pressure-Time Curve for Impact on Wall [Edinburgh 1994 Data; Large Air Bubble; Transducer Close to Foot of Vertical Wall (See Fig. 7)]

Figure 1.2: Typical wave load on wall measured by Deborah J. Wood, D. Howell Peregrine, and Tom Bruce, (2000)

Air Involvement

Bagnold (1939) modeled the wave with air compression, analyzed shock pressure set-up and described 'air cushion' effect. Moutzouris (1979) studied air pocket development on a slope in detail. Blackmore & Hewson (1984) considered air percentage contained in the incident waves and developed a rational expression for the estimation of wave impact pressures. Peregrine & Thais (1996) and Kisacik & Ozyurt (2017) has persisted on a systematic research in this topic for over 10 years. Peregrine & Thais (1996) developed a filling-flow model to study the effects of volume fraction of entrained air in cushioning water impact. Bullock & Crawford (2001) derived a relationship between the Pressure Reduction Factors (PRFs) and the estimated aeration level based on drop tests. Peregrine (2003) modelled air entrainment and investigated the role of entrained and trapped air as well as compressibility effects. Previous studies have laid a solid theoretical foundation and theories of wave impacts and air involvement will be applied for further study.

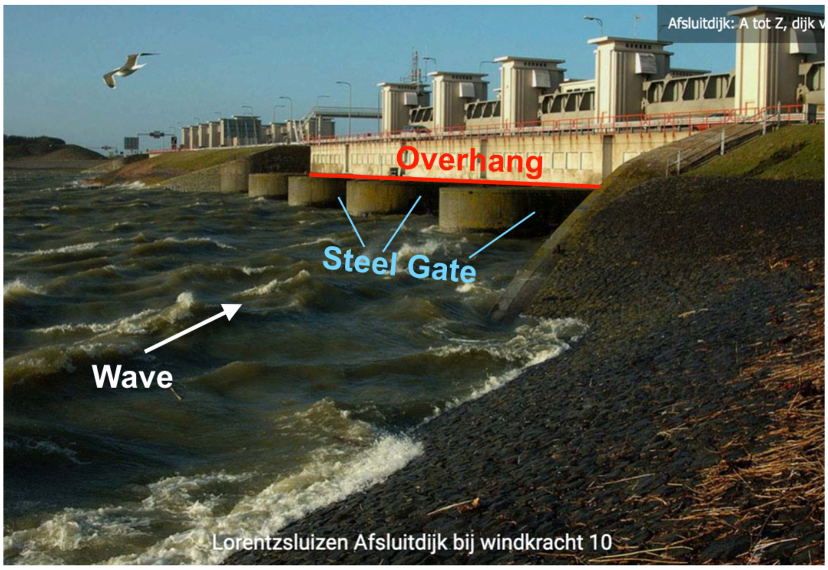

Figure 1.3: Stevin Outlet Sluis (Afsluitdijk), One typical vertical structure with overhanging (Kees Looijesteijn photography)

1.2. Problem description and objectives

Air influence on wave loads is the research focus. Over the last decades, studies of impulsive wave impacts mainly focused on vertical structures like breakwaters or caissons. Meanwhile, for wave impacts on composite hydraulic structures, such as vertical structures with overhangs (for example, Stevin Outlet Sluis in Afsluitdijk, figure 1.1 and 1.3), curved front seawalls (studied by Anand & Sundar (2010) and Chowdhury & Anand (2017)), the research also has its practical value. Violent waves loaded on hydraulic structures are usually mixture of air and water. Thus, besides structural complexity, air involvement also adds to the difficulty of wave impact study.

The main research question of this thesis is:

Research Question:
How are the impulsive wave loads on vertical structures with overhangs influenced by air?

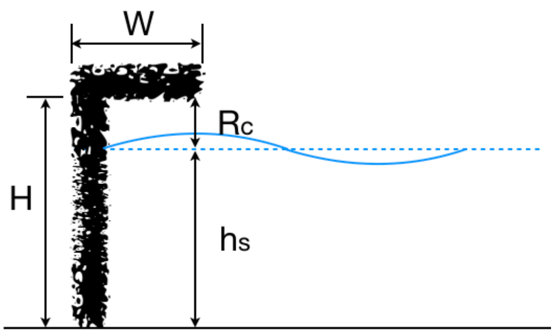

Figure 1.4: Dimensions influencing impulsive wave loads

Main influencing parameters of the impulsive wave loads on structures (Figure 1.4) are wave height (H_i), wave period (T), water depth at the toe of the structure (h_s), freeboard (R_C) and aeration level. Dynamic development of waves, air involvement, structure response and other uncertain factors make the loading process complicated, which should be studied both qualitatively and quantitatively. Thus research questions rise as follows:

Research Sub-questions:
1. How does the entrapped air change during the process of wave impacts?
2. How is the wave loading influenced by the presence of horizontal overhang?
3. How is the wave loading influenced by the presence of air pocket?

1.3. Research approach

Questions described in section 1.2 are addressed in 4 parts:

Part 1: Summarize important theories and concepts of wave impacts related in the following study and initiate research sub-question 1, 2 and 3;

Part 2: Address research sub-question 3 with numerical model;

Part 3: Address sub-question 1,2 and 3 with physical model;

Part 4: Compare results from part 2 and part 3 and make conclusions for research sub-question 1,2 and 3.
Methodology of this thesis is illustrated in Figure 1.5.

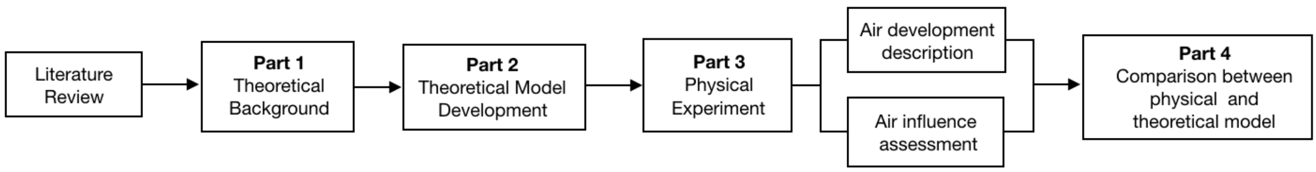

Figure 1.5: Research Approach

1.4. Thesis structure

Thesis structure is consistent with section 1.3. Chapters are summarized briefly as follows:

- **Chapter 1 - Introduction** ;
- **Chapter 2 - Literature Review:** Perform literature study on impulsive wave loads and develop theories of air influence on impulsive wave loads;
- **Chapter 3 - Theoretical model set up:** Select and study one theory in depth, develop a theoretical model of wave impacts on vertical structures with overhang under air influence;
- **Chapter 4 - Physical experiment:** Introduce the experiment tools and physical experiment scheme;
- **Chapter 5 - Test Data Analysis:** Analyze impulsive wave impacts on the structure according to recorded video and test data;
- **Chapter 6 - Theoretical model validation and Discussion:** Validate the theoretical model based on physical experiment results and discuss factors contributing to wave load difference;
- **Chapter 7 - Conclusions and recommendations:** Summarize the previous research results of air influence and proposes suggestions for future research.

2

Literature Review

This chapter presents a summary of the existing knowledge of impulsive wave impacts. It includes the most important study results and theories for wave impulsive impacts on vertical structures with and without overhangs. A summary of methods already used to study the wave impacts on such hydraulic structures, such as physically modelling and numerical modelling is also included, as well as the existing research conclusions.

2.1. General concepts

Main environmental loads exerted on coastal structures are caused by waves. Water in motion can be described by Navier-Stokes equation. Waves can be categorized by the breaker types, such as non-breaking waves, slight breaking waves, breaking waves with small air trap, breaking waves with large air trap, and broken waves (Dogan Kisacik (2014)). In the design of hydraulic structures, waves are normally classified into three types: non-breaking waves, breaking waves and broken waves (Figure 2-1). Wave loads on vertical structures can be classified as longer lasting, quasi-static loads and quickly-acting, more intense impulsive loads.

2.1.1. Wave types

Non-breaking waves

Waves in deep water are normally defined to be non-breaking waves. Non-breaking wave loads are treated as quasi-stationary. Theory of Sainflou (1928) is commonly used in the present Dutch manual Leidraad Kunstwerken (TAW, 2003), although this formula underestimates the maximum wave impact force. Formula of Goda (1974) is also commonly used in design guidelines.

Breaking waves

If a wave is very steep or the water is very shallow, particle velocity *u* may exceed wave celebrity *c*, and the particles would leave the the wave profile. The wave is no longer stable and wave-breaking occurs. Surging waves occur when the slope is steep. The breaking criterion is described by Miche:

$$H_b = 0.142 L tanh(2\pi h/L) \tag{2.1}$$

in which,
H_b: breaking wave height (m);
L: wave length (m);
h: water depth (m).

Kortenhaus & Oumeraci (1998) used a parameter map to classify breaker types. Hu & Mai (2017) carried both numerical and laboratory investigations to better understand the physical processes involved in offshore breaking wave impacts on a large offshore structure. Wave breaking is the most non-linear process and the process of violent waving breaking against coastal structures is beyond theoretical

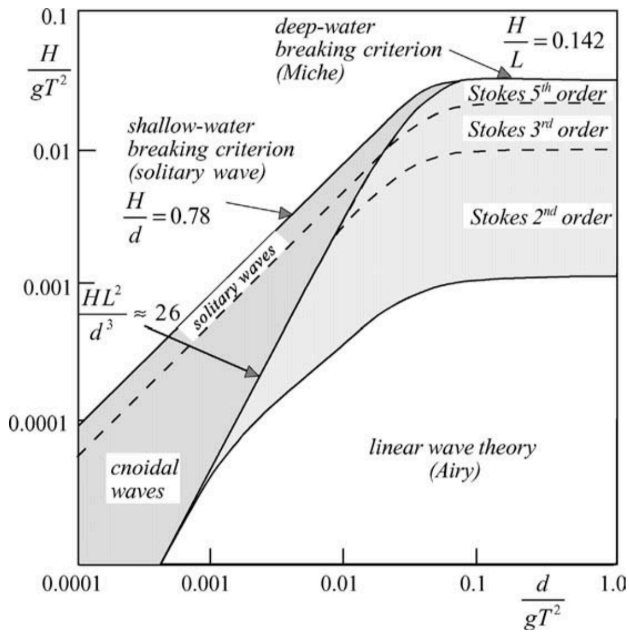

Figure 5.12 The ranges of applicability of the various wave theories (after LeMéhauté, 1976, Kamphuis, 2000, and SPM, 1973; see also Note 5C).

Figure 2.1: Validity of wave theories (LeMehaute, 1976)

modelling (Holthuijsen (2007)). Thus, in the physical experiment, non-breaking waves are generated.

2.1.2. Significant definitions

Some most frequently used *significant definitions* are described, which will be used throughout the whole master thesis:

a). Definitions by *Bagnold (1939):*

1. Duration of shock pressure (s): The time taken by a wave of compression to travel with the speed of sound in water (4,000 feet per second) from the seat of impact to the nearest free surface at which the compression of water can be relieved.

2. Clapoti (lapping of wave): In deep water, the advancing wave does not break, but contact with the wall deflects the water upwards. It is a non-breaking standing wave pattern.

b). Definitions by *Moutzouris (1979):*

3. Oscillation amplitude: Pressure difference between a maximum and the next minimum value of the pressure at the moment of the zero down-crossing time between the two considered values.

4. Oscillation period: Twice the time difference between the maximum and the next minimum values. Oscillation period decreases with decreasing air pocket radius continuously.

c). Definitions by *Peregrine & Thais (1996):*

5. Mach number: In fluid dynamics, the Mach number (M or Ma) is a dimensionless quantity representing the ratio of flow velocity past a boundary to the local speed of sound.

$M = \frac{u}{c}$,

where:
M: the Mach number;
u: the local flow velocity with respect to the boundaries (either internal, such as an object immersed in the flow, or external, like a channel);
c: the speed of sound in the medium.
It is an approximation with which a flow can be treated as an incompressible flow. When M < 0.2-0.3, the flow is considered to be incompressible.

d). Definitions by *Bullock & Crawford (2001):*
Bullock & Crawford (2001) described three most common air state between a structure and an approaching wave: expelled air, entrapped air and entrained air.

6.1. Expelled Air: Air is displayed by the water without the loss of connection with the surrounding atmosphere;

6.2. Entrapment Air: Air entrapment occurs when the crest of a plunging breaker curls over and makes contact with the structure in a way that completely encloses a significant quantity of air within water and structure boundaries.

6.3. Entrained Air: Air pocket is subdivided by the violence of wave impacts and turns into many bubbles. The resultant air bubbles remain entrained in water for a relatively long period of time, along with air bubbles entrained by turbulent waves.

e). Definitions by *Kisacik (2012) and Dogan Kisacik (2014):*
7.Impact pressure: In compressible fluid dynamics, impact pressure (dynamic pressure) is the difference between total pressure (also known as pitot pressure or stagnation pressure) and static pressure.

8. Wave impact peak: The wave impact peak is an increase in pressure caused when the water under motion comes in sudden contact with the structure. This peak is characterized by a large pressure gradient.

9. Peak pressure: The greatest pressure recorded at a given position as a function of time during impact.

10. Pressure impulse: Time integral of pressure through the impact, just as the impulse is the integral of the force.

11. Incident wave height H_i: The wave height that is not influenced by the existing structure.

12. Total wave height H_T: The total wave height measured in front of the structure.

13. Rise Time t_r: The time interval from the wave-impact pressure exceeds the noise level to the pressure reaches the peak pressure.

14. Uplift quasi-static force F_{v-qs}: The maximum quasi-static force due to the downward or backward acceleration of the water body which first hits slab and then free falls. Quasi-static loads are slowly-acting wave loads.

15. Flip through: According to Peregrine (2003), flip through refers to the phenomenon that the very violent pressures occur without any actual impact on the wall but with a smooth irrotational flow in wave profile measurement. The smaller the region into which the free surface "focuses," the smaller and more violent is the resulting jet formation. Dogan Kisacik (2014) found that the vertical acceleration of a wave component reaches the highest value just before the flip through for both regular and irregular waves.

2.2. Impulsive wave loads on hydraulic structures

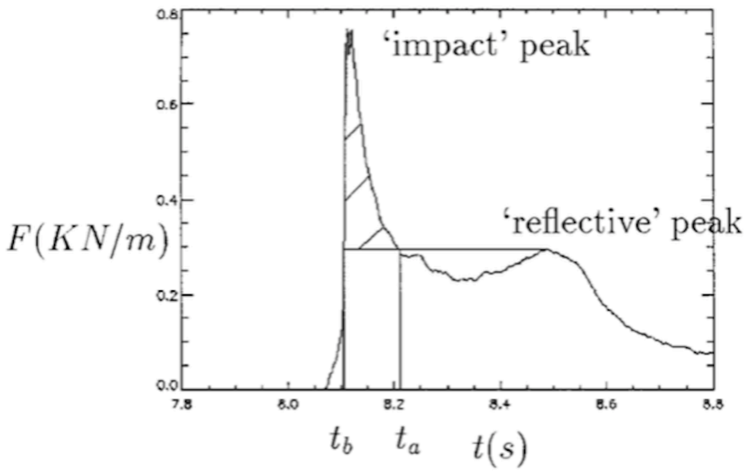

FIG. 9. Horizontal Force *F* on Wall for Impact of Plunging Breaker Trapping Large Air Pocket from Edinburgh Data; from Figure B-5 of Oumeraci et al. (1997), Plotted Using Analysis Program (A. Kortenhaus, Private Communication, 1997); Shaded Area Is Impulsive Force

Figure 2.2: Typical wave load on wall measured by Deborah J. Wood, D. Howell Peregrine, and Tom Bruce, (2000)

Wood & Peregrine (2000) found that waves in the process of breaking often produce impulsive loads on a structure. As can be seen, there are 2 peaks in the graphs above: a high peak of short duration (impact pressure: more intense but shorter lasting), a more slowly varying peak (reflective pressure). The variance of peak pressure can be quite large while the pressure impulse shows great consistency.

This section presents the most fundamental descriptions, methods and formulae for impulsive wave loads on vertical structures with and without overhangs. It describes basic research methods, the development of theories along the time and recently developed formulae for impulsive wave loads on two typical coastal structures: vertical walls and vertical walls with horizontal overhangs.

2.2.1. Influencing factors of wave loads on the vertical structures

The influencing factors of the wave loads are analyzed, which helps to understand loading process better.

Wave parameters: Impulsive wave loads are exerted by waves. Wave parameters (wave height, wave period, wave length, etc.) are the most important influencing factors. A large number of empirical formula related to the outcome of wave impacts directly to wave height (H) and wave period (T). Kisacik & Troch (2012) found that incident wave height is better related horizontal wave impulsive force (F_h) than total wave height. Big scatter of force data ranges between 1<H_i/h_s<1.2, in which situation the waves break with small and large air traps. Rattana Pitikon & Shibayama (2000) found that wave heights are better predicted with $H_{1/3}$ values than with H_{max} values.

Hydrodynamic conditions/ Boundary conditions: The hydrodynamic conditions can be influenced by the boundary conditions, which is studied by Kisacik & Ozyurt (2017) in detail. Wave shoaling may occur during wave propagation along a slope, which can be reflected by wave height $H_{1/3}$ or H$_{max}$.

Wave reflection (C_r): Wave reflection may influence energy distribution near the hydraulic structure because it increases the turbulence. It is influenced by both wave parameters (such as wave length L, water depth h, wave height H at the toe of the structure, wave overtopping amount, breaker shape and so on) and structural parameters (such as foreshore slope, foreshore steepness, vertical structure rigidity). According to Allsop(1999),

$$\begin{cases} C_r = 0.70\text{-}0.90, \text{ for little breaking} \\ C_r = 0.50\text{-}0.70, \text{ for heavy breaking} \end{cases} \quad (2.2)$$

Wave breaking also influences the wave impact since energy is distributed through turbulence. Since in the physical experiment, non-breaking waves are generated, wave breaking effect is not studied in detail.

Trapped Air: Air entrapped by the over-turning wave forms air cavity, which periodically contract and expand due to compressibility. Accordingly, the hydrodynamic pressure as well as the pressure in the cavity would also oscillate. When the entrapped air is compressed to its maximum pressure, the air starts to rebound and the water surface would be accelerated upward the wall. Then the water is splashed around. Free inner jets form periodically inside the entrapped air cavity. The free jets tends to impinge the cavity surface and this results in the cavity division. During this process, rich bubbles are formed during the wave impact process. According to the conservation law of energy, smaller non-dimensional air pressure may result in a larger maximum cavity pressure in the contraction stage of a cavity.

Wood & Peregrine (2000) found the air trapped in the wave can be present in two forms: 1) trapped bubble, 2) dispersed air. Wave bounce back may occur due to the compressibility of trapped air. For a given wave, a higher impulse at impact is caused by an air pocket because there is some rebound of water. Bagnold (1939) found the impulsive wave load is maximum when the trapped air is least (but not zero) while the following researchers found Bagnold overestimated the influence of trapped air.

Based on the conventional simulations with boundary element method (BEM), Song & Zhang (2018) achieved the complete process simulation of wave impact with air entrapment, beyond the wave over-turning stage. An equation is deduced based on the conservation law of energy for general wave impact problems with air entrapment.

Bounce Back: Considering the compressibility of trapped air, when the water approaches the wall with velocity U while the trapped air is at the wall, it takes time for the air to be compressed and then re-expand, which is likely to extend the duration of the impact peak. Also, the water does not lose its wall-normal velocity component, but instead rebounds. This "bounce-back" implies an elastic collision between water and wall that leads to an increase in the impulse imparted to the wall. The measured pressure impulse is greater than that which results from the simple pressure-impulse calculation. In addition, leakage of trapped air may cause cushioning and reduces the effect of bounce back. The bounce back model predicted pressure impulse distribution better than Cooker and Peregrine model, especially when the air pocket depth is less than half the water depth.

Plunging Angle: The initial impact caused by the wave crest generates local pressure peaks on the vertical coastal structure, alongside with rapid deformation of the impinging free surface along the wall. The peak pressure is influenced by the incident angle between the wave surface and the wall. The peak pressure decreases quickly if the plunging angle increases.

Structure Slope: Bagnold (1939) found that if the slope is steep, the wave has no time to adjust its velocity and amplitude. Thus the wave velocity and amplitude remains constant. The wave front steepens and becomes vertical. Finally wave energy is driven out in the form of a water jet. Kirkgoz (1991) generated regular waves and measured the impact pressures of breaking waves on sloping walls with different degrees.It is found that the impact pressures and resulting forces on sloping walls can be greater than those on a vertical wall. The most frequently measured position of the maximum impact pressures is slightly below the still-water level. The pressure around the peak pressure tends to be longer if the maximum pressure decreases.

Rise Time t_r: Weggel and Maxwell(1970) firstly developed a formula based on wave flume test and wave momentum consideration:

$$p_{max} = a[t_r]^b \tag{2.3}$$

in which,
p_{max}: maximum pressure in one wave impact (Pa);
t_r: rise time (s);
a, b: empirical coefficients, values of a and b are listed in the Table below.

Researchers	Scale of experiments	a	b
Weggel & Maxwell, 1970	Small	232	-1.00
Blackmore & Hewson, 1984	Full	3100	-1.00
Kirkgoz, 1990	Small	250	-0.90
Witte, 1990	Small	261	-0.65
Hattori et al., 1994	Small	400	-0.75
Bullock et al., 2001	Full	31000	-1.00

Table 2.1: Values of coefficients a and b for enveloping curves of impact maximum versus rise-time (from previous measurements)

Source of Error:
In theoretical model, trapped air are usually simplified as bubbly mixture in the fluid (Topliss, 1994) or ”filling flow” model (Peregrine Thais, 1996). Estimation of wave velocity, wave height, bubble position and boundary conditions is also a source of error. Apart from simplification of air bubble, PIV measurements and analysis is difficult at the time of impact because the duration of impulse is really short.

2.3. Air Influence Analysis

2.3.1. Air Influence Description

Air in waves mainly exists in two forms (also check section 1.1.2 d):
1) Air pocket;
2) Scattered air bubbles.

Bagnold (1939) found that the trapped air pocket spreads the impact pressure in both time and space. The smaller the trapped-air is, the larger the nearby pressure would be. The pressure peaks only occur in the area of air cushion. The compression of air pressure is applied simultaneously over the finite water surface and the wave's momentum is reduced. Thus a resultant large force occurs. Above the area of air cushion, no shock pressure is observed while beneath the air cushion, shock pressure decreases rapidly with increasing depth. Shock pressure maximum varies from one impact to another. It is influenced by the dimension of the air pocket. It increases in intensity when the air cushion thickness decreases. When the thickness of the air cushion exceeds half of the cushion height, the shock pressure is then negligible. However, the area enclosed by pressure-time curve is similar and never exceeds an exact value. The energy of breaking wave is stored in the compression of air cushion.

Usually,the pressure-time curve is a sharp initial rise of pressure followed by a second longer period during which the high pressure is maintained. It is because a jet of water strikes the structure first and caused a sharp pressure rise. In the next moment, the pressure is distributed over a larger area of the area. Thus the pressure the becomes less in density while longer in period.

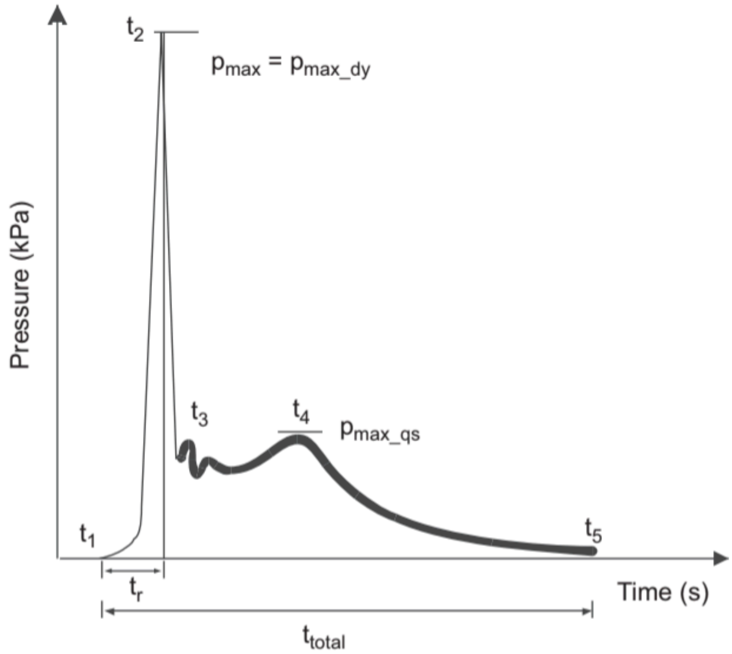

Figure 2.3: Idealized time-history of an impact pressure associated on the vertical part (Peregrine, 1995)

In another situation, when the average width D of the air cushion is smaller than the distance (s) between the wave prominences and water surface, the air cushion cannot be continuous and will be split into several isolated air pockets. Then the compression of air pockets occurs separately and the compression of air is possible to be relieved by air pocket sideways movement to a lower pressure area without compression. The air cushion compression is applied successively over different filaments of the finite water surface. As a result of air being able to escape, the shock pressure is then much less violent and even disappears.

Bagnold (1939) laid the study foundation of air influence on wave-pressure. Bagnold studied the air influence in condition of breaking waves and found that wave impacts on seawalls consist of two parts:
1) hydrostatic pressure;
2) shock pressure.
In deep water, there is only one type of impact- -*clapoti*, thus the pressure on the wall is merely the hydrostatic pressure calculated by the top height of the clapoti. This kind of pressure is long-lasting and small. While at low tide, the wave may strike the wall at the same time of breaking. The wave front is almost parallel to the wall. Pressure shock of great density and short duration is then superimposed on hydrostatic pressure in this case.

Peregrine & Thais (1996) found that entrained air makes water compressibility increase greatly. Air cushions an impact by air entrainment and suspension as small bubbles in water. Or the wave may shoot up the wall without trapping any air bubble.

Theories of air influence on wave impacts is summarized in the order of time development.

2.3.2. Air Influence Theory

The existence of air is a primary reason which makes the mathematical problem of breaking waves hard to be solved. Theory and mathematical background for the mechanism of air influence is still insufficient. The air-water emulsions, froths and foam is hard to describe mathematically, thus the initial conditions of the impact cannot be defined.

1) BAGNOLD's Piston model of Air Cushion with Vertical Hydraulic Structures, 1939

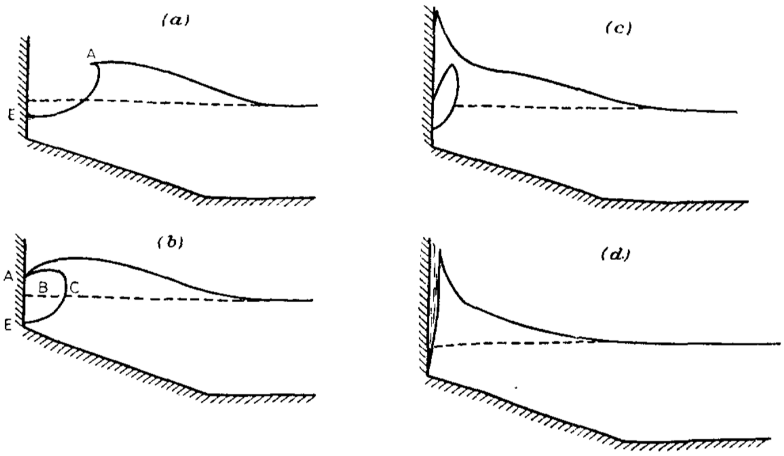

Figure 2.4: Air cushion development against a vertical wall during wave breaking (Bagnold, 1939)

Air cushion development:
As can be seen from the figure above, once the top of water jet strikes the structure before it falls, an air pocket would be enclosed between the vertical structure and the water surface. The air cushion will be compressed as the wave front advances. Once the air pressure reaches the maximum value, the air would escape upward and burst out in the form of much spray. The air then appears in the form of small isolated bubbles. Bagnold imagined a column of fluid, which has an equivalent volume of the moving fluid, and defined the length **K** of the moving column.

Cause of shock pressure:
When a wave strikes against a vertical sea-wall, high pressures can be measured on the structure, which is defined to be shock pressure. The violent simultaneous retardation of a certain limited mass of water is brought to rest by the action of a thin cushion of air. The air is compressed by the advancing wave front, as can be seen in Figure 2.5. Shock pressure occurs since the water column acts as a heavy free piston and compresses the air cushion adiabatically. Accordingly, on the wall, the main pressure zone occurs only over the area, which is covered by the air cushion.

Preconditions for shock pressure
Shock pressure can be tested only when the following conditions should be satisfied simultaneously:
1) A very flat wave front;
2) A thin enclosed air cushion between the wave front and the vertical structure;
3) The air cushion exists for a very short duration.

Assumptions:
1) Fluid associated with the motion of the body is imagined to be a equivalent volume with particles all move with the velocity u of the body;
2) Wave impact pressures are due to the adiabatic compression of a thin lens of air trapped between wave front and seawall;
3) The air layer compression is adiabatic;
4) The advancing water water face is smooth and continuous.

Calculation method:
The maximum pressure can be calculated according to the equation below:

$$(p_{max} - p_0) = 2.7\rho U^2 \frac{K}{D} \tag{2.4}$$

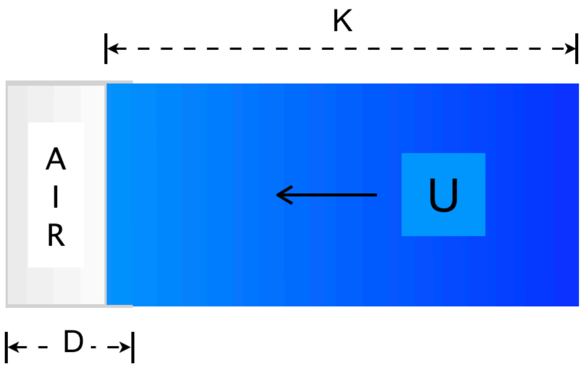

Figure 2.5: Bagnold's Piston model

in which,
D: the initial thickness of the air cushion;
K: length of water volume;
U: approaching velocity of water volume.

Limitations of Bagnold's study:
1) Not correlating the pressure maximum with the characteristics of the incoming wave;
2) The physics of short-period shock pressures production cannot be described and get related to air impact in a mathematical approach;
3) The maximum shock pressures recorded for full-scale waves are relatively small compared with model-experiment after the general linear scale effect is added.

Improvement suggestions (Bagnold (1939)):
1) Attempt to repeat maximum shock pressures in wave-tank with accuracy to find out which wave gives the most consistent results;
2) Try to solve the process of breaking waves mathematically so that the initial conditions of the impact can be defined;
3) The difference between sea-water and fresh-water, as well as scale effect, is important.

2) Ramkema Theory of a model law for wave impacts, 1978

Ramkema (1978) combined various mathematical models for wave impacts and slamming into one mass-spring system, as can be seen in Figure 2.5(a). Piston model of Bagnold (1939) is the basic theory of Ramkema's analysis. Because the specific air layer is considered.

Assumptions:
1) The air compression varies between adiabatic and isothermal;
2) Forces due to the acceleration of gravity are neglected;
3) Compressibility of water is considered;

Formula:
Equation of motion:

$$M_w \frac{d^2 z}{dt^2} = p^2 L - p_0^2 L \tag{2.5}$$

Impulse Equation (formulated in Lagrange coordinates):

$$\frac{\partial^2 z}{\partial t^2}\frac{\partial z}{\partial a} + \frac{1}{\rho}\frac{\partial p_w}{\partial a} = 0 \longrightarrow \frac{\partial^2 z}{\partial t^2} - c_w^2 \frac{\partial^2 z}{\partial a^2} = 0 \tag{2.6}$$

Continuity equation:

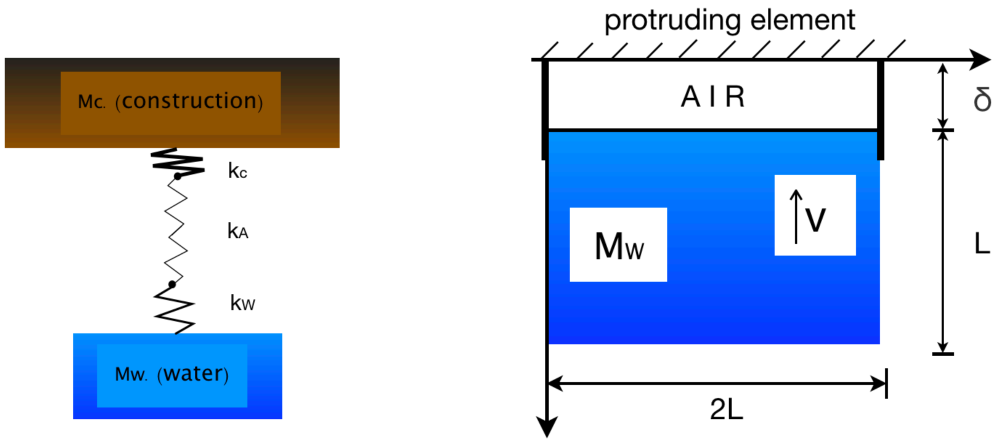

a). Mass-spring system b). Piston model

Figure 2.6: Theoretical models for the water, air and protruding structure system (Ramkema, 1978)

$$\rho \frac{\partial z}{\partial a} = \rho_0 \tag{2.7}$$

Boundary conditions:

At z=h, x>0 and at z=0, 0<x<L:
$$\frac{\partial \phi}{\partial z} = 0 \tag{2.8}$$

At 0<z<h,x=0:
$$\frac{\partial \phi}{\partial x} = 0 \tag{2.9}$$

At z=0, L_1<x<2L:
$$p = p_m cos 2\pi f t \tag{2.10}$$

At z=0(free surface):
$$g\frac{\partial \phi}{\partial z} + \frac{\partial^2 \phi}{\partial t^2} = -\frac{1}{\rho}\frac{\partial \rho}{\partial t}, \tag{2.11}$$

where,
M_w: two dimensional mass of water, the equivalent hydraulic mass;
M_c: the mass of the construction;
k_w, k_A, k_c: the spring constant of water, spring and construction;
p: pressure in the air layer;
p_0: atmospheric pressure (100,000N/^{2});
2L:the width of the two-dimensional mass of water;
v: the velocity of water travelling upward;
z: vertical coordinate;
a: position of the water particles at t=0;
δ: thickness of air blocked from the atmospheric pressure p_0;
γ: the ratio between the specific heat at constant pressure and that at constant volume;
ρ: local density of water;
ρ_0: the local density of water at t=0;
ϕ : velocity potential.

3) Blackmore and Hewson Theory of Entrained Air in Incident Wave, 1984

Blackmore & Hewson (1984) found empirical designing formulas are rarely related to service condition reality. So he collected all the previous full-scale experiments results. It is proven that formulas of Gaillard(1904) and Bagnold (1939) are not generally applicable to full-scale wave impacts.
Blackmore developed an expression for wave impacts estimation according to local wave parameters and included a coefficient reflecting the percentage of entrained air in waves. Air impact is described

qualitatively

Assumptions:
1) Momentum impulse relationship:

$$\int_{t=t_i}^{t=0} Fdt = \int_{v=0}^{v=v_b} Mdv \tag{2.12}$$

in which, F: External force [N];
t: Force time [s];
M: Object quality [kg];
v: Object movement speed [m/s].

2) The horizontal water velocity (v_b) at the moment of impact can be replaced by wave celerity C_b;
3) Water mass M remains constant throughout the impact;
4) The force on wall may be replaced by a pressure P acting over a constant area A;

Formula:
Blackmore derived an equation from momentum impulse relationship:

$$P_i = 2K * \rho * T * C_b^2/t_i \tag{2.13}$$

in which,
P_i: Maximum impact pressure;
C_b: Wave celebrity;
K: A dimensionless coefficient, which is a function of wave steepness;
t_i: rise time, the time period over which the impact pressure rises zero to its maximum value;
This equation fits well with full-scale data and model-scale data. The rise time is dependent on the entrained air percentage. Entrapment of large volumes of air means waves need to break and reform several times. The more air is contained in the waves, the longer the rise time is and the smaller the impact pressure would be. Air content is hard to measure in real waves and it is dependent on beach type, beach slope, near shorewater depth and so on.

4) Peregrine and Thais Filling In Model of Entrained Air in Water Wave Impacts, 1996

Peregrine & Thais (1996) developed a theory on a flow where air is dispersed as small bubbles. They provided a method to estimate the cushioning effect of air in violent free-surface flows. Peregrine focused on the flow in a flip-through wave impact and compared it to a flow rapidly filling a confined region, which shares a lot of similarities while easier to calculate, as is shown in the figure below.

Assumptions:
1) Incompressible water contains homogeneously distributed small air bubbles and the mixture behaves as a compressible fluid;
2) Gravity is neglected;
3) The pressure is constant along the free streamline;
4) There is no "slip" velocity or relative transnational movement between the phases;
5) In regions of highest pressures, the effect of air is neglected since bubbles have a nearly negligible volume fraction (air is eliminated at high pressure);

Formula:
A theoretical model is set for assessing the air influence on wave impacts, given the inflow parameters are prescribed:

$$p - p_1 = \frac{2}{\epsilon + \beta_1}, p_m - p_1 = \frac{1}{(\epsilon + \beta_1)^2} \tag{2.14}$$

in which,
β_1: the incoming volume fraction of air bubbles;

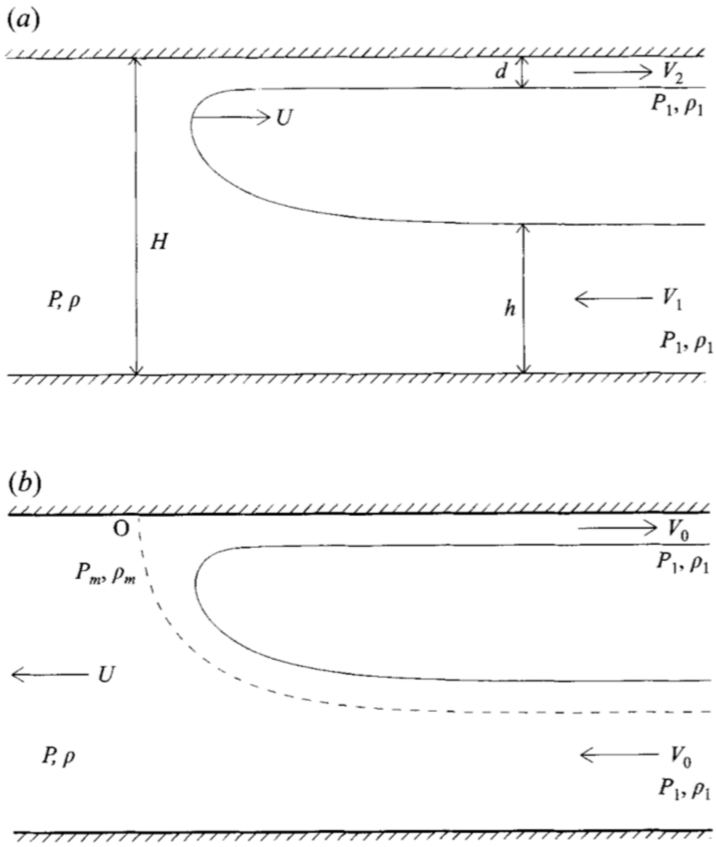

Figure 2.7: Configuration of the filling flow: (a) Static coordinate system; (b) Moving coordinate system (Peregrine, 1996)

ϵ: the clearance of the incoming wave, ϵ = (H-h)/H, which determines the violence of the flow;
p: the background, or filling, pressure in the space already filled with water;
p_1: the atmospheric or equilibrium pressure in the coming and outgoing mixture;
p_m: the maximum pressure during the wave impact.

Conclusions:
Depending on the theoretical model analysis, Peregrine found that 1) With the increase of ϵ, the clearance of the incoming flow is increased, the flow turns less violent and the background pressure is increased;
2) Pressures decrease with increasing wave Mach number based on the sound speed in the air-water mixture and with the violence of the flow;
3) Both peak pressure and background pressure decrease with the increase of air.

Disadvantages:
1) Aspects of bubble migration should be studied further;
2) In practical use, the volume fraction of entrained air β is hard to estimate properly;
3) The theory still needs to be validated with experimental measurements.

5) Wood and Peregrine Theory for Wave Impact beneath a Horizontal Surface, 1996
Wood & Peregrine (1996) considered the wave impact on the underside of a projecting surface and set up a mathematical model, as is shown in Figure 2.9. Assumptions are the same as that of Peregrine & Thais (1996). Laplace equation is solved. Solutions under infinite depth, infinitely long deck and general conditions are proposed. Pressure-impulse contours under different parameters are plotted.

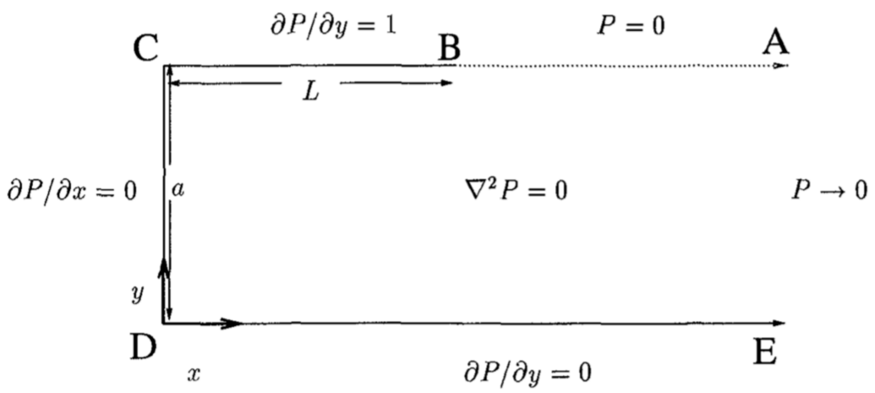

Figure 2.8: Mathematical Model (Wood Peregrine,1996)

6) Wood and Peregrine Theory for Wave Bounce Back, 2000

Wood & Peregrine (2000) developed a theoretical model considering "bounce back" effect due to trapped air and compared it with experimental data. The model is used for flip through impact, where just before impact the wave face is nearly parallel to the wall.

Assumptions:
1) The impact occurs in a short period. So gravity and the nonlinear terms involving a spatial derivative of **u** can be neglected if Δt«H/U;
2) The water is incompressible;
3) Flow into solid boundaries is zero;
4) The horizontal component of the nondimensional velocity after impact is a cosine distribution.

Simplifications:
1) Neglecting the shape of the bubble;
2) The region in which we solve Laplace's equation (the domain of solution) is taken as the simple rectangular shape, which means the bubble has zero thickness.

Formula:
1) For no wave bounce back:
Equation of motion (Laplace's Equation):

$$\mathbf{u}_a - \mathbf{u}_b = -\frac{1}{\rho}\nabla P^D \longrightarrow \nabla^2 P^D = 0 \tag{2.15}$$

in which,
$\mathbf{u}_a$-$\mathbf{u}_b$: Velocity fields just after and just before impact;
ρ: Liquid velocity;
P: Pressure impulse;
Boundary conditions (as is shown in Figure 2.8):

At solid boundary where no impact occurs:

$$\partial P^D/\partial n = 0 \tag{2.16}$$

At solid boundary where impact occurs, the horizontal velocity goes to zero on impact:

$$\partial P^D/\partial n = \rho U = 1 \tag{2.17}$$

Along the upper free surface:

$$P = 0 \tag{2.18}$$

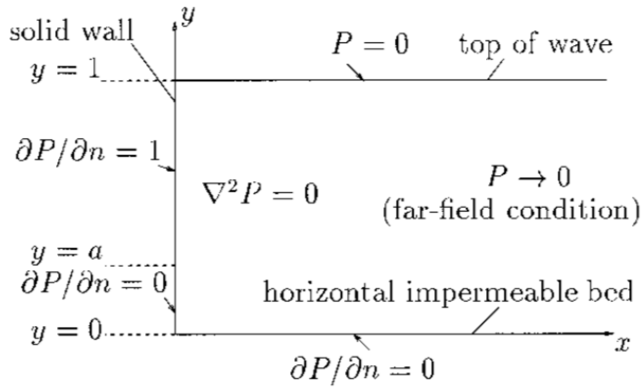

Figure 2.9: Dimensionless Boundary Conditions on Pressure Impulse for Impact on Wall with No Bounce Back (Cooker and Peregrine 1990, 1992, 1995)

Solution to Laplace's equation:

$$P = \sum_m A_m e^{-\alpha_m x} cos(\alpha_m y) \tag{2.19}$$

where

$$A_m = \frac{2}{(m+\frac{1}{2})^2\pi^2}[(-1)^m - sin(\alpha_m a)] \tag{2.20}$$

2) For wave bounce back:
The boundary condition on the middle section of the left-hand side wall (a<y<b), as is shown in Figure 2.10:

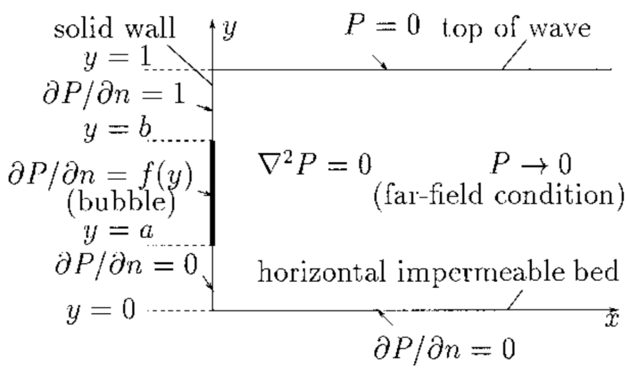

Figure 2.10: Dimensionless Boundary Conditions on Pressure Impulse for Impact on Wall with Bounce Back (Peregrine 2000)

$$\frac{\partial P}{\partial n} = 1 + cos(C(y - D)) \tag{2.21}$$

The Fourier series solution is:

$$P = \sum_m A_m e^{-\alpha_m x} cos(\alpha_m y) \tag{2.22}$$

where

$$A_m = \frac{1}{\alpha_m}[\frac{sin(C(b-D)+\alpha_m b}{\alpha_m + C} + \frac{sin(C(b-D)-\alpha_m b}{C-\alpha_m}] - \frac{1}{\alpha_m}[\frac{sin(C(a-D)+\alpha_m a}{\alpha_m + C} + \frac{sin(C(a-D)-\alpha_m a}{C-\alpha_m}] + \frac{1}{\alpha_m^2}[sin(\alpha_m) - sin(\alpha_m a)] \tag{2.23}$$

in which:
a and *b* : the non-dimensional position of the bottom and top of the air bubble;
C=π/(b-a) and D=(b+a)/2;
$\alpha_m = [m + (1/2)]\pi$.

Disadvantages: Complicated distribution along the boundary is not really justified as real velocity profiles since detailed velocity profiles of waves are not available at impact.

7) Bullock Theory of Air Influence on Wave Impact Pressures, 2001

Bullock & Crawford (2001) did laboratory drop tests to study the relationship between aeration level and impact pressure, using both fresh water and sea water. Difference of air characteristics in fresh water and sea water is compared.

Assumptions:
1) The air-water mixture behaves as a homogeneous compressible fluid, the air and water act independently of each other;
2) All the 'as measured' compressed air is assumed to be compressed in an adiabatic process. The volume is converted to the equivalent value at atmospheric pressure in analysis;

Formula:
The aeration level is represented by the percentage voids ratio of water β:

$$\beta = \frac{V_a}{V_a + V_w} \tag{2.24}$$

in which,
V_a: the volume of air;
V_w: the volume of water.
Normally, β is hard to decide during tests. An estimate of aeration level is by taking the average of aeration measurements obtained during the period from the occurrence of $P_m ax$ to the end of the impact.
Bullock developed Pressure Reduction Factors (PRFs) to reflect air aeration effect on wave impact:

$$PRF = 1.0 - 0.2\sqrt{M}(1.0 - e^{-k\beta}) \tag{2.25}$$

in which,
M (in kg m/s): the violence of the impact characterised by the momentum of the traveller at the instant of first contact with the water;
k: an empirical coefficient.

8) Peregrine Theory of Trapped and Entrained Air in Water-Wave Impacts, 2003

Peregrine (2003) described and computed pressure field of flip-through. He pointed out that air entrapment changes compressibility of air-water mixtures, thus increases pressure peak duration and reduces peak pressure. Accordingly, pressure oscillations occur following the peak because air pocket breaks into small air bubbles during the following process. Peregrine described "bounce back" effect and proposed 2 approaches to study the air-water case.
One approach is to consider the compressibility of trapped air. The according 'bounce back' effect implies that the collision between wall and water increases the impulse impact on the wall.
Another approach is to eliminate the compressibility effect of air pocket. This approach is only feasible when the air pocket is small enough that its oscillation period is much less than the impact duration.

9) Bredmose and Peregrine Theory of Modelling the Effect of Air in Violent Breaking Wave Impacts, 2009

Bredmose & Peregrine (2009) modelled compressible computations for areated wave impacts of the flip-through type through to overturning. The results coincide well with main characteristics of violent breaking-wave impacts observed by Bullock & Obhrai (2007).

Assumptions:
1) Flow condition: Incompressible, inviscid, irrotational two-dimensional flow;
2) The compressible aerated fluid is composed of incompressible liquid (pure water) and compressible gas (air), which is only applied in a domain close to the wall.

Equations:
Flow model consists of conservation equations for mass, x-momentum, y-momentum, gas mass and energy.

Suggestions:
The presence of air may reduce the magnitude of the maximum pressures. While the entrapment of air can also increase the impact forces and impulses because the spatial and temporal extent is increased. The process is complicated and three-dimensional flows is suggested to be modelled in the future to study the role of compressibility better.

2.4. Existing prediction methods of wave impact loads

2.4.1. Prediction methods of wave impact loads on vertical structures

Goda (2000) presents a landmark prediction method in the assessment of wave loads at walls. Blackmore & Hewson (1984) developed a prediction formula for average pressures under broken waves (λ range between 0.3 for rough and rocky foreshores, 0.5 for more regular beaches). Allsop (1996) defined a variable $F^*_{h,imp}$, which is assumed to obey a Generalized Extreme Value (GEV) distribution. Cuomo (2007) introduces a variable α to calculate both wave impacts on seawalls and uplift force on the hydraulic structure. Cuomo & Allsop (2010) improved the formula and described the spatial distribution of normalized quasi-static (shoreward) pressure as a function of the relative location of pressure transducers up the wall. Blackmore & Hewson (1984) considered the effect of entrained air.

2.4.2. Impulsive wave loads on vertical structures with horizontal overhangs

Structures with horizontal slabs prevent most of over-topping because the closed angles stop incident waves from dissipating. This makes the loading condition more severe. Studies on vertical structures with overhangs is limited, compared to studies of vertical structures. From 2011-2017, Kisacik & Troch (2012) carried a continuous systematical research on this topic.

Kisacik's study is based on experimental measurements in the wave flume of Ghent University (Belgium) including three more water depths. The pressure distribution is described as a function of breaker types. An expression is also proposed for the location of maximum pressures p_{max}.

The pressure shape measured for each impact on the vertical part is shown in Figure 2.3, in which the rise time t_r, maximum dynamic pressure ($p_{max,dy}$) and quasi-static pressure ($p_{max,qs}$) is defined. The maximum dynamic pressure is caused by the breaking wave on the vertical wall, while the maximum quasi-static pressure is caused by the downward acceleration of the water body which free falls after first rising on the wall and then rebounded by the horizontal slab. Rise time t_r is defined as the time interval from the pressure exceeds the noise level to the maximum dynamic pressure is reached.

Ramkema (1978) developed a theoretical model of upward wave impact against the tip of the protrusion element. Cooker & Peregrine (1995) developed a model of flip through impact on vertical structure. Wood & Peregrine (2000) extended the pressure-impulse model to allow for a 'bounce back' effect due to trapped air cushion. On this basis, a new theoretical pressure-impulse model of vertical structure with horizontal overhang considering air influence can be further developed and applied in Chapter 3.

Calculation of uplift impact forces

Dogan Kisacik (2014) compared the tested results of uplift impact forces resulted from regular and irregular waves. It is found that the incident wave height at the toe of the foreshore (H_1), water depth at the structure toe (h_s), the incident wave period (T) and geometric properties (c'/h_s) are the main influencing factors of the uplift impact forces.

For incident wave heights, regardless of regular or irregular waves, it is found that the wave induced forces show high scattering in the breaking wave zone.

According to the experimental measurements, the measured force values are very sensitive to the variation of the water depth and becomes larger with the increase of the water depth. However, for the highest water level, horizontal forces hit on the walls are relatively low because under such conditions, some waves first hit the free end of the horizontal overhang during the wave breaking process. Thus the wave's kinematic energy is damped. As a result, the ability to form high impact forces is also reduced. Vertical forces exerted on the horizontal overhang are more sensitive to the ratio of water depth to the clearance between SWL and the horizontal overhang (c'/h_s). It should be noticed that the increase of water depth would decrease the clearance simultaneously. The incident wave period may influence the wave breaking type while does not influence the wave impact forces on the hydraulic structures as much as wave period (T) and water depth (h_s).

For integrated force maximum per impact F_{max}, McConnell and Kortenhaus (1996) derived that :

$$F_{max} = a[t_r]^b \tag{2.26}$$

$$\frac{F_{max}}{F_{max-qs}} = a'[\frac{t_r}{T}]^{b'} \tag{2.27}$$

in which,
F_{max}: maximum integrated force per impact (N);
t_r: rise time (s);
a, b, a', b' : empirical coefficients, values of a and b are listed in the Table below.

Dogan Kisacik (2014) derived a prediction formula for uplift forces acting on the overhanging slab. The formula is derived from scaled test results so the formula should be corrected for the prototype dimension (a scale correction is necessary). Also, the structural response, wave induced vibrations should be studied to improve the existing prediction formula. In addition, the prediction equation should also be validated with different data sets and physical experiments.

Table 2.2: Coefficients a, b,a' and b' in equations above from previous studies

Researchers	Bottom Slope	Scale	a	b	a'	b'
Walkden et al.(1996)	1/4.5	Small	21.4	-0.92		
Walkden et al.(1996)	-	Full	1900	-1.00		
Cuomo et al.(2010a)	1/13	Full	7.00	-0.60		
Kisacik (2014) for horizontal force (F_h)	1/20	Small			0.35	-0.67
Kisacik (2014) for vertical force (F_v)	1/20	Small			0.22	-0.56

Location of maximum pressure

For vertical part of the structure, maximum pressure is found to be around SWL (Richert 1968, Partensky 1988, Chan and Melville 1988. Bullock & Obhrai (2007) found the location of the largest pressure ranges between SWL and the hitting point of the wave crest. Formulas of the p_{max} location are already developed:

Kirkgoz (1982) :
$$\frac{z_{max}}{d_b} = 0.58 + 0.16cot\theta - 0.008cot\theta^2 \tag{2.28}$$

in which:
z_max: location of the maximum pressure; d_b: water depth; θ: incident angle of wave.
Kisacik & Ozyurt (2017) :
$$\frac{z_{max}}{h_s} = -23.2H_1/L_0 + 1.4 \tag{2.29}$$

in which:
H_1: the incident wave height at the toe of the foreshore;
h_s: water depth at the structure toe;
L_0: wave length.

Besides, at the upper corner of the vertical structure, relatively high local pressure is also observed because of secondary impact from rising jets. The influencing area is rather small and the impact decreases sharply. Structural integrity may be endangered if cracked or weak point exists.

For horizontal part of the structure, the maximum pressure tends to be measured at the attached corner. High local impacts may also happen in other areas once the wave crests slam the horizontal slab under high water level. The pressure on horizontal part is normally less than that on the vertical part and it is not the study content in this thesis.

In conclusion, empirical formulas have been developed for wave forces and wave impulses, which laid solid foundation for further study. However, researches about wave loadings are mostly carried out in flumes with slopes and structures are loaded with breaking waves. The following research in this master thesis will focus on regular waves developed in flume with flat bottom, which can fill in gaps in the research field.

3

Theoretical Model Set Up

3.1. Theory development and model set-up

Chapter 3 describes set up of theoretical model and compares calculation results under two situations, as is shown in Figure 3.1:

1) Wave impacts on the bottom of horizontal deck without bounce effect (without air);
2) Wave impacts on the bottom of horizontal deck with bounce effect (with air).

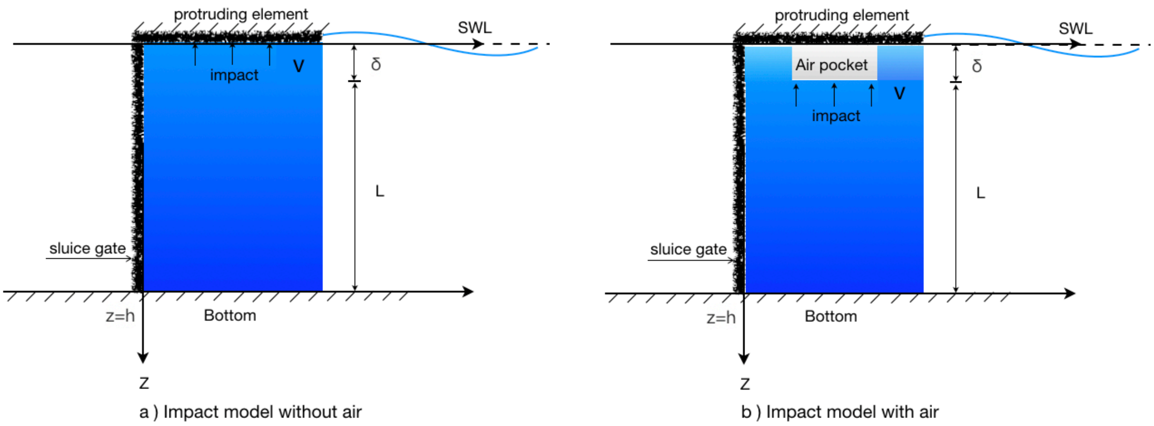

Figure 3.1: Mathematical models of wave impacts under a horizontal deck

Theories summarized in chapter 2 are all relevant to the research topic while they have different limitations. Bagnold (1939) piston model failed to relate pressure maximum with incoming waves and air impact mathematically. Based on Bagnold's piston model, Ramkema (1978) combined wave impacts and slamming under a horizontal deck into one mass-spring system. Blackmore & Hewson (1984) discovered that Bagnold's theory is not generally applicable to full-scale wave impacts and derived an equation from momentum impulse relationship, introducing rise-time t_r to reflect air entrapment influence. Peregrine & Thais (1996)'s filling in model simulated a flow filling in a confined region, where air is dispersed as small air bubbles but not air pocket. Thus models mentioned above are not suitable for simulated situations.

Wood & Peregrine (1996) have systematically studied wave impacts in different situations for over twenty years and build solid foundation for study of both physical experiment and numerical modelling. They validate the theoretical model considering bounce back effect by comparing results of numerical model and analytical solution. Also, they already set up theoretical model of vertical structures with overhang and develop theories for wave impact beneath a horizontal surface considering trapped air (Wood & Peregrine (2000)), which is exactly the study content of this master thesis. The difference is this thesis, breaking waves are changed into regular waves and sloping flume is changed to be flume with flat bottom. Thus bounce back theory of Wood & Peregrine (1996) is selected to be the cornerstone of theoretical research.

New theoretical model of vertical structure with horizontal overhang is set up:

Assumptions:

1) Air pocket is compressible. Peregrine (2003) suggested that when the air pocket is so small that the oscillation period is much less than the impact duration, air pocket can be taken to be incompressible. According to experimental data, the oscillation period is longer than the impact duration, thus compressibility of air is considered.

2) The flow is considered to be incompressible, inviscid, irrotational and 2-dimensional. In conclusion, the aerated fluid is considered to be composed of compressible air phase and incompressible water phase;

3) The duration of impact is so short that gravity and nonlinear terms can be neglected.

4) Flow into solid boundaries is zero.

Simplifications:

1) Shape and thickness of air bubbles is neglected;

2) Position of air is assumed to be at the corner of the horizontal and vertical structure according to the video observation from physical experiment (described in Chapter 4);

3) Ratio of the length of horizontal overhang to the height of vertical structure is $\frac{1}{6}$, simulating the dimension ratio in physical experiment (described in Chapter 4).

Equation of motion (Laplace's Equation):

$$\mathbf{u}_a - \mathbf{u}_b = -\frac{1}{\rho}\nabla P^D \longrightarrow \nabla^2 P^D = 0 \tag{3.1}$$

in which,
$\mathbf{u}_a$-$\mathbf{u}_b$: Velocity fields just after and just before impact;
ρ: Liquid velocity;
P^D: Dimensional pressure impulse;

Equations can also be checked in *Chapter 2 - Wood and Peregrine Theory for Wave Bounce Back, 2000*.

3.2. Theoretical model without air pocket

For theoretical models with bounce back and without bounce back, equation of motion is the same. The difference is boundary conditions.

Boundary conditions:

At solid boundary where no impact occurs (along the vertical structure):

$$\partial P^D/\partial n = 0 \tag{3.2}$$

At solid boundary where impact occurs, velocity goes to zero on impact (along the horizontal overhang):

$$\partial P^D / \partial n = \rho U \tag{3.3}$$

in which, U: velocity of water impact. Actually, value of U may be different at different positions along the horizontal overhang. Since we know nothing about its variation, we take U to be a constant and it is determined to be velocity unit.
Thus, equation (2.3) can be non-dimensionalized:

$$\partial P / \partial n = 1 \tag{3.4}$$

in which, P=$P^D/\rho U$, P is non-dimensional pressure impulse.

Along the upper free surface:

$$P = 0 \tag{3.5}$$

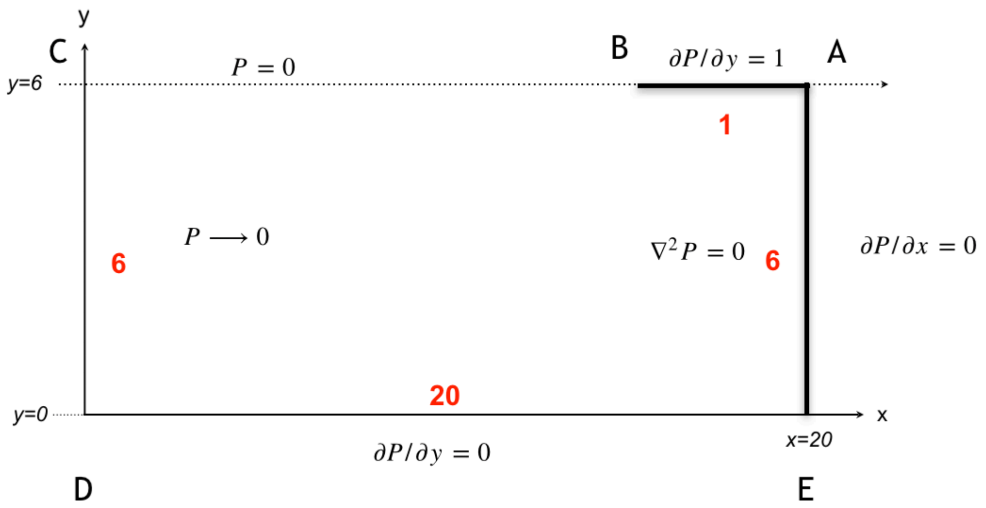

Figure 3.2: Dimensionless boundary conditions on pressure impulse for impact under horizontal deck with no bounce back

Boundary conditions for wave impact without bounce back, including model size ratio, are summarized and shown in Figure 3.2. Horizontal overhang and vertical structure is placed at the right end of the model, shown by bold lines. Red numbers are unit length representing dimension ratio of the flume and structure. Ratio of horizontal overhang length and vertical structure is $\frac{1}{6}$ and water depth is assumed to be the same as overhang length, which is consistent with experimental model described in chapter 4. Theoretically, flume length should be infinitely long. Thus ratio of horizontal overhang and flume length is $\frac{1}{20}$ to ensure water wave can be fully developed at the free end. For theoretical model without air pocket, equations are solved using Matlab. Programme codes in this case are downloaded and altered by *Bas Hofland*.

Non-dimensional result is shown in Figure 3.3. Area affected by the presence of hydraulic structure ranges from x=17 to x=20. Pressure impulse decreases with the increase of water depth and the increase of distance away from the hydraulic structure.

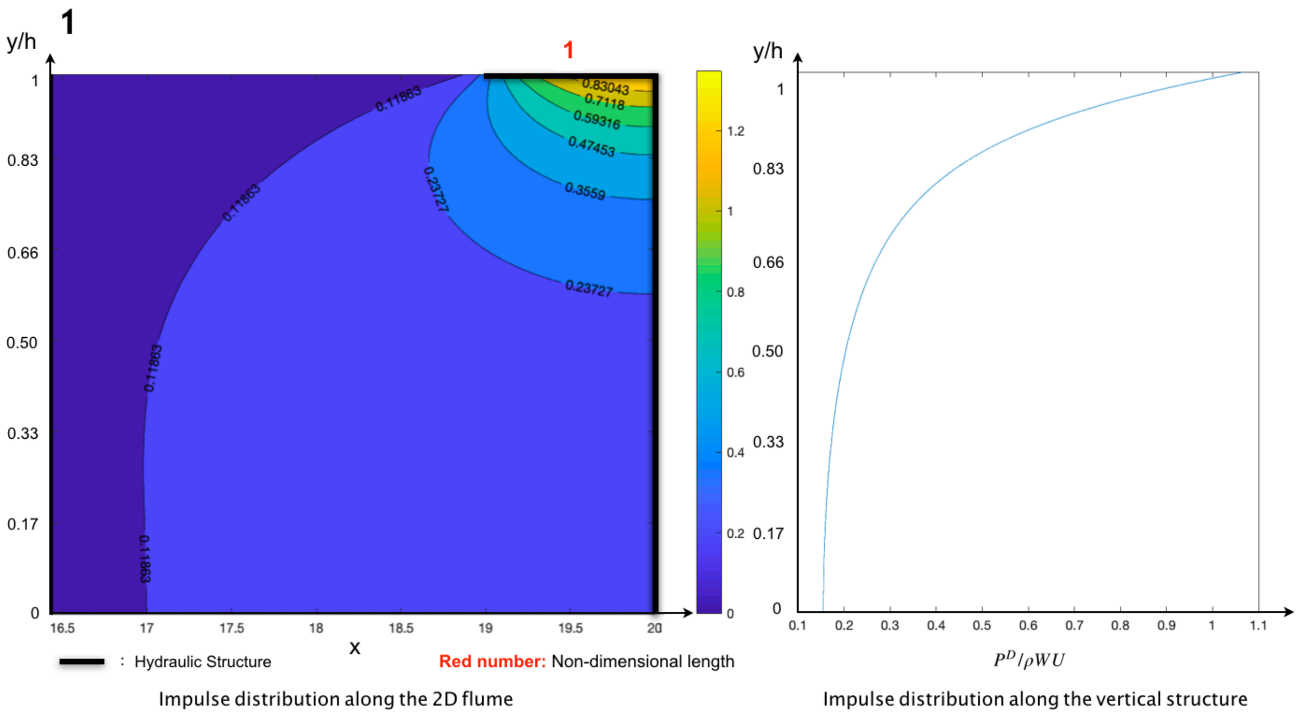

Figure 3.3: Situation 1: Pressure-impulse distribution with no air effect (h: water depth, 6; y: water level)

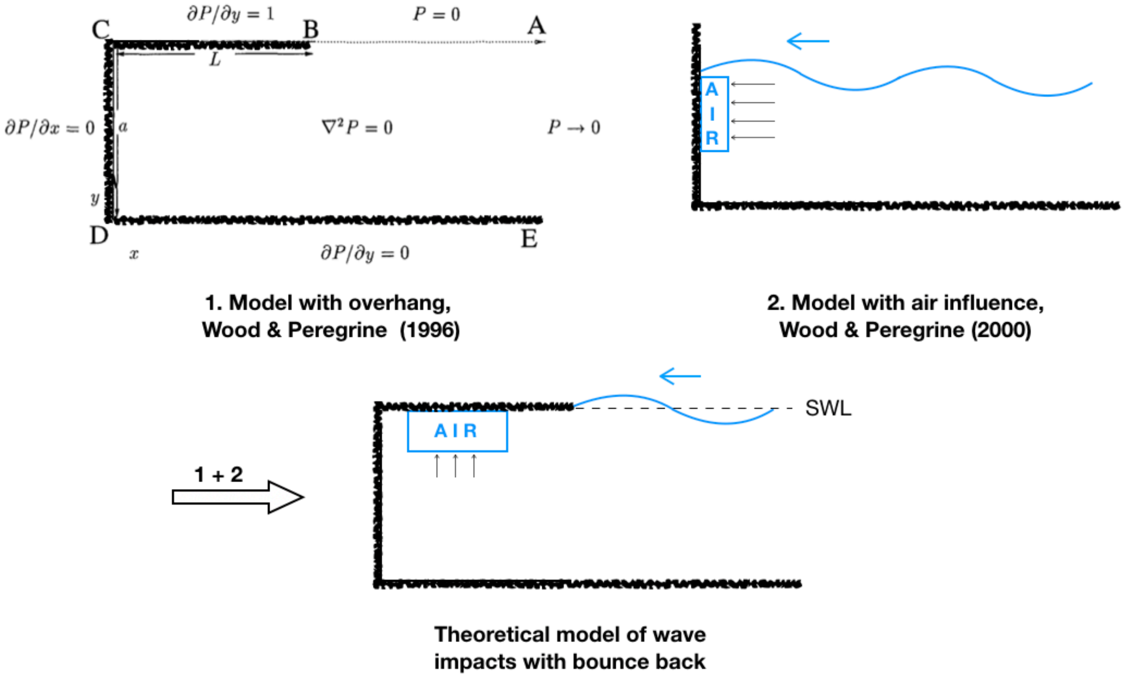

Figure 3.4: Set up of theoretical model with air pocket

3.3. Theoretical model with air pocket

Air is considered to influence wave impact in the form of air pocket. Thickness of the air pocket is neglected and air size refers to the length of air. Wave touches the air pocket and bounces back. Theoretical method solving with air pocket refers to Peregrine (2003). Here we combine the model for an overhang (Wood & Peregrine (1996)) and the model for air influence (Wood & Peregrine (2000)) into a new model (Figure 3.4). The difference between 2 theoretical models in chapter 3 is the presence of air pocket. Thus boundary condition is changed. Bounce back effect is considered to be air pocket influence. Definition of bounce back effect can be checked in section 2.2.1.

Assumption:

Since air influence is considered to be bounce back effect (definition check section 2.2.1), value of impact velocity does not change while the direction changes from upward to downward under air influence. Thus velocity constant is taken to be 2 at solid boundary where impact occurs. Since the velocity constant is influenced by bounce back effect, we can define the velocity constant as the **bounce back coefficient** β. Thus, β=1 represents wave impacts with no bounce back effect and β=2 represents wave impacts with bounce back effect.

Variables:
For model with air effect, influencing factors are air position and air size at the impact moment. Since air thickness is neglected for simplification, air size can be represented by the length of air. Variables *a* and *b* are assumed to be the left and right end of the air pocket, as is shown in the Figure 3.5. Seven situations (Table 3.1) are calculated to study the sensitivity of pressure-impulse distribution to the change of air.

Table 3.1: Variables in theoretical model with air influence

Air size	Situation	a	b	Result
0	(1)	20	20	Fig.3.3
1/3	(2)	19 2/3	20	Fig.3.6
	(3)	19 1/3	19 2/3	Fig.3.7
	(4)	19	19 1/3	Fig.3.8
2/3	(5)	19 1/3	20	Fig.3.9
	(6)	19	19 2/3	Fig.3.10
1	(7)	19	20	Fig.3.11

Boundary condition of bounce back:

Difference of boundary condition between model with air and without air lies at the bottom of horizontal overhang, where impact occurs. Velocity constant is taken to be 2 under bounce back effect.

At solid boundary where impact occurs (a <x <b):

$$\partial P/\partial n = 2 \tag{3.6}$$

in which, P=P$^D/\rho U$, P is non-dimensional pressure impulse.
At solid boundary where no impact occurs (19 <x ≤a ∪ b ≤x <20):

$$\partial P/\partial n = 1 \tag{3.7}$$

in which, P=P$^D/\rho U$, P is non-dimensional pressure impulse. Other boundary conditions are the same as model with no bounce back.

Boundary conditions are summarized in Figure 3.5. Blue bold font *B* in Figure 3.5 represents air pocket boundary. 7 cases are theoretically modelled with non-dimensional air pocket size increasing from 0 to 1 and air position moving from structure corner A to overhang free end B. Calculation result is shown in Figure 3.3 and from Figure 3.6 to Figure 3.11. In these figures, red number represents air size, bold black lines represent contour of hydraulic structure and bold blue lines represent contour of air pocket. Pressure-impulse distribution along the vertical structure under 7 situations are presented in Figure 3.12.

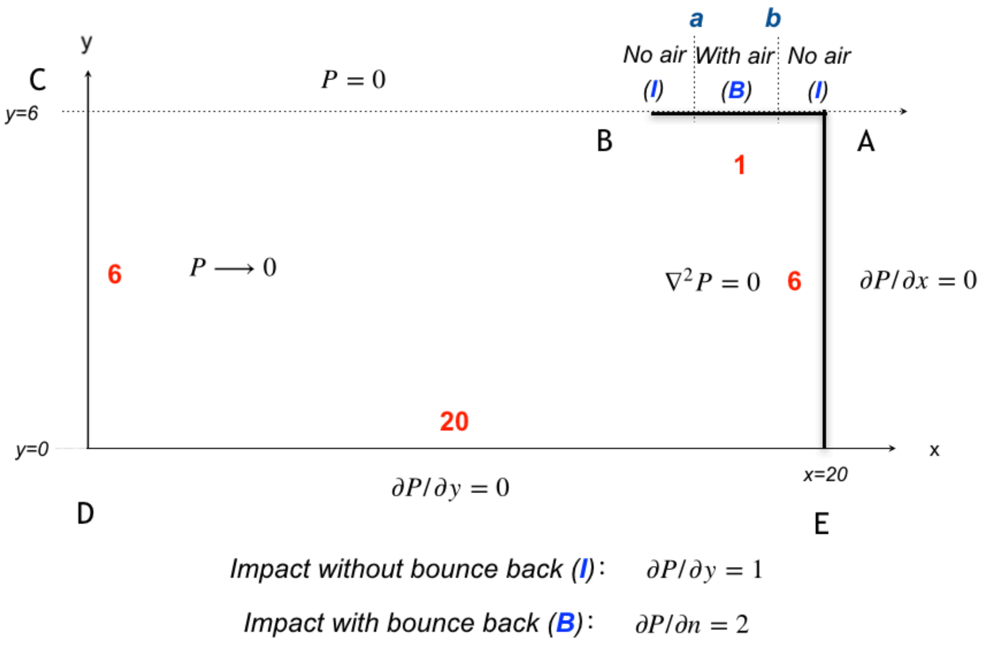

Figure 3.5: Dimensionless boundary conditions on pressure impulse for impact under horizontal deck with bounce back effect

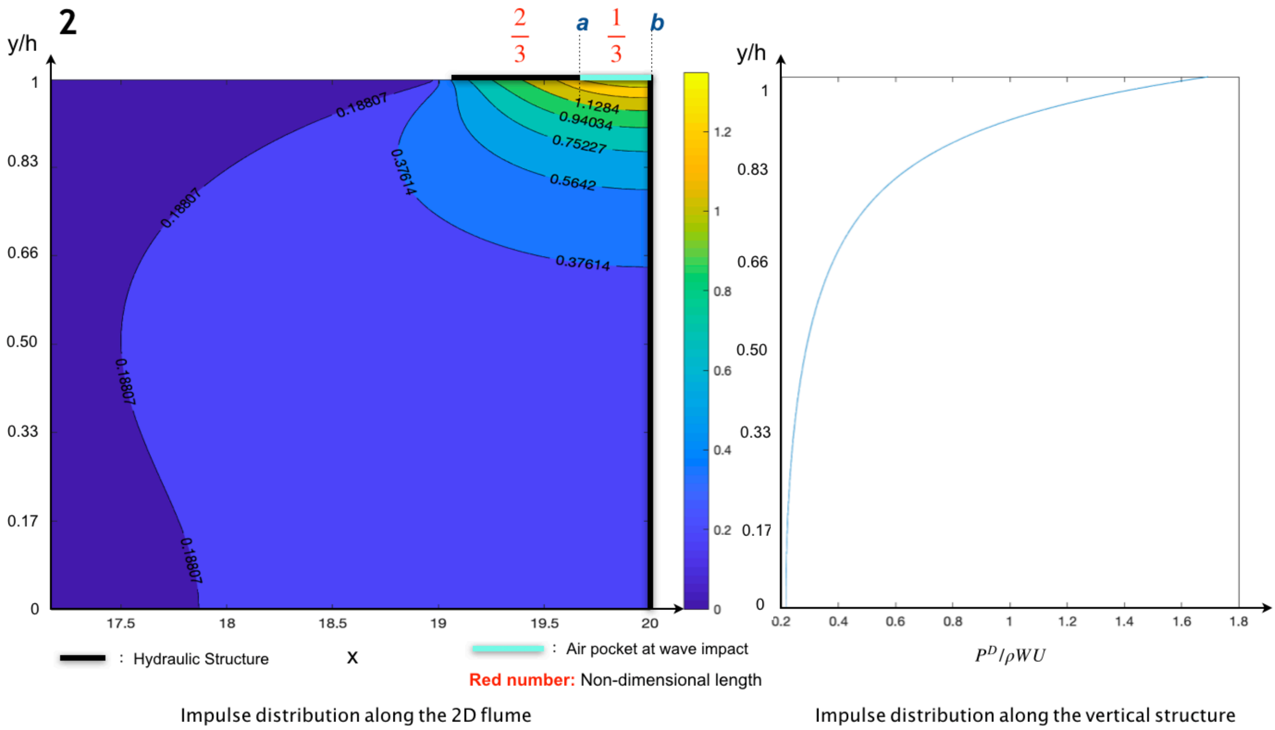

Figure 3.6: Situation 2:Pressure-impulse distribution of wave impact with bounce back effect (h: water depth, 0.6; y: water level, a = 19 2/3, b = 20)

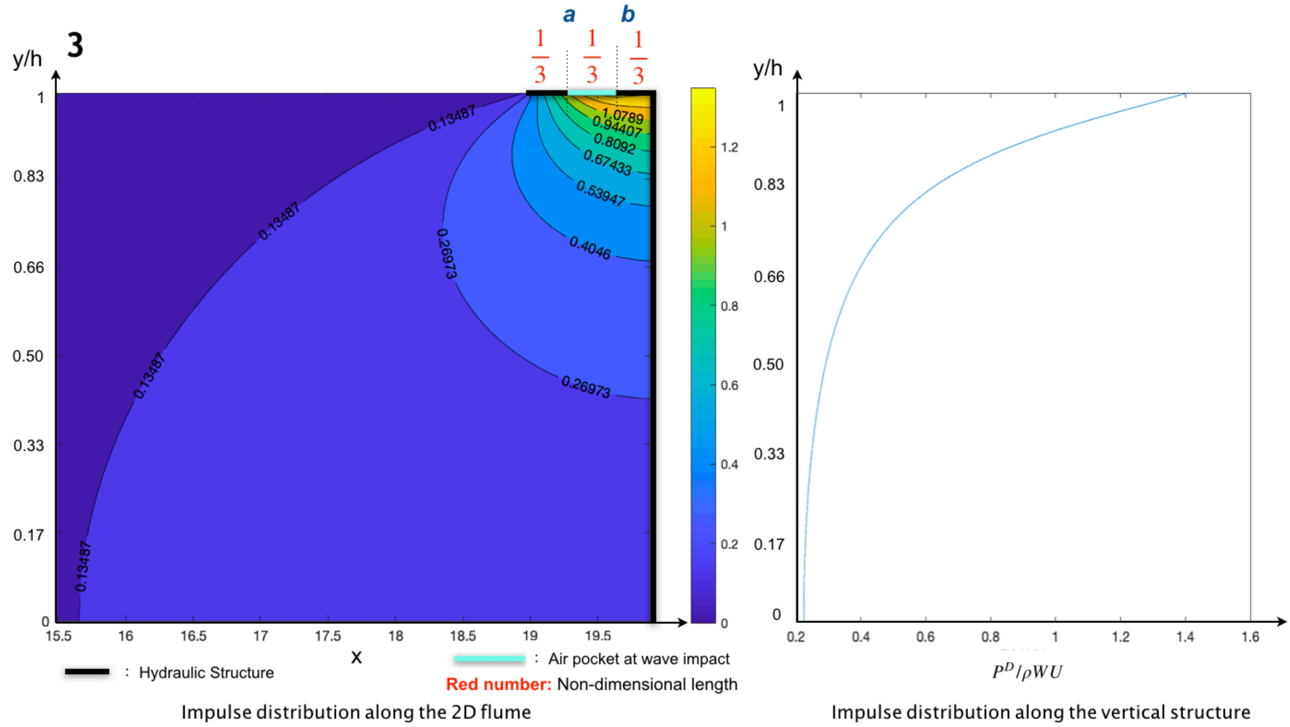

Figure 3.7: Situation 3:Pressure-impulse distribution of wave impact with bounce back effect (h: water depth, 0.6; y: water level, a = 19 1/3, b = 19 2/3)

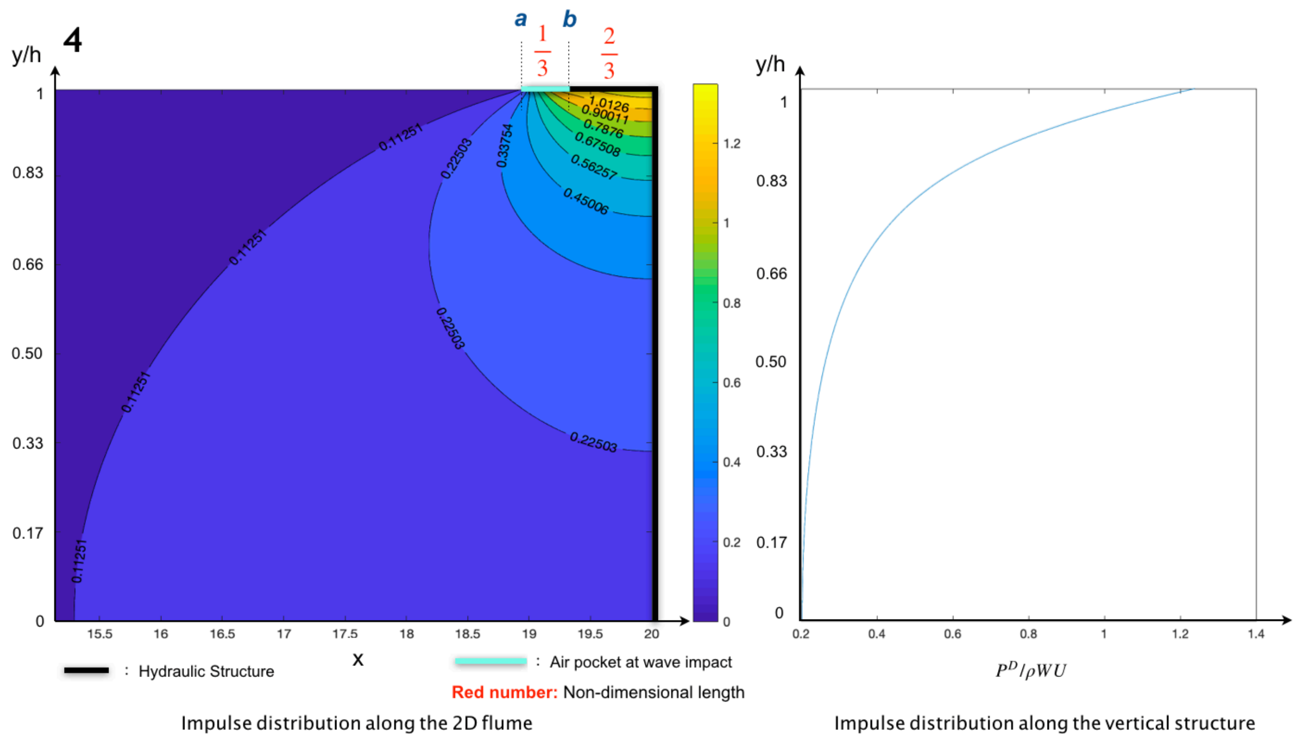

Figure 3.8: Situation 4:Pressure-impulse distribution of wave impact with bounce back effect (h: water depth, 0.6; y: water level, a = 19, b = 19 1/3)

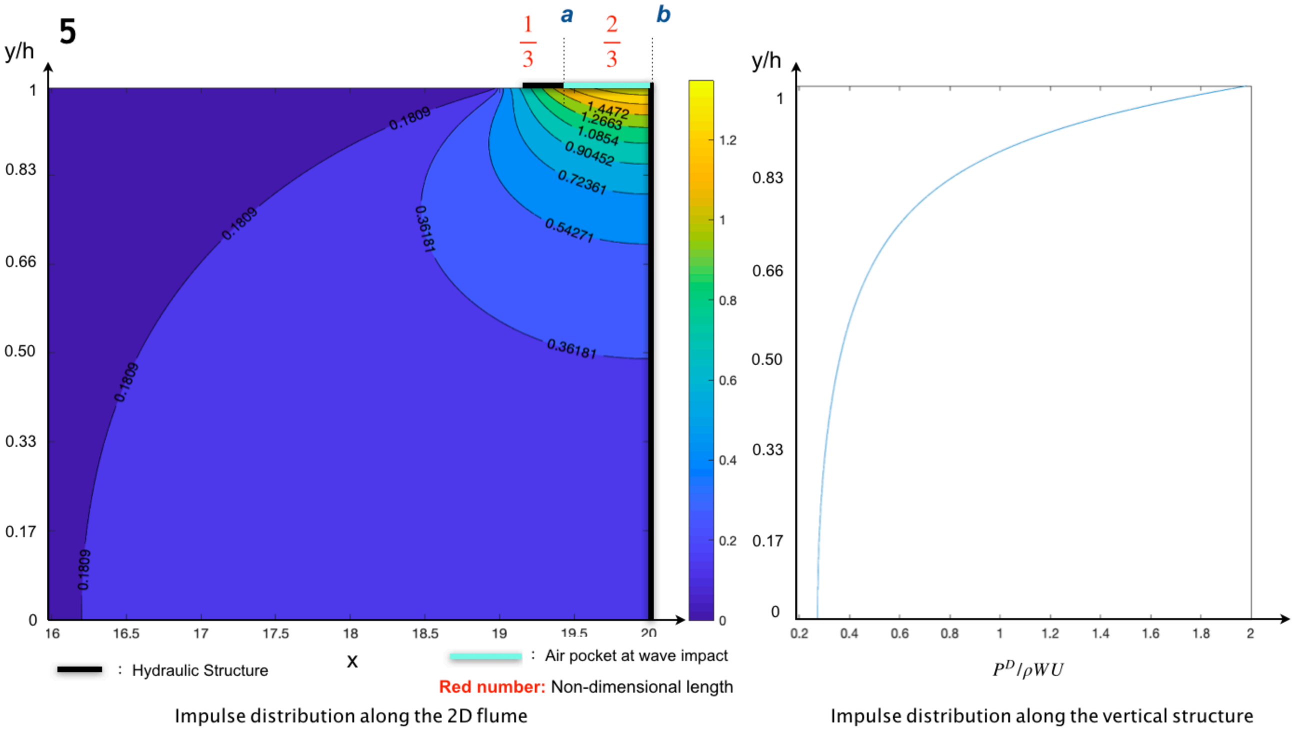

Figure 3.9: Situation 5:Pressure-impulse distribution of wave impact with bounce back effect (h: water depth, 0.6; y: water level, a = 19 1/3, b = 20)

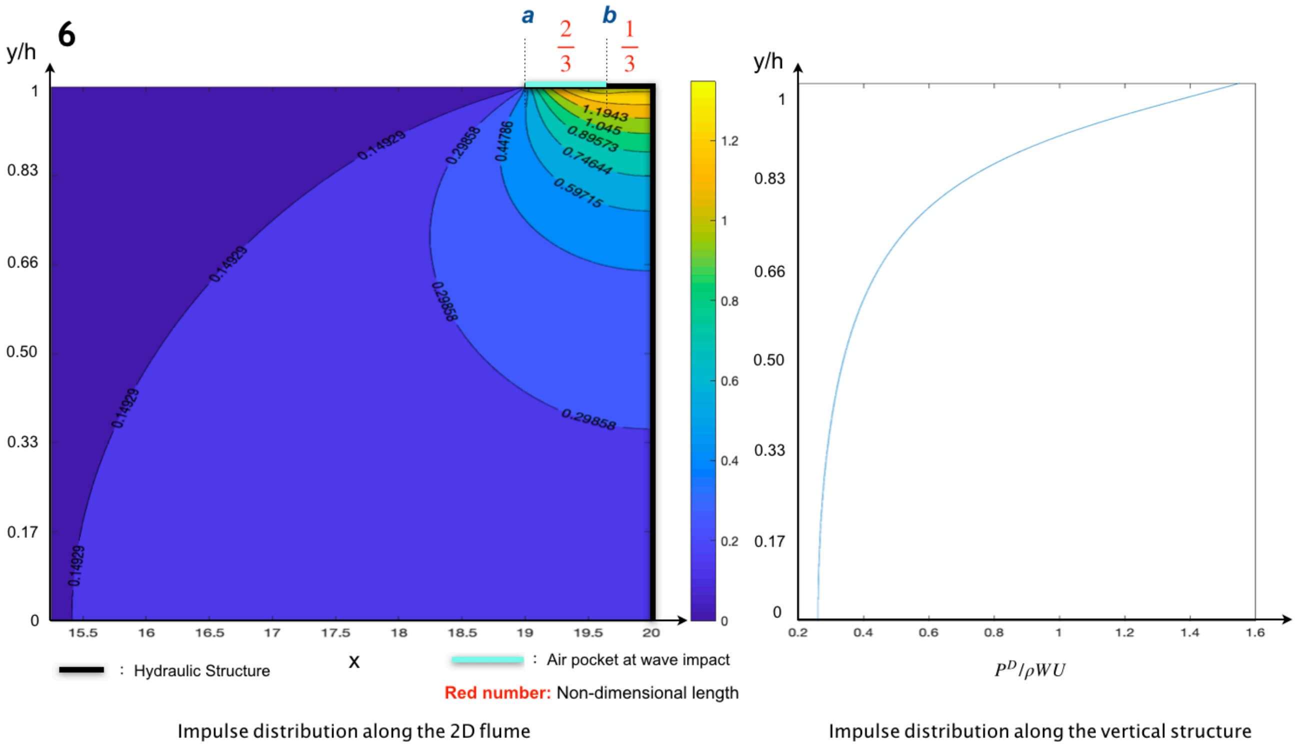

Figure 3.10: Situation 6:Pressure-impulse distribution of wave impact with bounce back effect (h: water depth, 0.6; y: water level, a = 19, b = 19 2/3)

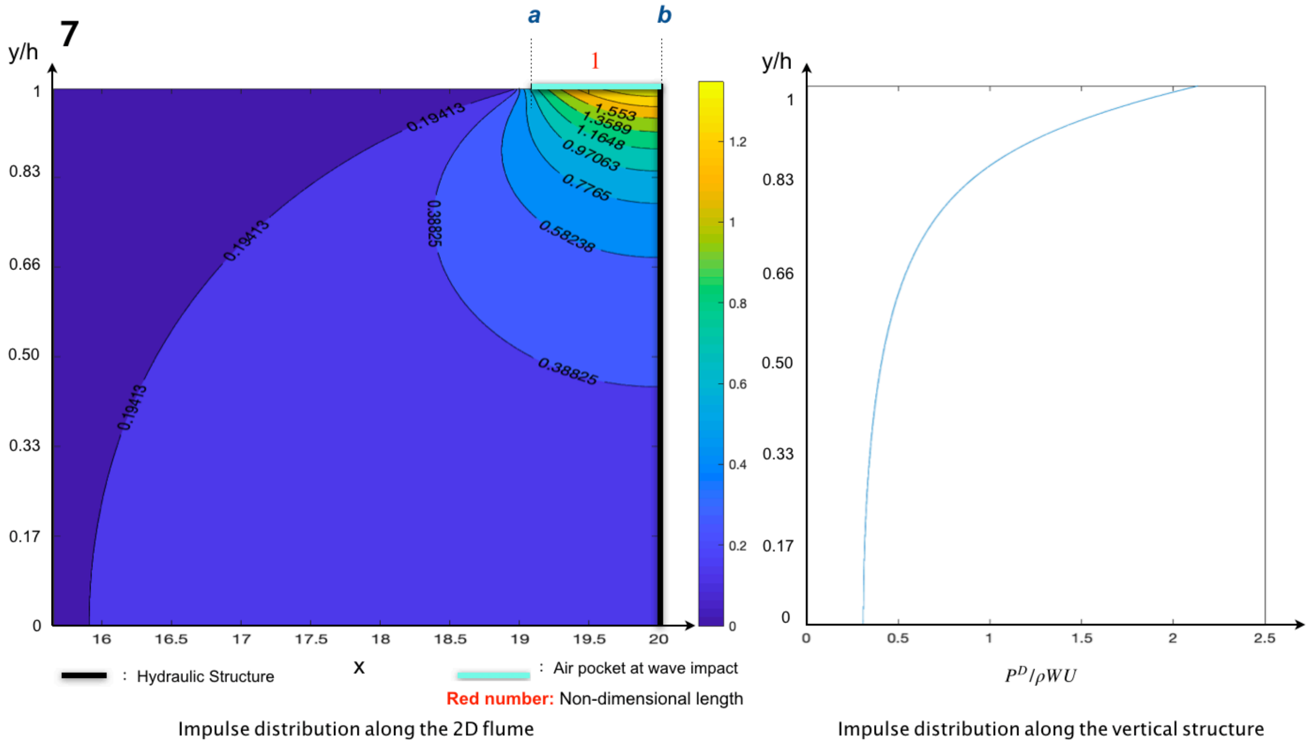

Figure 3.11: Situation 7:Pressure-impulse distribution of wave impact with bounce back effect (h: water depth, 0.6; y: water level, a = 19, b = 20)

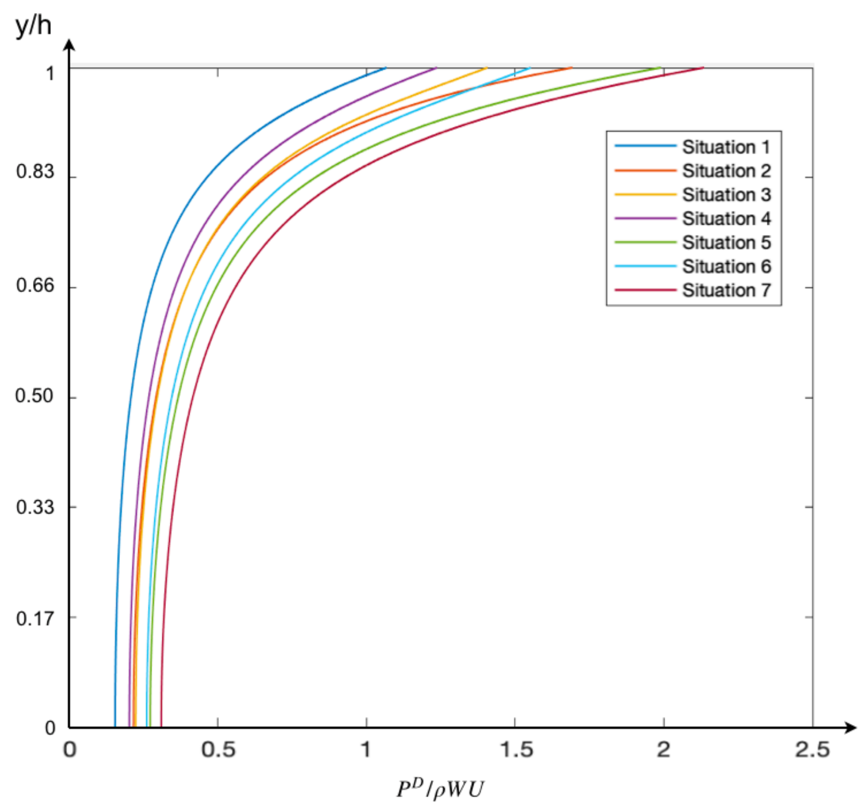

Figure 3.12: Wave impact pressure-impulse distribution along vertical structure (7 situations altogether, check Table 3.1)

3.4. Air influence on pressure impulse distribution

Air mainly influences wave loads from 2 variables:
1) Air position;
2) Air size.

Influence of these 2 factors are illustrated in Figure 3.13, Figure 3.14 and 3.15. In these figures, bold black lines represent structure contour. Bold blue lines represent air pocket size and air pocket position *in the horizontal direction*. **Note:** Actually, vertical position of air pocket is right under the bottom of horizontal overhang. Air pocket drawn in Figure 3.13, Figure 3.14 and 3.15 is not consistent with its actual vertical position in order to illustrate horizontal air position more clearly.

Air pocket moves from structure corner to overhang free end with the same size from situation (2) to situation (4). When distance between air pocket and vertical structure increases, area affected by wave impact along the 2-D flume is also increased from x= 17.5-20 to x=15.3-20 (check Figure 3.6 to Figure 3.8). At the same time, less impact impulse is loaded on the vertical structure (see Figure 3.13). Change from situation (5) to situation (6) (see Figure 3.9, Figure 3.10 and Figure 3.14) also reflects the same variation trend. Thus it can be concluded that when other conditions are the same, pressure impulse loaded on vertical wall decreases if air pocket moves away from the structure.

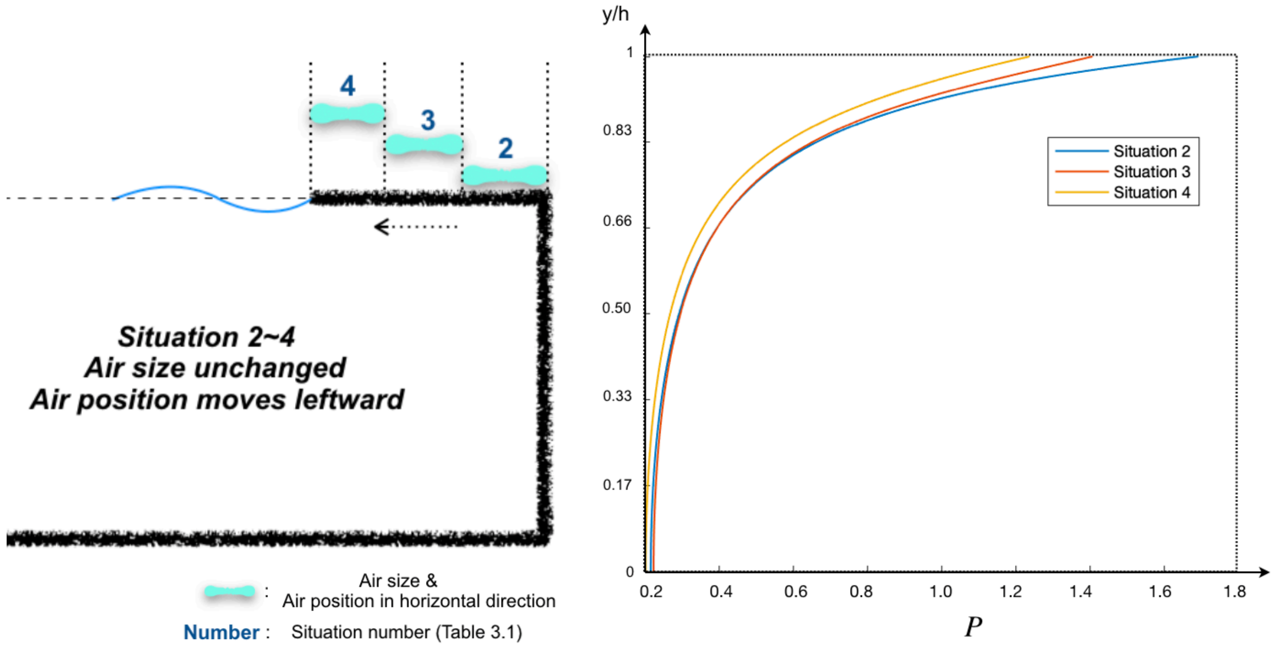

Figure 3.13: Situation 1, 2, 4 (Left figure: Schematic diagram of air size and position in horizontal direction; Right figure: Non-dimensional pressure impulse distribution along the vertical wall)

Air pocket position in situation (1), (2), (5) and (7) remains the same – at the structure corner while air pocket size increases progressively (Figure 3.15). It is observed that area affected by wave impact along the 2-D flume increases from x= 17-20 to x=15.8-20 (check Figure 3.3, Figure 3.6, Figure 3.9 and Figure 3.11). Meanwhile, impact impulse loaded on the vertical structure also increases.

It can be concluded that with the increase of air pocket size and decrease of distance between air pocket and the structure, impact pressure-impulse loaded on hydraulic structure is increased. Presence of air (bounce back effect) increases wave impact pressure-impulse, which is consistent with the conclusion from Wood & Peregrine (2000) that air involvement increases wave loads.

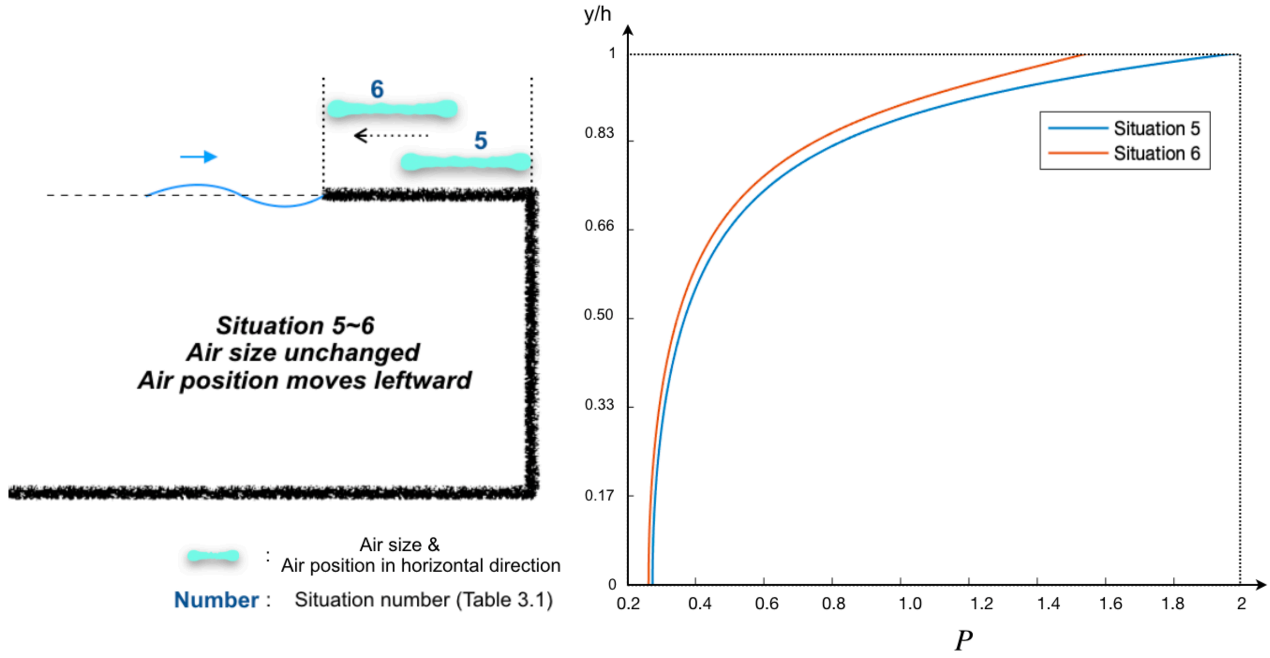

Figure 3.14: Situation 5, 6 (Left figure: Schematic diagram of air size and position in horizontal direction; Right figure: Non-dimensional pressure impulse distribution along the vertical wall)

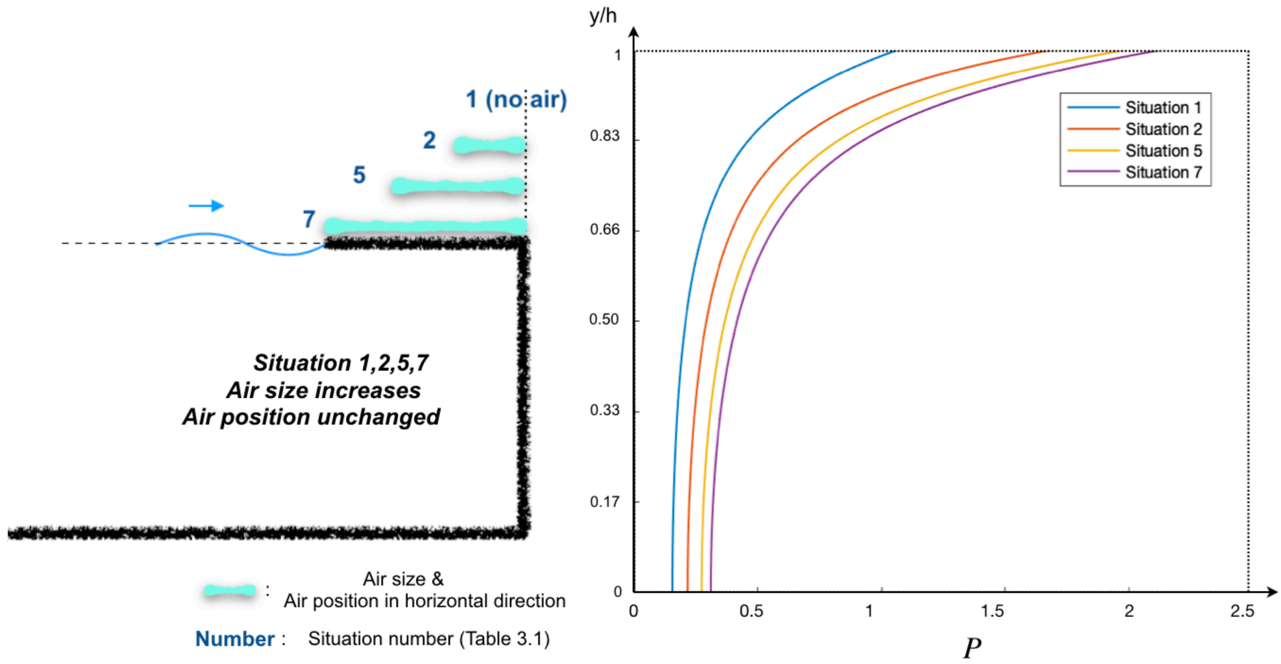

Figure 3.15: Situation 1, 2, 5, 7 (Left figure: Schematic diagram of air size and position in horizontal direction; Right figure: Non-dimensional pressure impulse distribution along the vertical wall)

4 Physical Experiment

Chapter 4 introduces experimental equipment and experimental scheme in detail. Also, typical features during wave and air development are described with recorded pictures. Physical experiment is carried out in the wave flume (40m* 0.8m *1m, L*W *H, Figure 4.1) at the Water Lab of Technology University of Delft. During the tests, pressure sensors are installed to measure impact loads. The whole experiment scheme is carried out by Ermano de Almeida.

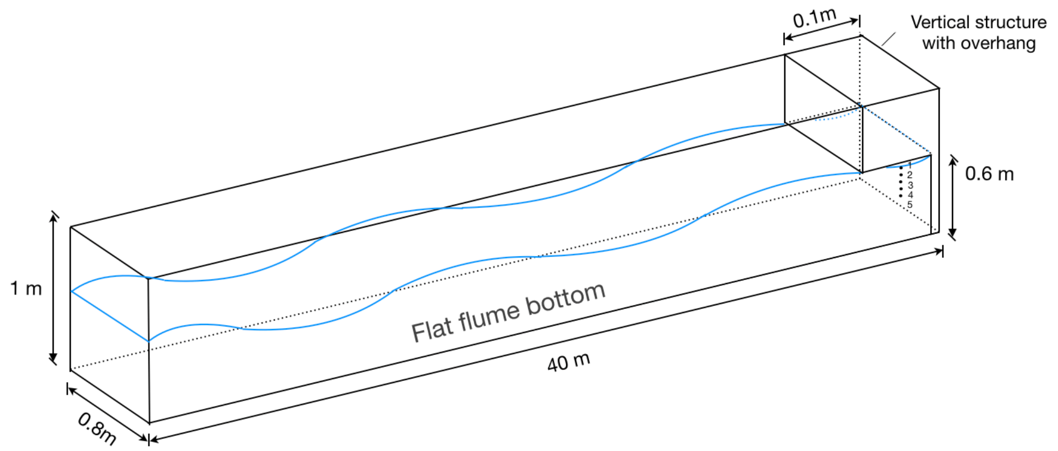

Figure 4.1: Experimental setup: overall view with pressure sensors

Study focus is wave impact impulse caused by the presence of horizontal overhang. Pressure sensors are installed on vertical walls. Pressure distribution on the vertical wall is recorded by pressure sensors connected to a data logging system. Thickness of the vertical structure is designed to be 1.0 centimeters, creating a rigid boundary for waves.

4.1. Experimental Scheme

4.1.1. Experimental Equipment

1) Wave flume;

Physical experiment is performed in the state-of-the-art wave flume (0.8 m wide, 1 m deep, 40 m long, wave paddle with active reflection compensation) at the Water Lab of Technology University of Delft, as is shown in Figure 4.2.

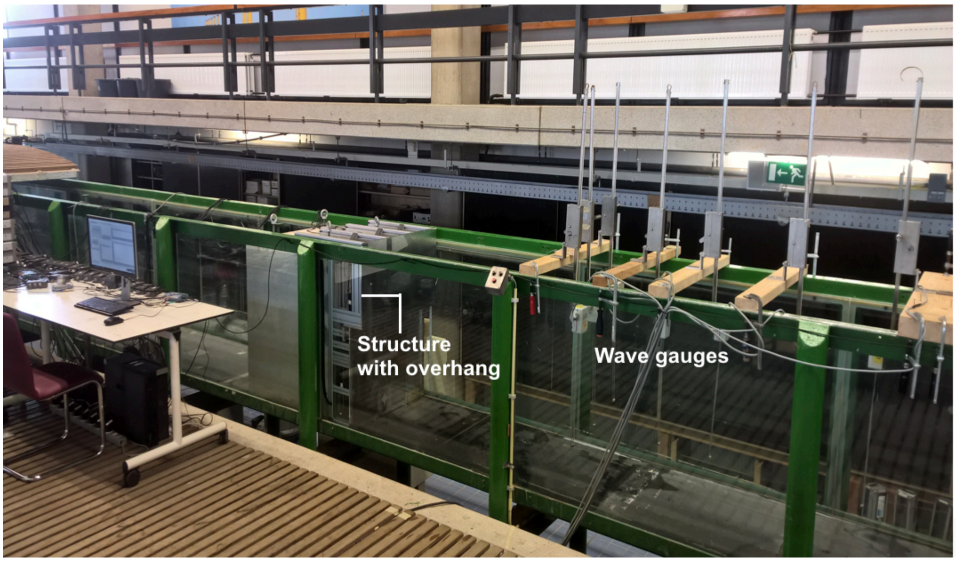

Figure 4.2: Wave flume used in physical tests (Ermano de Almeida)

2) Wave generator;
Wave generator is placed at one end of the wave flume and generates waves according to experimental schemes.

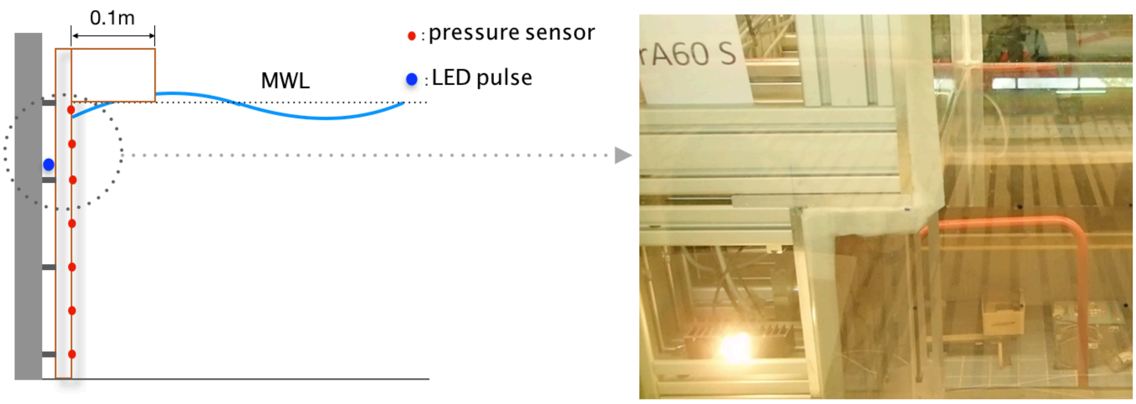

Figure 4.3: Position of LED pulse

3) LED pulse;
LED pulse starts to flash when the first wave impact occurs. In this way, measurements of pressure sensors and videos can be related properly with reference to the LED pulse. LED pulse flashes every 5 seconds.

4) Camera;
Cameras (Olympus) are installed around the structure to record wave shape during the development of wave impacts from 3 perspectives. Sampling frequency of cameras is 59.935 Hz. Details and positions of cameras are shown in Figure 4.4.

5) Wave gauges;
8 wave gauges are installed along the wave flume to measure real-time water level height. Positions

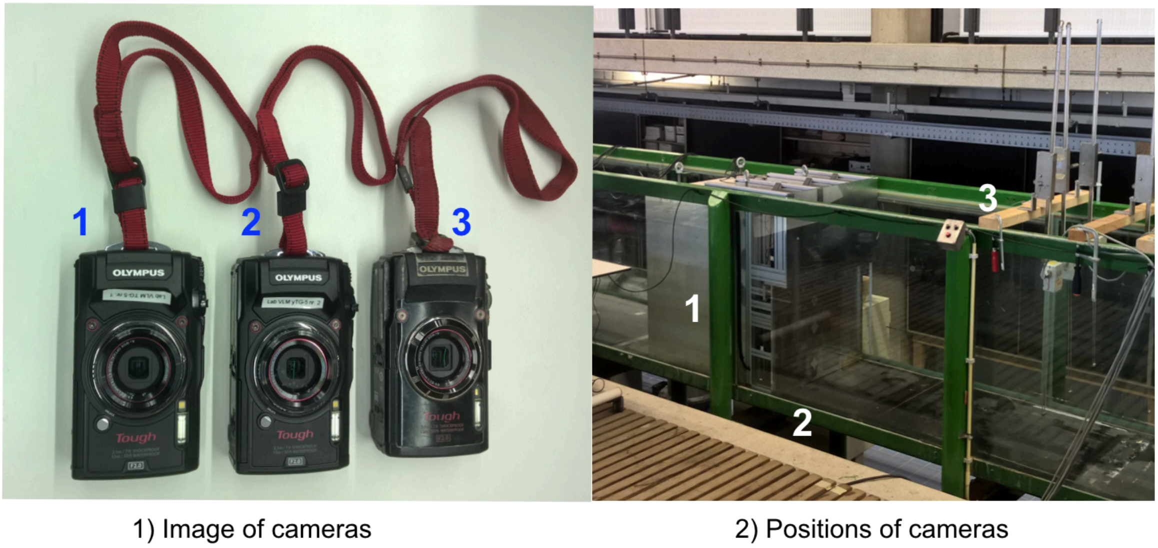

Figure 4.4: Cameras used in physical tests

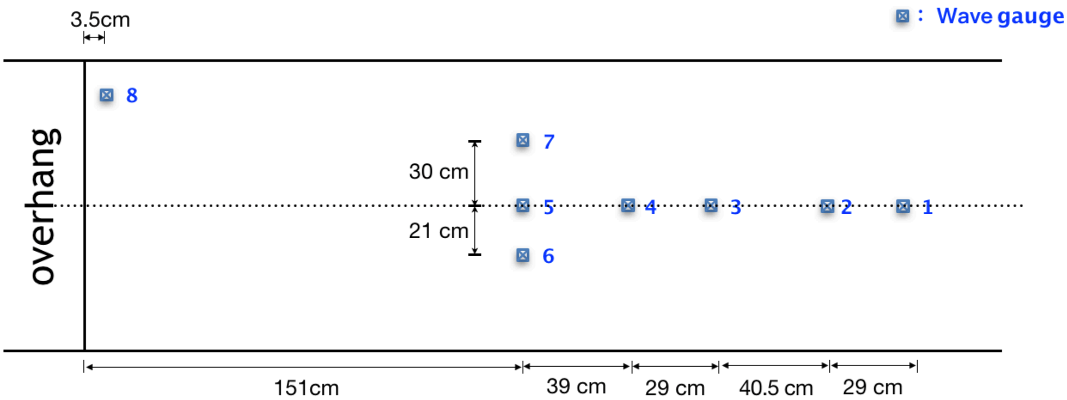

Figure 4.5: Positions of wave gauges

of wave gauges are shown in Figure 4.5.

6) Pressure sensor;

HKM-375(M) transducer from Kulite are selected to measure wave pressures. Sampling frequency is 1,000Hz. Under dynamic wave loads, the load difference is first revealed by voltage difference Δv. The voltage difference is then calculated to find out the pressure difference Δp. Positions of pressure sensors and front view dimension of the structure is shown in Figure 4.6.

4.1.2. Experimental Program

Physical experiment schemes are explained in detail in the following sections.

Structural Dimensions

Two types of structures are tested and analyzed in physical experiment (see Figure 4.7):
1) structure without overhang;

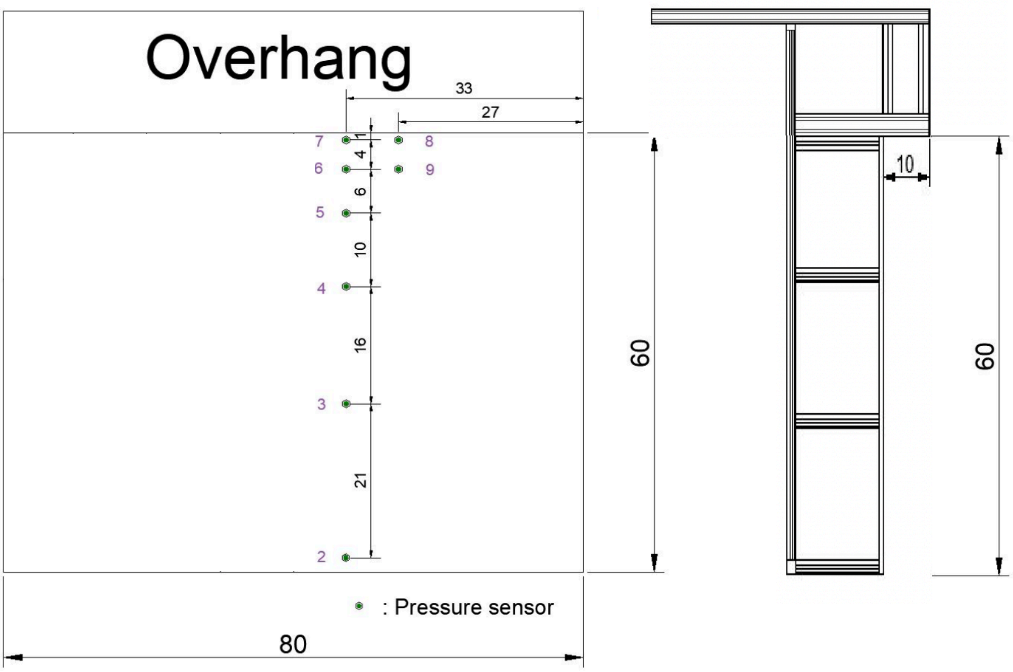

Figure 4.6: Dimension of overhang structure and pressure sensor position

2) structure with short overhang (overhang length= 10 cm).

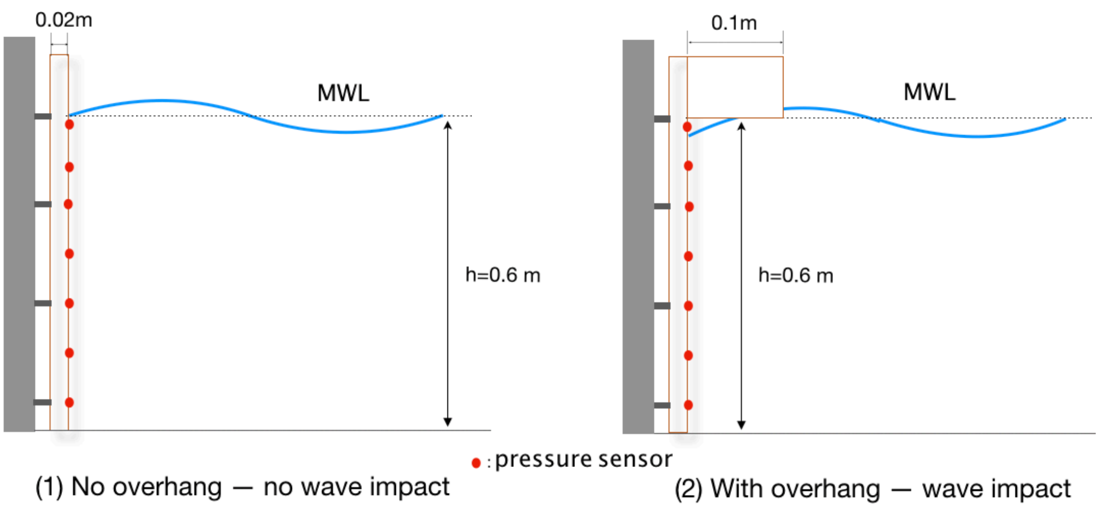

Figure 4.7: Experiment scheme diagram

To measure the peak pressures more comprehensively, 8 pressure sensors are placed the vertical structure, separated in 2 columns. Structure dimensions and pressure sensor positions are shown in Figure 4.6. Height of overhang is h=0.6m.

Test Parameters

Variables in physical tests are incident wave period (T), incident wave height (H), freeboard (R_c) and water depth (h) at the wall toe. Both regular waves and irregular waves are generated under two conditions – vertical structure without overhang and vertical structure with overhang. Only regular wave cases will be analyzed in detail. Wave height is H_i = incoming wave height = 0.06m, wave period is T_p=1.30s, freeboard is R_c=0m, mean water depth in the flume is h = 0.60m. Test parameters are listed in Table 1.1. Besides impact pressure measured by pressure sensors, water level along the flume is also measured by wave gauges. Images of wave gauges can be seen in Figure 4.2. Position of wave gauges is shown in Figure 4.5.

Table 4.1: Test parameters

Wave Conditions	**Symbol**	**Wave height(m)**	**Wave period(s)**	**Water depth h**(m)
Regular Waves	$r_A 60s$	0.06	1.3	0.6
Irregular Waves	A60s	0.06	1.32	0.6

4.2. Phenomenon Description

In physical experiments, waves generated are all non-breaking waves.

4.2.1. Wave development description

1) Regular waves:

1.1) For vertical structures without overhang, no air pocket would be entrapped because regular waves are generated and no water jet occurs during the whole process. The wave surface simply moves up and down along the vertical wall and no wave impacts are tested;

1.2) For vertical structures with overhang, when the sum of water depth and half of the wave height is no larger than the height of overhang(d +H_i< h), wave crest is beneath the overhang bottom and the wave surface has no contact with overhang. Under this circumstance, Wave pressures exerted on vertical structure are the same as the situation of vertical structures without overhang and no wave impacts are measured.

When d+ H_i ≥ h, the approaching wave front touches the bottom corner of the overhang and a certain volume of air is trapped between the wave surface and the structure. As the wave front keeps moving forward, the wave surface rises to clap the bottom of the overhang. The air volume first splits into several air pockets of smaller size and then move away from the vertical structure with reflected waves. The majority of wave pockets split into small air bubbles and float up along the outline of the overhang structure, finally escape to atmosphere and disappear. Wave impacts are tested during the process.

2) Irregular waves:
Wave combinations are quite random for irregular waves.

2.1) Vertical structures without overhang, wave impacts occur rarely if water jet is formed by irregular wave when it touches the vertical structure;

2.2) Vertical structures with overhang, when water depth plus half of the wave height of irregular waves is no larger than the overhang height (d +H_s < h), wave impacts occur rarely if one wave with large height comes and air would be trapped.

When d+ H_s ≥ h, it is observed that wave surface claps overhang bottom frequently and impact pressures are tested frequently. The air-trapping process is similar to that of regular waves while for irregular waves, it is more complicated for random combination of waves

4.2.2. Air development description

1) Regular waves r$_A$60s

In the situation of $r_A 60s$, the water depth is 0.6m, which equals to the height of the horizontal overhang. Under the influence of waves (H_i=0.06m), the air volume involved under such situation is limited. Figure 4.8 to Figure 4.10 display changing process of wave surface and air (figures are processed to be more understandable in chapter 5).

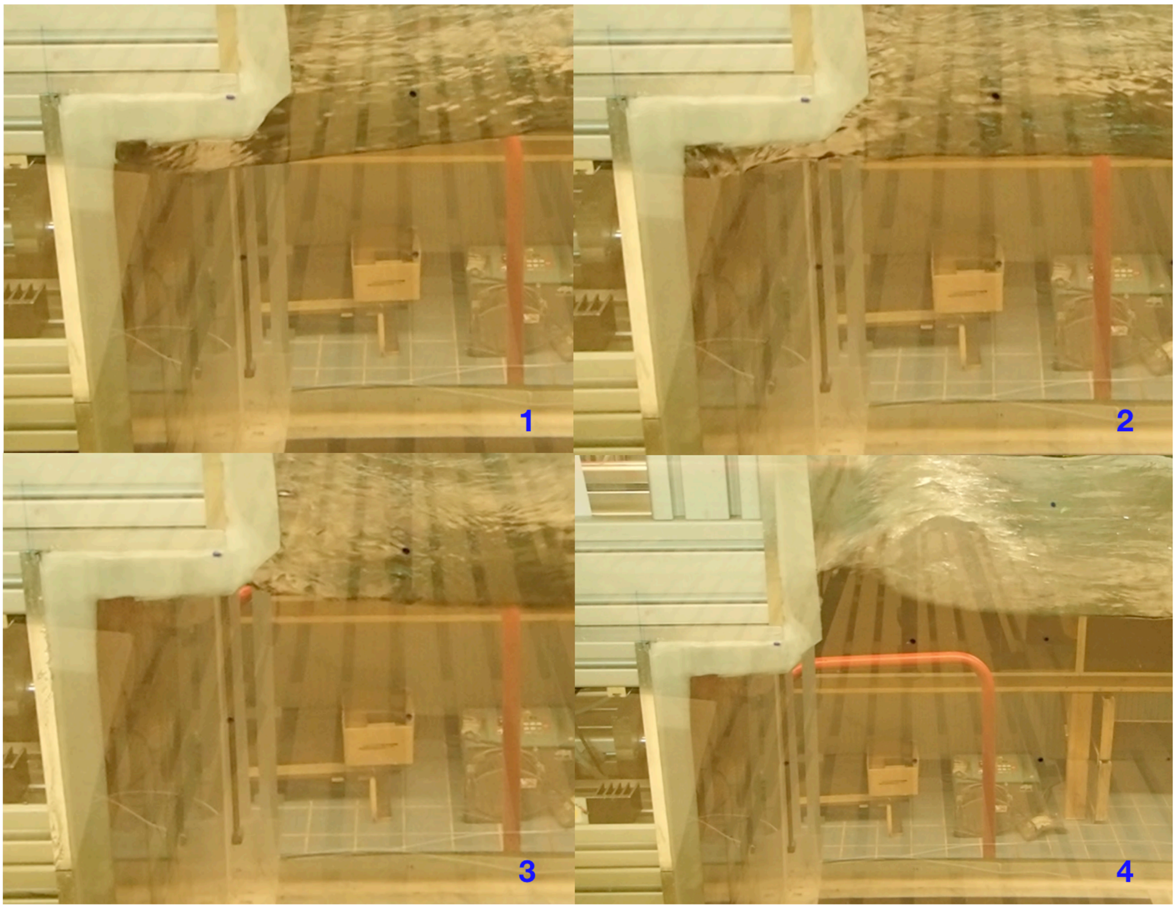

Figure 4.8: Side view of wave shape and air involvement changing process under $r_A 60s$

As one wave profile approaches the structure and the wave surface rises, a certain amount of air pocket is trapped between the bottom of the overhang and the wave surface. When the wave surface continues to rise, the trapped air volume is squeezed into many air bubbles (entrained air), moves away from the structure with the deflected water and finally escape into atmosphere. White spray appears during this process. Peak impact pressure occurs with the trapped air pockets and then minor vibration of peak pressures appear when the unstable air cushion breaks into many small escaping air bubbles.

Figure 4.9: Bottom view of wave profile and air involvement changing process under $r_A 60s$

Figure 4.10: Top view of wave profile and air involvement changing process under $r_A 60s$

2) Irregular waves A60s

For irregular waves A60s, the wave impact with the maximum peak pressure is selected for analysis. Evolution of wave shapes are shown in Figure 4.11 to Figure 4.13.

Figure 4.11: Normal pressure measurement situation under irregular waves A60s

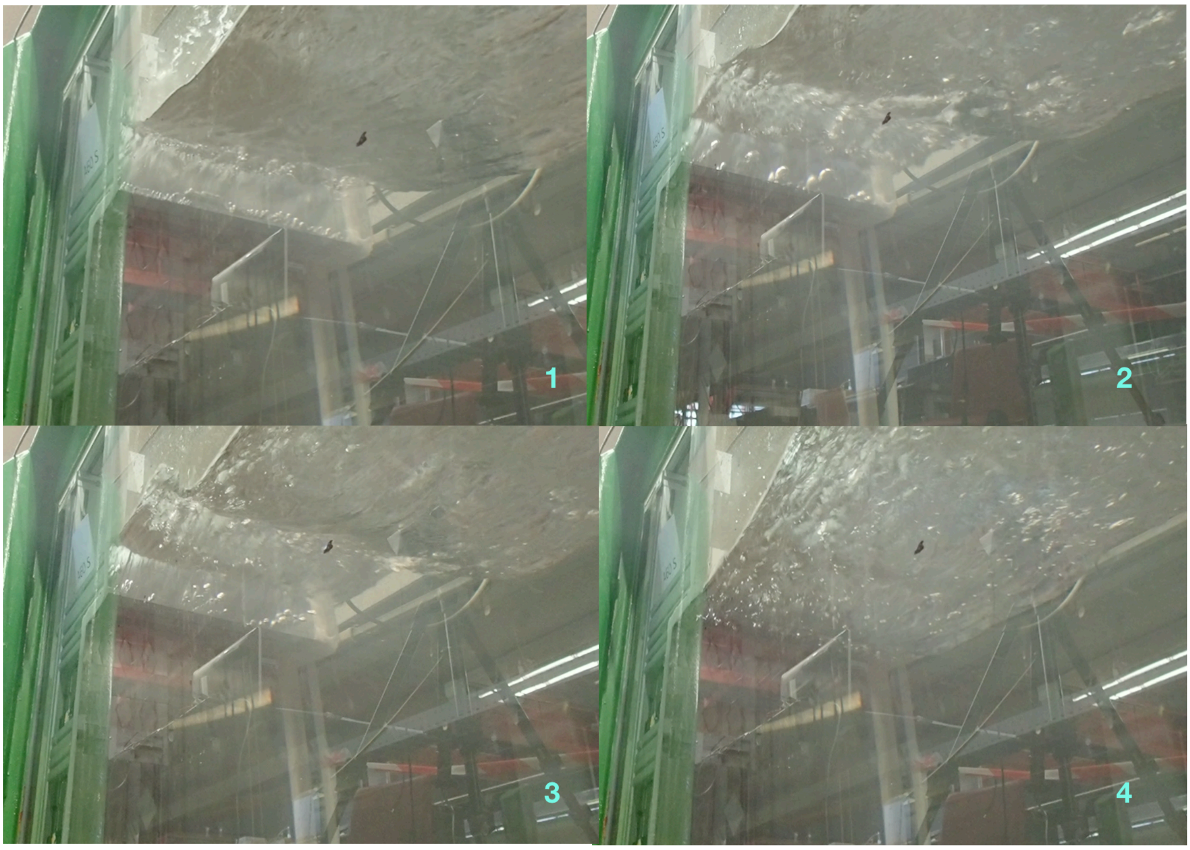

Figure 4.12: Normal pressure measurement situation under irregular waves A60s (bottom view)

Measured data is analyzed with combination of videos. It is shown that waves with relatively small wave heights usually entrap less air and measured pressures are relatively large. For waves with larger wave heights, more air is trapped and more air bubbles are produced. Relatively larger air volume escapes from water body and water splash usually appear, as is shown in Figure 4.12 and Figure 4.13. It is observed that smaller impact pressures are measured.

Figure 4.13: Normal pressure measurement situation under irregular waves A60s (Top view)

Images more understandable and explanations in depth are presented in Chapter 5.

5

Test Data Analysis

In chapter 5, impulsive wave impacts on the structure are analysed according to recorded video and test data. During physical experiment, wave heights are measured by wave gauges. Shape of waves and air content can be checked from video records from side view and bottom view. Wave impacts against the structure are measured by pressure sensors. Test data analysis in chapter 5 composes of 3 parts (see Figure 5.1). Signal noise is first removed by low-pass filtering. Pressure distribution and impact impulse distribution along the vertical structure under wave impacts is calculated. Relationship between air and wave loading is described. Wave impact pressures are sensitive to incoming wave parameters while pressure impulse are less sensitive. Non-dimensionalization of pressure impulse is applied at the end of chapter 5 so that experiment result and numerical modelling result in chapter 3 can be related. Considering process of wave impacts is influenced by various factors, data analysis starts from simple wave conditions – regular waves rA60s and rA60 (Table 5.1). Test results of regular waves are analyzed in detail since wave parameters of each impact are known and the influence of air can be analyzed more precisely.

Figure 5.1: Original signals of pressure measured under regular waves (with overhang)

Conditions analyzed in this thesis are listed in the table below. Also, pressure impulse is selected to be the critical research variable for 2 main reasons:

1) Compared to peak pressures, pressure impulse is more typical and representative because it is more constant for different wave impacts;

2) Load which is exerted on and has an effect on structures is not peak pressure but pressure impulse.

Table 5.1: Tested conditions

Structure	**Wave conditions**	**Wave height H_i**	**Wave period T_p**	**Water depth**
With overhang(rA60s)	Regular Wave	0.06m	1.316s	0.60m
Without overhang(rA60)	Regular Wave	0.06m	1.316s	0.60m

5.1. Signal filtering scheme

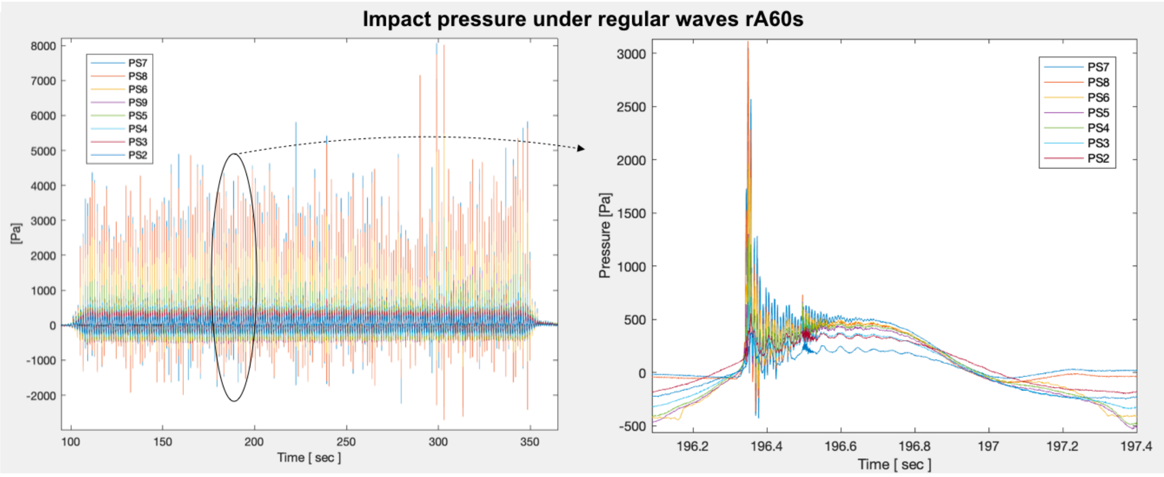

Figure 5.2: Original signals of pressure measured under regular waves (with overhang)

Figure 5.2 shows pressure distribution over time under regular waves *rA60s*. Violently vibrating signals and irregular pressure distribution over time can be observed. For example, obviously large wave pressure is measured from around 280s to 320s. This is because noise is involved in original signals measured by pressure sensors. Much noise is caused by vibrations of the structure and pressure sensors, frictions between wave water and structure surface, dynamic interaction between wave and structure, air bubble breaking and movement, and so on. Noise should be filtered and signals of waves should be kept. Low frequency filtering is applied to smooth the curves so that rules hidden in graphs could be better observed and analyzed. Thus first of all, experiment data should be filtered to remove signal noise.

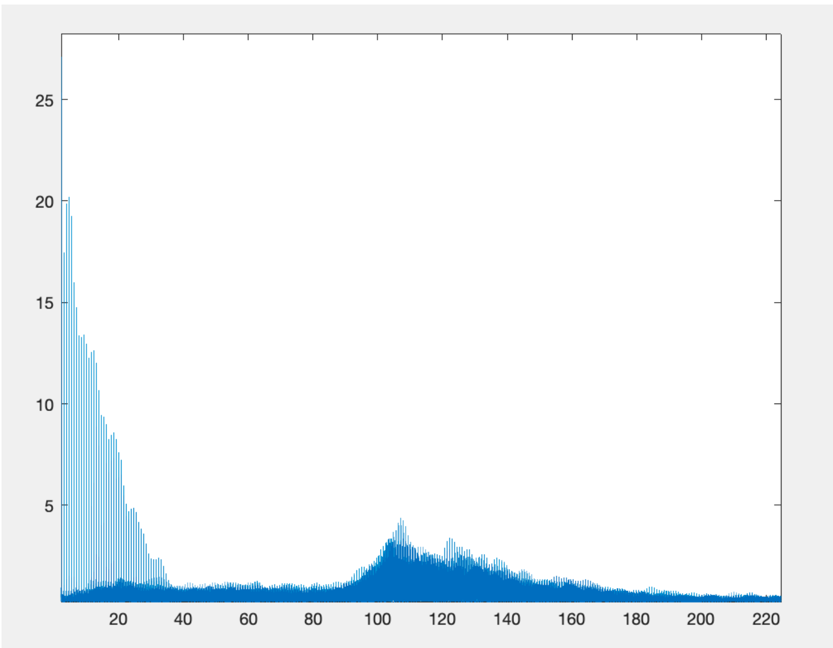

Figure 5.3: Frequency spectrum of original signal (detrend + FFT function)

To decide the filtering frequency, frequency spectrum is drawn in advance. Detrend and FFT (Fast Fourier Transform) function is applied (Figure 5.3) and signals with frequencies from 0Hz–40Hz are maintained because this is the range of wave loads. Butterworth filter is selected for data processing and smoother curve is achieved after filtering (Figure 5.4). Details of cut-off frequency determination and low-pass filtering choice can be checked in **Appendix A**. Contents related to filtering is also stated in section 5.4.

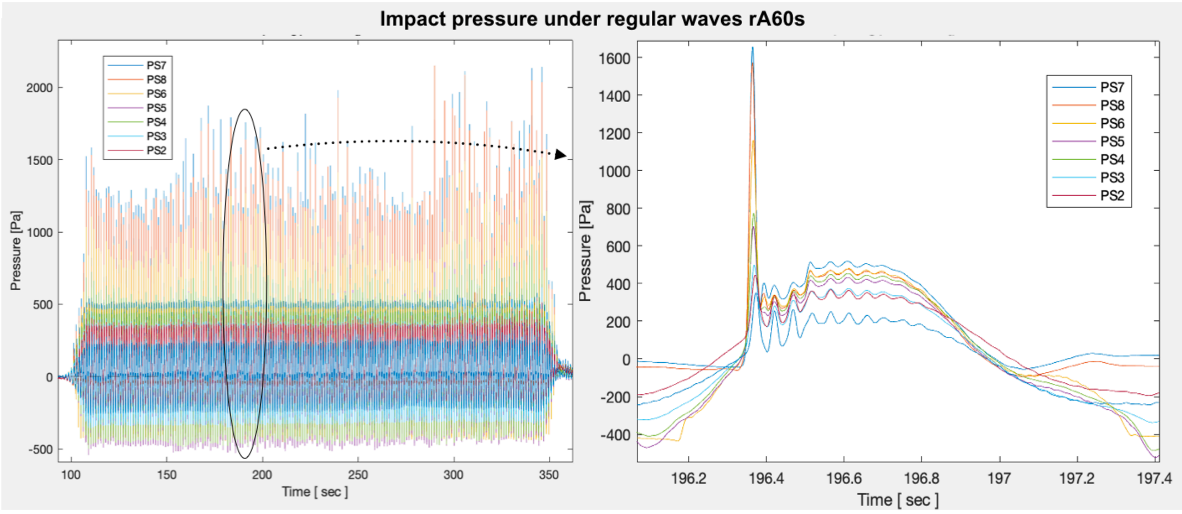

Figure 5.4: Filtered signals of pressure measured under regular waves (with overhang)

5.2. Relationship between peak pressure and air content

Data from pressure sensor 7 is analyzed as typical impact pressure because pressure sensor 7 is located in the key junction area of air and water. It can be observed that for pressure sensor 7, initial pressures are smaller than zero (Figure 5.5). This is because pressure sensor 7 located 1 centimeter below the horizontal overhang (Figure 5.6). When wave impact occurs, pressure sensor 7 is 1 centimeter below the original wave surface. Thus negative pressure of 1 centimeter water column occurs there (P_{t0}=-ρ g h_w=-10^3 ×10 ×0.01= -100 Pa). Tested result is -117.7Pa, which is close to theoretical value. Considering vibrations of waves, structure and pressure sensors and other influencing factors, the difference is acceptable and reasonable. Also, it testifies the rationality of experimental measurement.

6 wave impacts (Table 5.2) are selected to analyze, as is shown in Figure 5.5. 2 of them are wave impacts with the biggest peak pressures among all tested waves. One is a wave impact with medium peak pressure and the other 3 selected wave impacts have the smallest peak pressures. The purpose of this section is to study the relationship between peak pressure and air entrapment. Relationship between air entrapment and measured pressures will be explained with images.

Table 5.2: Peak pressures analyzed in detail

	Number	**Peak Pressure (Pa)**	**Moment (s)**
Maximum Peak Pressures (Pa)	(1) (2)	2139.61 2130.58	345.937 340.729
Medium Peak Pressure (Pa)	(3)	1375.03	293.927
Minimum Peak Pressures (Pa)	(4) (5) (6)	1047.69 987.27 986.06	288.726 300.432 245.827

Maximum peak pressure (1) is analyzed in detail (peak pressure = 2139.61 Pa, t=345.937 s). The

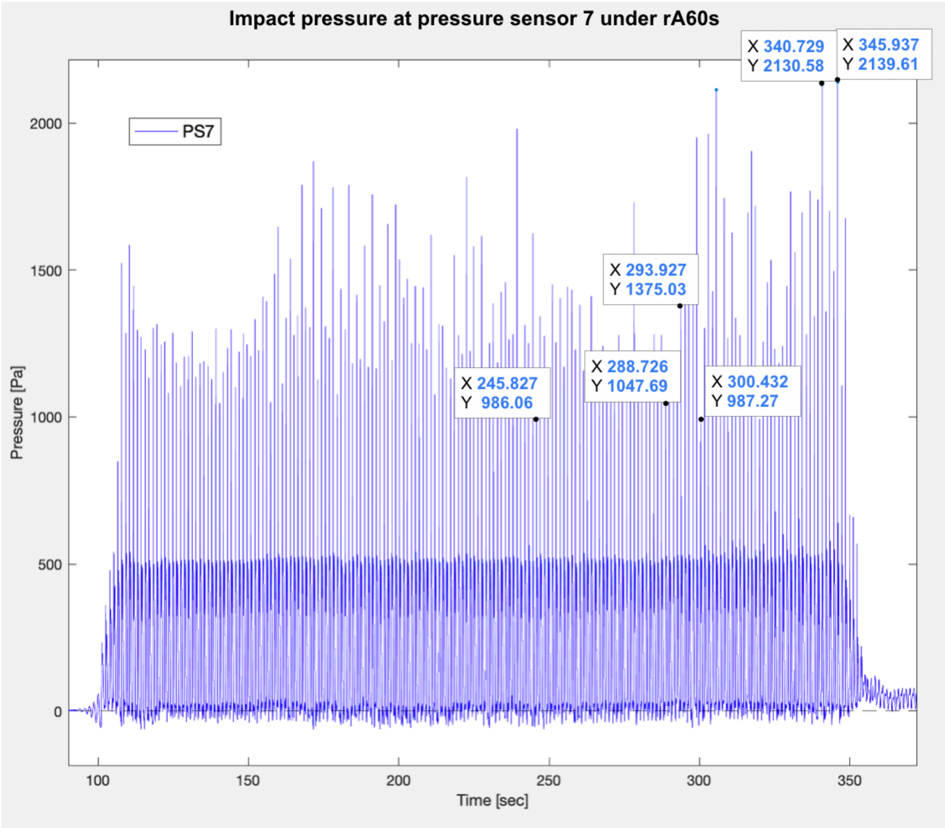

Figure 5.5: Measurement data of pressure sensor 7

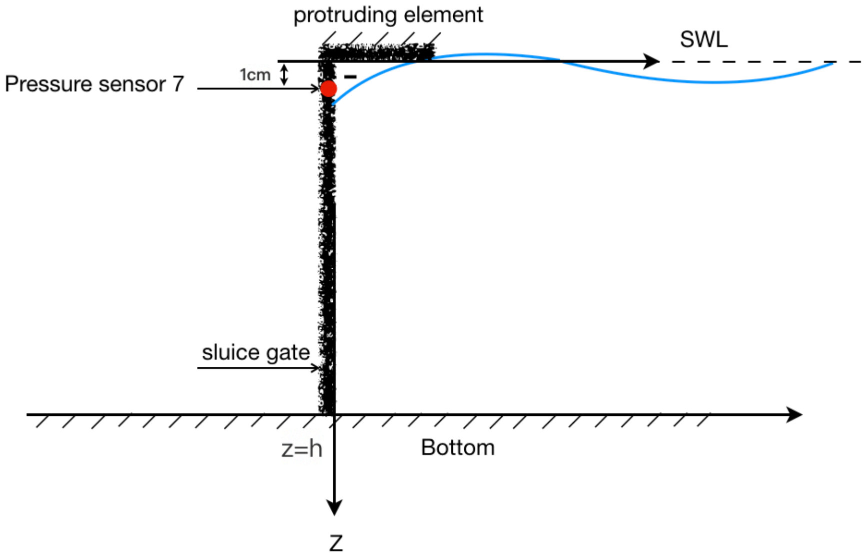

Figure 5.6: Pressure sensor 7 under wave impacts

other 5 wave impacts (2-6) are analyzed in the same method. Corresponding figures of the other 5 wave impacts can be checked in **Appendix B.**

Maximum peak pressure (1): P=2139.61 Pa, t=345.937s

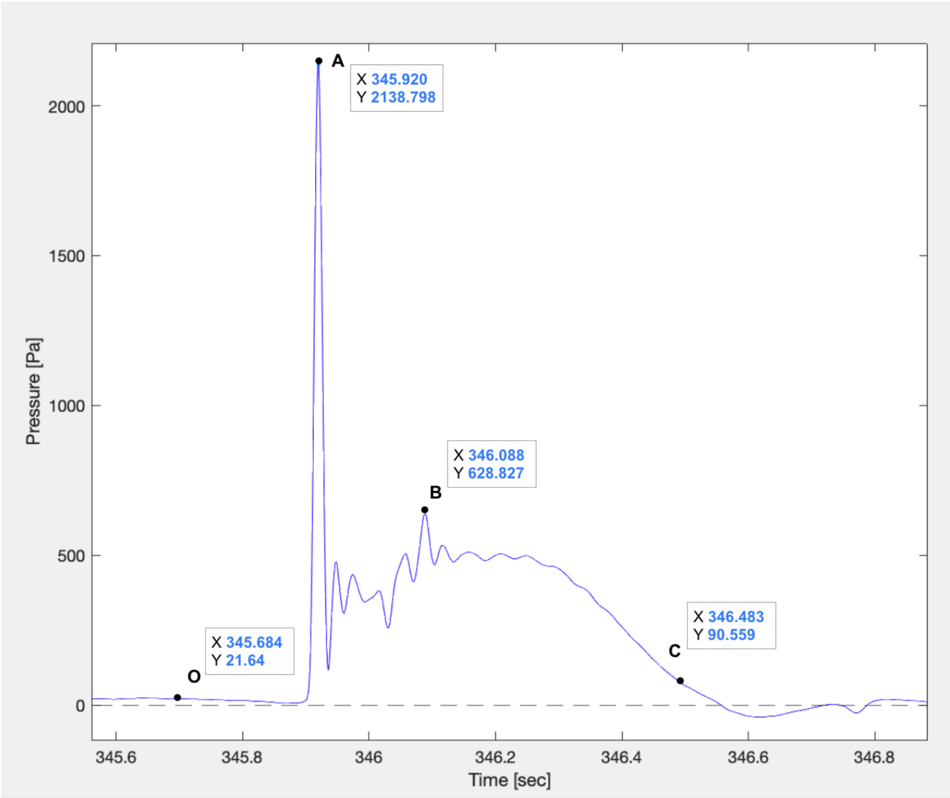

Figure 5.7: Pressure-Time Curve (Pressure sensor:7, Peak pressure = 2139.61 Pa, t = 345.937s; X:Time(s),Y:Pressure(Pa)

5.2.1. Representative moments description in one wave impact

Four typical points (O, A, B and C) in the pressure-time curve of wave impact (1) can be observed and wave images corresponding to these moments are recorded, as is shown in Figure 5.8.

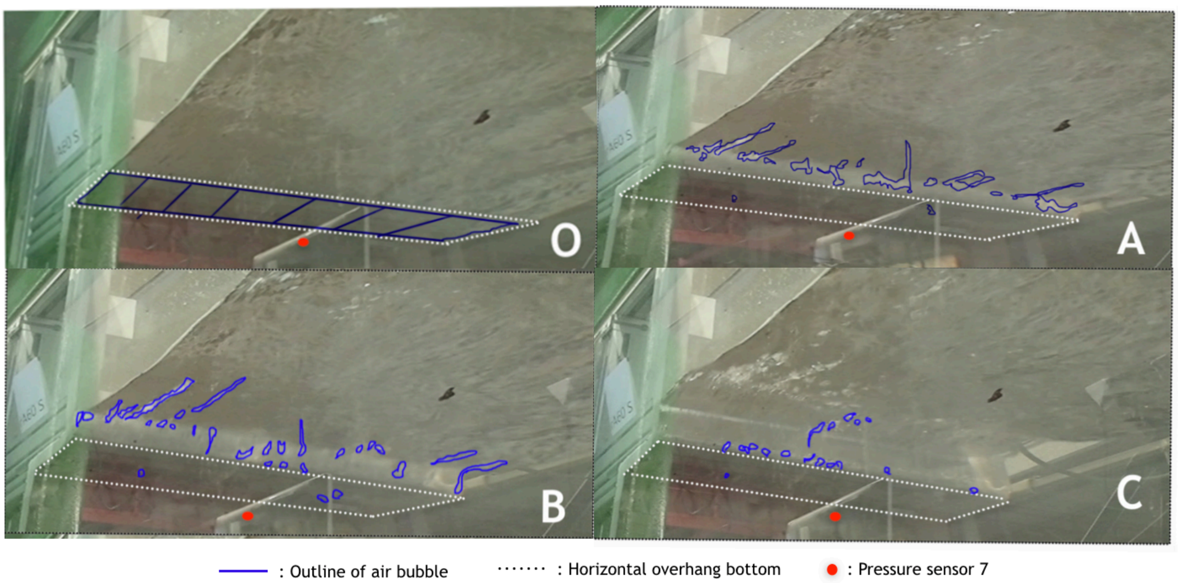

Figure 5.8: Bottom view of air bubble distribution (Pressure sensor:7, Peak pressure = 2139.61 Pa, t = 345.937s, air shape is estimated from colour difference in blurred image and outlined in blue)

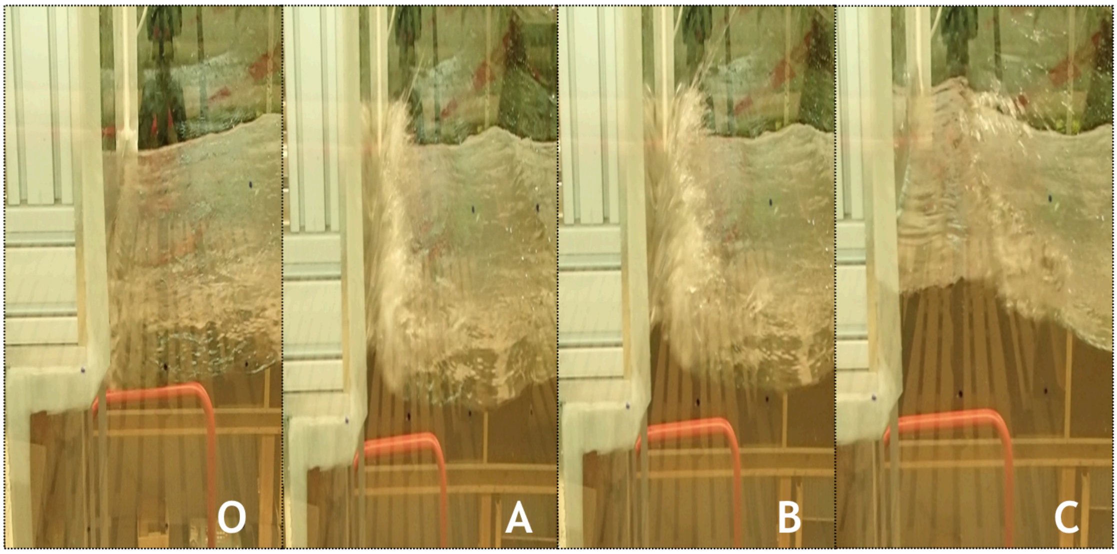

Figure 5.9: Side view of wave shape(Pressure sensor:7, Peak pressure = 2139.61 Pa, t = 345.937s.)

a). Moment before wave impact (O):

At moments before wave impact, the previous wave has retreated and a new wave crest is coming, creating conditions for the next wave impact. Vertical structure only undergoes hydro-static pressure and water surface is stable from all angles and no air is mixed in water. Since water surface has not touched the overhang bottom, air spreads all over the overhang bottom.

b). Moment of the maximum primary peak pressure (A):

1) Bottom view: Entrapped air is pressed out by the uprising wave surface. After that, the impulsive peak pressure occurs while air left under horizontal overhang is the least. Since images are of poor quality, air bubbles are outlined in blue in Figure 5.8;

2) Side view: Wave surface rises above the lower right corner of the structure and water splashes quite violently.

As can be seen, phenomenon observed coincides with the conclusion of Bagnold (1939): During each wave impact, peak pressure occurs when very little air is entrapped between water and structure.

c). Moment of the reflected peak pressure (B):

1) Bottom view: Moment B is right after moment A and there is still air left under the horizontal overhang;

2) Side view: Wave surface rises above the lower right corner of the structure and splashing water begins to drop back to water surface.

d). Moment after the reflected peak pressure (C):

1) Bottom view: Large percent of air is already pressed out and large amount of bubbles has come to water surface;

2) Side view: Reflected wave is developed and crest of the reflected wave has already moved a certain distance away from the right end of the overhang, which means the reflected wave has left the overhang for seconds. Water surface is more gentle.

5.2.2. Relationship between air content and peak pressure

During each wave impact, it is observed that air pocket usually breaks into two parts with the presence of the first wave peak. As is shown in Figure 5.10, a whole air pocket splits into two parts under the curve of wave peak surface. After that, two parts of air bubbles present in wave water, as the red and blue part in Figure 5.10. In addition, six moments selected in Figure 5.11 share the same characteristic in common and prove this regularity.

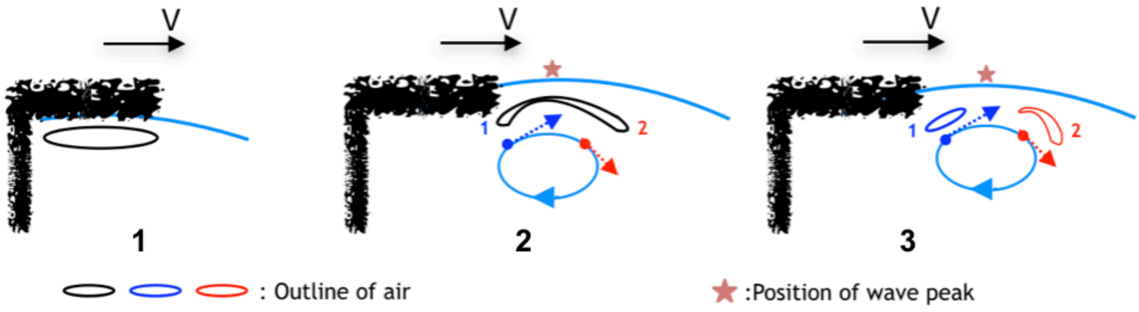

Figure 5.10: Air pocket breaks into 2 parts at wave peak under the horizontal overhang

To study the relationship between peak pressure and entrapped air content, volume of air entrapped (V$_{air}$) under overhang at the moment of peak pressure occurrence (t$_{peak}$) should be found out. However, because of the poor light at the overhang bottom, strong reflection of glass sink and limitation of image quality, V$_{air}$ right at the moment of t$_{peak}$ can not be determined from recorded videos with naked eyes correctly. Thus, it is decided to observe total volume of air contained during each wave impact (V$_{all}$) because air pressed out in water wave is easier to observe. Air bubbles pressed out in wave water can reflect volume of entrapped air (V$_{all}$). Images at the moment when most air bubbles present in wave water is selected since almost all entrapped air volume is squeezed out and V$_{all}$ can be estimated most accurately at this moment. To sum up (see Figure 5.10), air pocket size at moment 1 is what needed but hard to be identified. Thus, moment 3 is selected to estimate air pocket size roughly during the same wave impact. This approach may induce error.

Figure 5.11 shows the presence of most air bubbles (moment 3 in Figure 5.10) and the value of primary peak pressure during wave impacts selected in Table 5.2, which to some extent presents the whole air volume entrapped by each regular wave. As can been seen in Figure 5.11, air content is relatively small in (1) and (2), medium in (3) and large in (4) to (6) (corresponding the picture number in Figure 5.11 to 'Number' in Table 5.2 and Table 5.3). Total entrapped air content and corresponding primary peak pressure in each selected wave impact is described in Table 5.3.

Conclusion: When other parameters are the same, the larger the air volume (V$_{all}$) is entrapped during a whole wave impact, the smaller the impulsive peak pressure would be. Experiment result is consistent with Peregrine & Thais (1996) (Air entrainment increases water compressibility. Air cushions the wave impact since the pressure is spread in both space and time.).

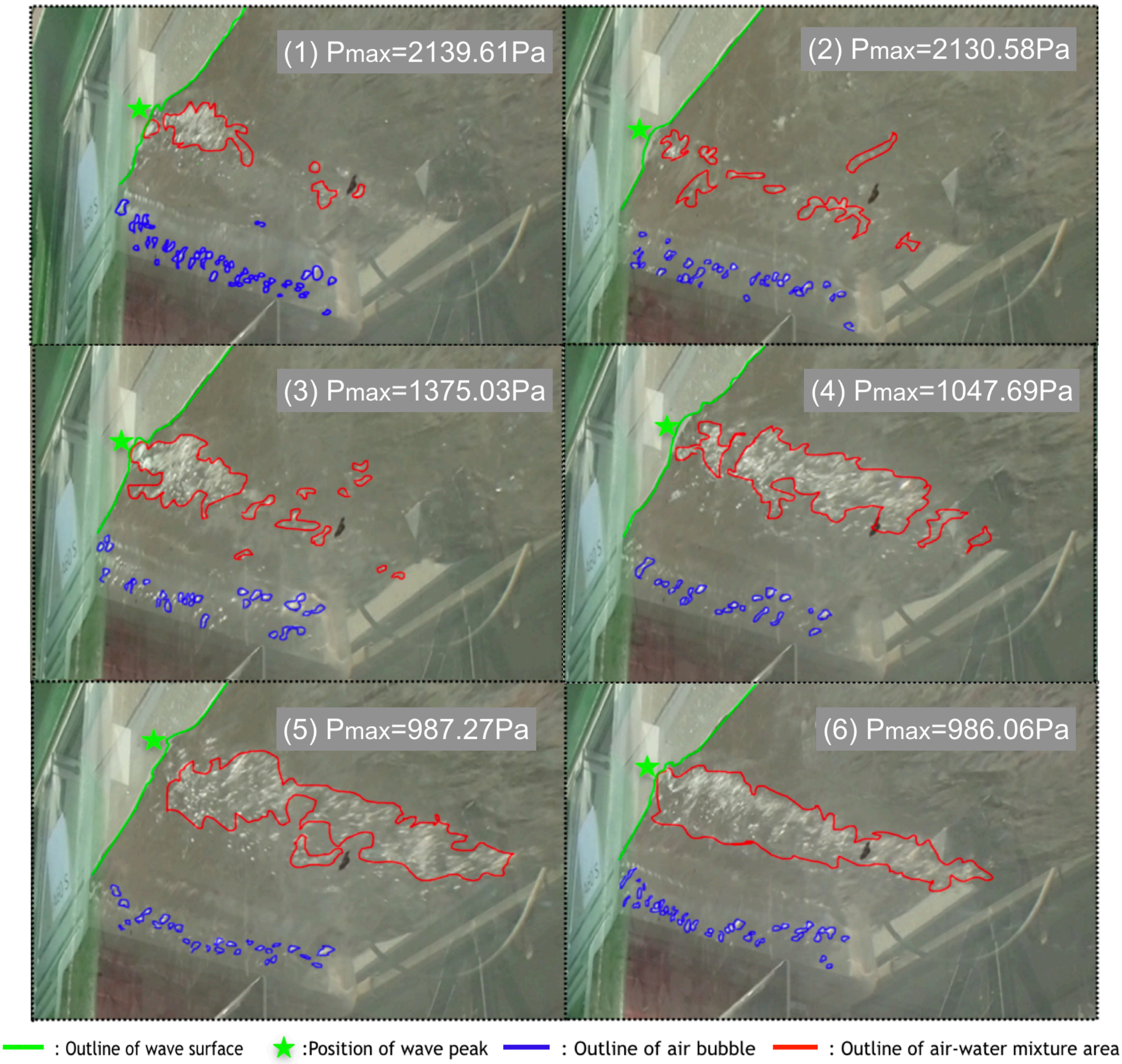

Figure 5.11: Presence of the most air in selected wave impacts

Table 5.3: Peak pressure and total entrapped air volume during selected wave impacts

	Number	**Peak Pressure (Pa)**	**Air Content**
Maximum Peak Pressures (Pa)	(1)	2139.61	small
	(2)	2130.58	small
Maximum Peak Pressure (Pa)	(3)	1375.03	medium
Minimum Peak Pressures (Pa)	(4)	1047.69	large
	(5)	987.27	large
	(6)	986.06	large

5.3. Pressure distribution along the structure

As is mentioned in Chapter 4, pressure sensors are installed on the vertical structure to measure impulsive wave pressures.

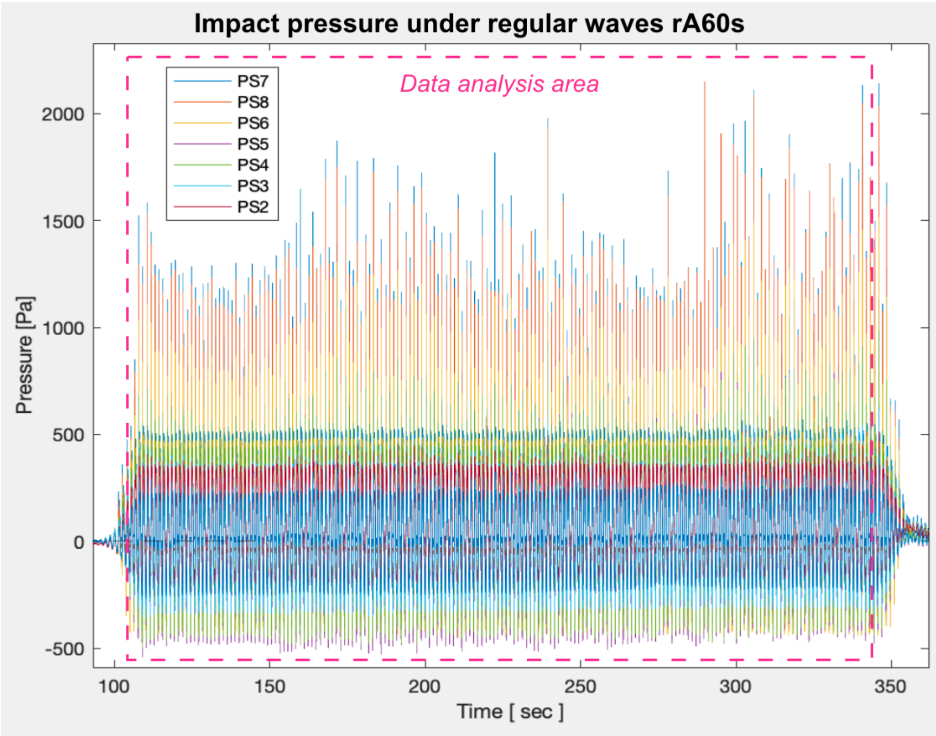

Figure 5.12: Analysis area of measured data

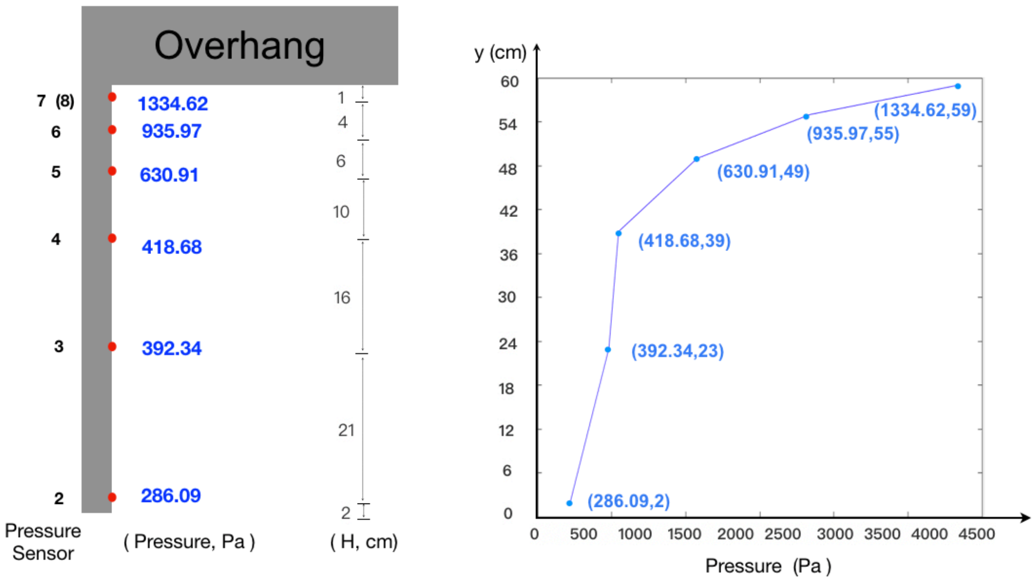

Figure 5.13: Pressure distribution along the structure in experimental measurement

For regular waves, each measurement takes about 2 minutes. Period from 108.8s to 342.8s is the analysis area because wave development is stable and typical during this period and almost the whole range of measured data is included. There are 180 waves, so 180 primary peak pressures are measured during the selected period. Average value of 180 peak pressures is selected to be the representative pressure and the result is shown in Figure 5.13. The maximum impulsive pressure occurs at the highest point of the vertical structure and impact pressure decreases with the increase of water depth, which means influence of wave impact and air entrapment decreases away from the water surface.

5.4. Pressure impulse distribution along the structure

Pressure impulse of each wave impact is the result of pressure integration over impact period. For vertical structures without horizontal overhang, no impact occurs under regular waves. Pressure impulse is calculated and represented by P_i^D. For vertical structures with horizontal overhang, pressure impulse is calculated and represented by P_j^D. Thus impact impulse ΔP^D resulting from the presence of horizontal overhang is achieved by removing P_i^D from P_j^D.

$$\Delta P^D = P_j^D - P_i^D \tag{5.1}$$

in which,
P_i^D: pressure impulse for vertical structures without overhang;
P_j^D: pressure impulse for vertical structures with overhang;
ΔP^D: impact impulse caused by the presence of horizontal overhang.

Impact impulse at the location of pressure sensors 2–7 are all calculated. Pressure-time curve varies greatly from one impact to another. For vertical structures with overhang, record of 180 regular waves is exported and analyzed. For vertical structures without overhang, regular waves do not induce wave impacts (see green line in Figure 5.14). Thus the structure and pressure sensors do not undergo much vibration and there is no need to filter the data. Original and filtered data is shown in Figure 5.14.

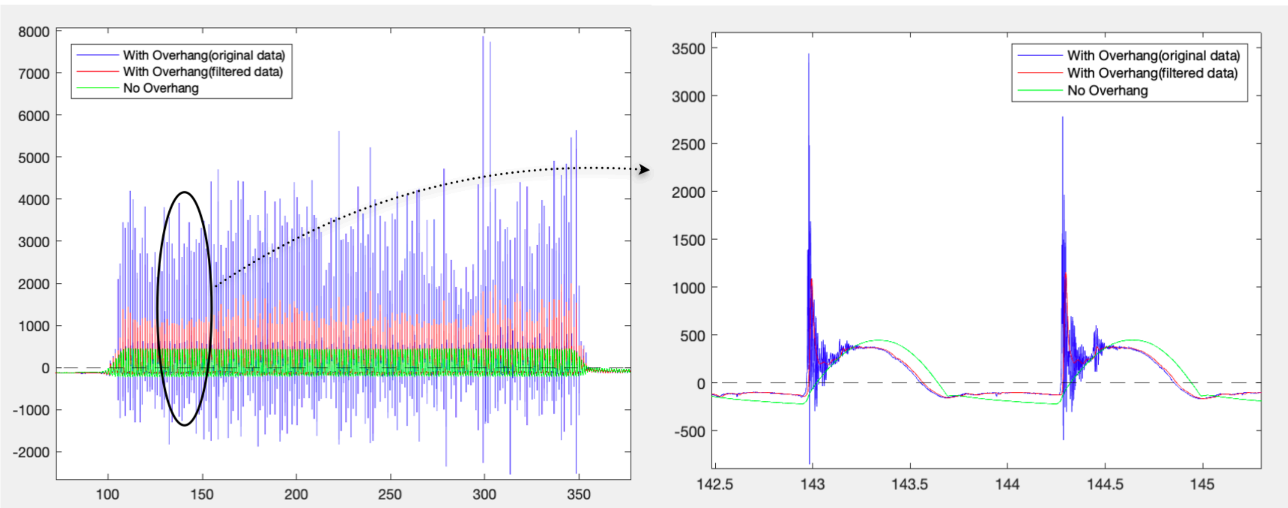

Figure 5.14: Pressure–time curve under regular waves(pressure sensors 7–with and without horizontal overhang)

5.4.1. Impulsive pressure impact definition

Pressure integration over impact period is the impact impulse. Analysis range is taken to be 108.8s–342.8s and 180 waves are included, which is almost the whole range of measured data. For vertical structures without overhang under regular waves, no impact occurs. P_i^D is regular wave pressure impulse without impact. Presence of horizontal overhang results in wave impact. P_j^D is the pressure impulse with impact. Thus (P_j^D-P_i^D) is the impact pressure impulse, which is the shaded area in Figure

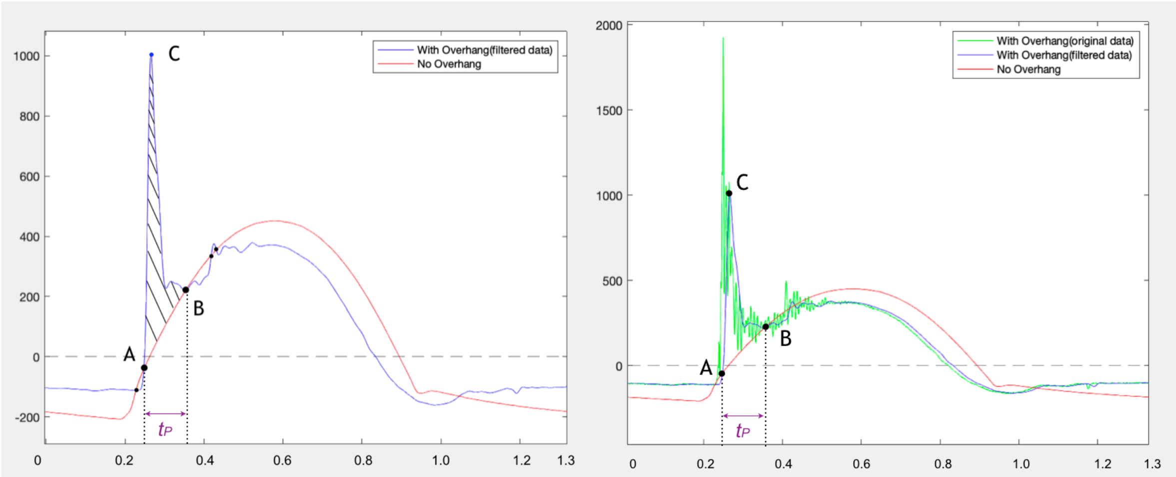

(a) (b)

Figure 5.15: Definition of impact pressure impulse $\Delta\ P^t$

5.15. It is defined to be the area of the impulsive peak ($\Delta\ P^D$). Because Pressure-Time curve vibrates violently, graphs with and without impact tends to have several intersections. For simplification, the nearest intersections on the left (point A in Figure 5.15 (a)) and right side (point B in Figure 5.15 (b)) of peak pressure point (point C in Figure 5.15 (a)) are defined to be the left and right border of the impulsive peak. Time period between point A and point B is defined to be the impulsive peak period (t_p).

Besides, to study the influence of low-pass filtering on calculation result, wave impact impulse of both filtered case and unfiltered case is calculated. Since unfiltered pressure-time curve vibrates quite violently, there are too many intersections between 2 curves (cases with and without horizontal overhang). For simplification, impulsive peak period under unfiltered situation is determined to the same as the filtered situation, as is shown in Figure 5.15 (b).

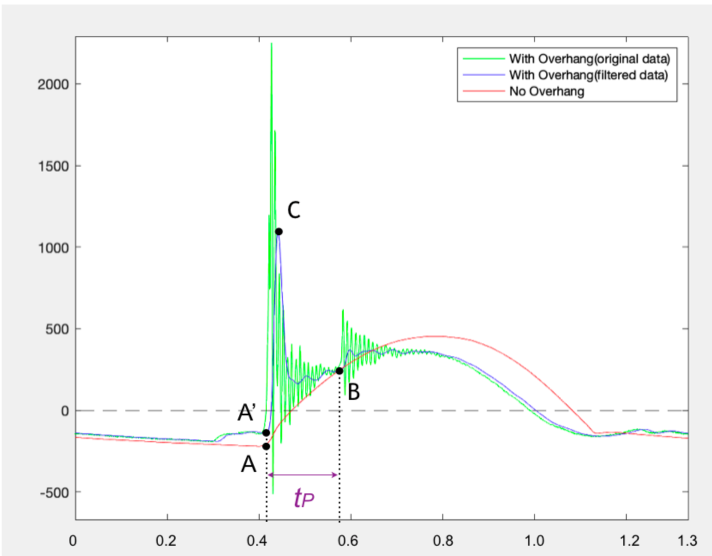

Figure 5.16: Determination of impulsive impact left boundary

Actually, in data processing, situations are more complicated since Pressure-Time curve vibrates irregularly. For some waves, there is no intersection on left side of peak pressure point. Left end of the impulsive peak period is then defined to be the point where difference between the vertical ordinates is the smallest (Figure 5.16).

5.4.2. Pressure integration — impact impulse calculation

Calculation process of data from pressure sensor 7 is described in detail.

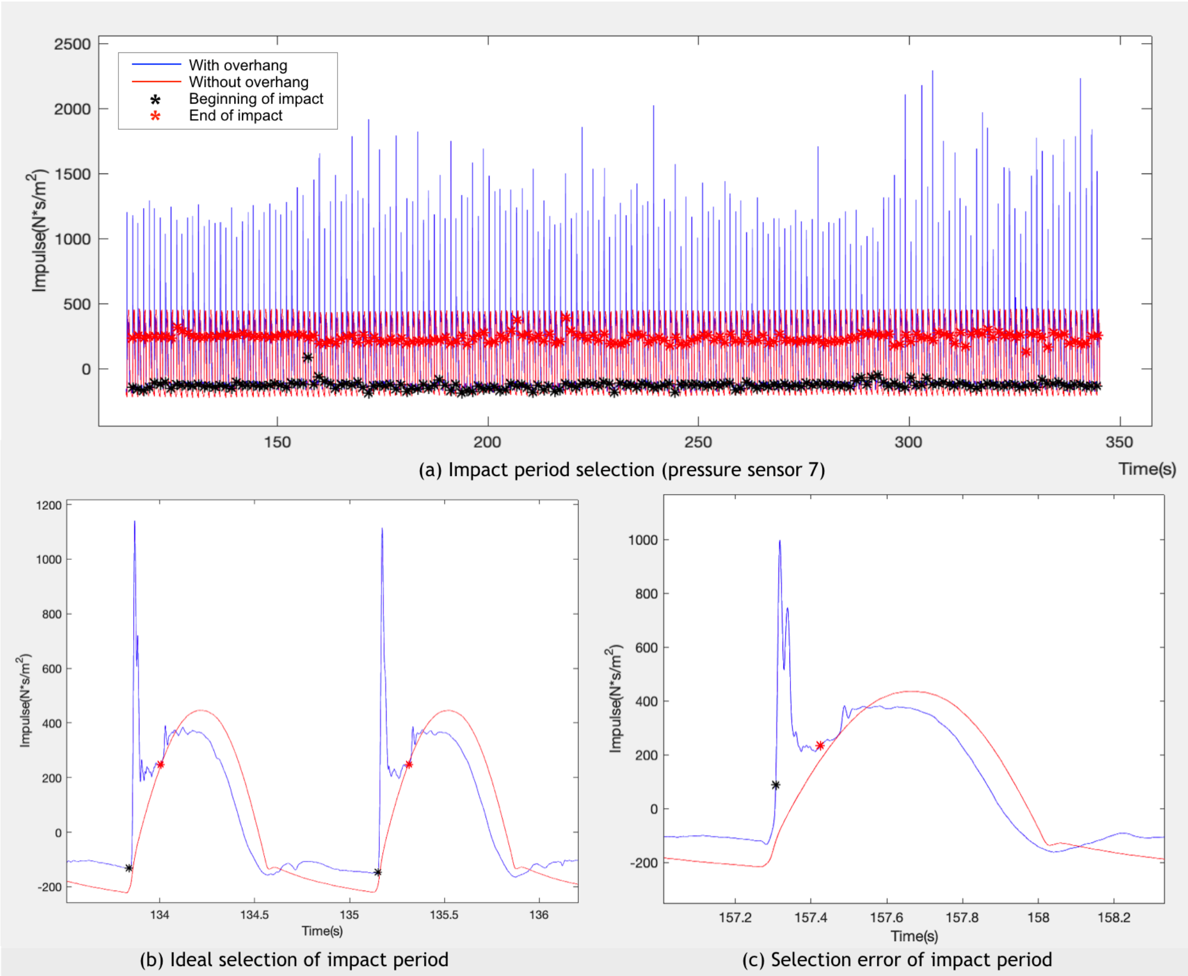

(a) Impact period selection (pressure sensor 7)

(b) Ideal selection of impact period

(c) Selection error of impact period

Figure 5.17: Impact period selection in Matlab programming

For 180 waves tested by pressure sensor 7, impulsive peak pressure period is first defined and then impact pressure impulse is calculated (Figure 5.17).

Value of impact impulse of 180 waves is shown in Figure 5.18 (a) and ratio between filtered impact impulse and unfiltered pressure impulse is shown in Figure 5.18 (b). As can seen, ratio between filtered impulse and unfiltered impulse ranges from 0.97-1.08, which means impact impulse after filtering almost equals to that before filtering. Thus it can be concluded that low-pass filtering does not influence the value of of impact impulse. Pressure impulse ranges from 22 Pa*s to 43 Pa*s. For pressure sensor 7, the average value of impulse after filtering is taken to be the measured wave impact impulse, which is 32.136 Pa*s.

Impact impulse at other pressure sensors are processed and calculated in the same way, which can be checked in **Appendix C**. Result is shown in Table 5.4 and Figure 5.19.

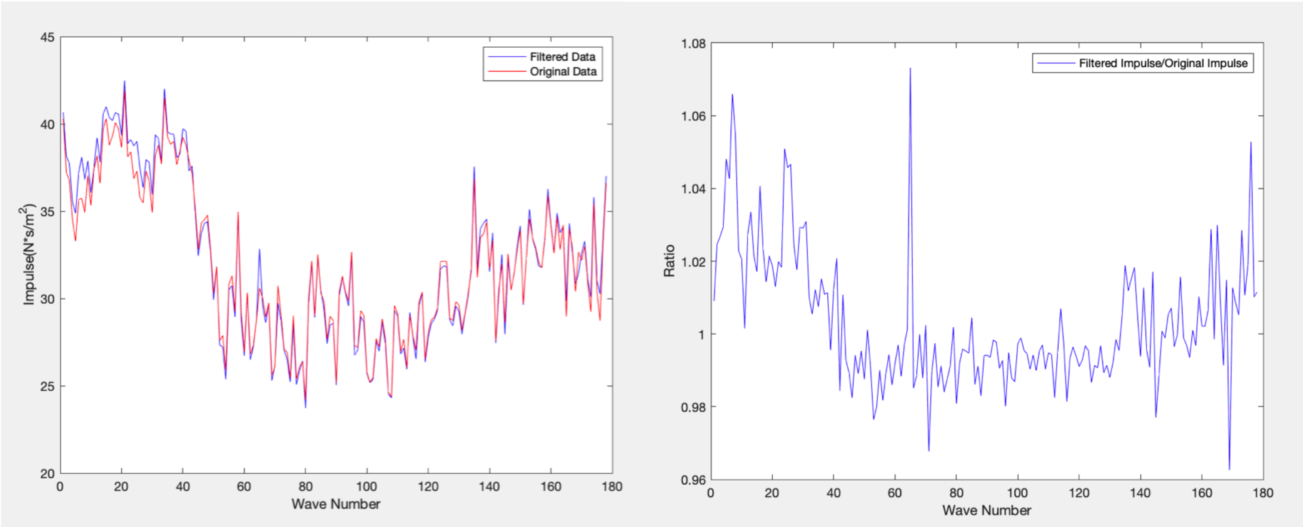

(a) Pressure impulse under filtered and unfiltered situation

(b) Ratio $\frac{P^t_{7,filtered}}{P^t_{7,unfiltered}}$

Figure 5.18: Impact impulse calculated under filtered and unfiltered situation

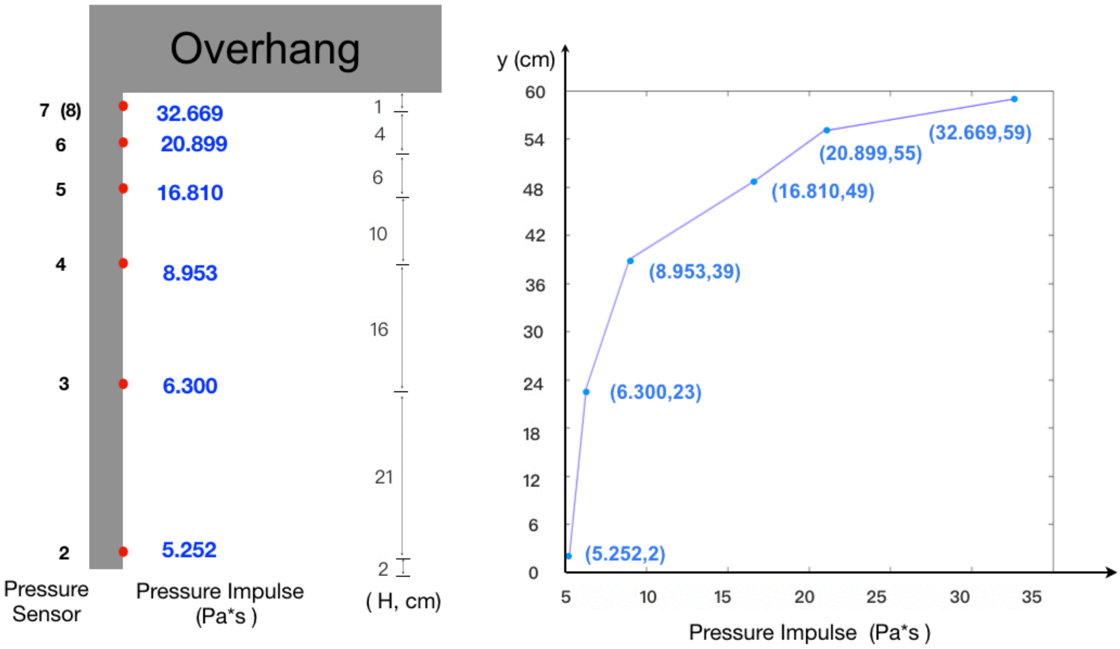

Figure 5.19: Physically measured dimensional impact impulse (filtered) distribution along the vertical structure

5.4.3. Impact impulse vibration analysis

In Figure 5.18, vibrations of impact impulse can be observed. It is found through calculation that such vibrations do not affect the average value of pressure impulse. Three main reasons can account for this phenomenon:

1) Uncertain factors during wave impact. Although regular waves are produced, air involvement and wave water turbulence may still make wave loading of each impact differ from each other;

Typical waves 1, 2, 3 and 4 are selected and shown in Figure 5.20. At moments around wave 1, waves

Table 5.4: Dimensional impact impulse measured at different pressure sensors

Pressure sensor	Height (cm)	Pressure impulse (Pa*s)
2	2	5.252
3	23	6.300
4	39	8.953
5	49	16.810
6	55	20.899
7	59	32.1363
8	59	33.2013

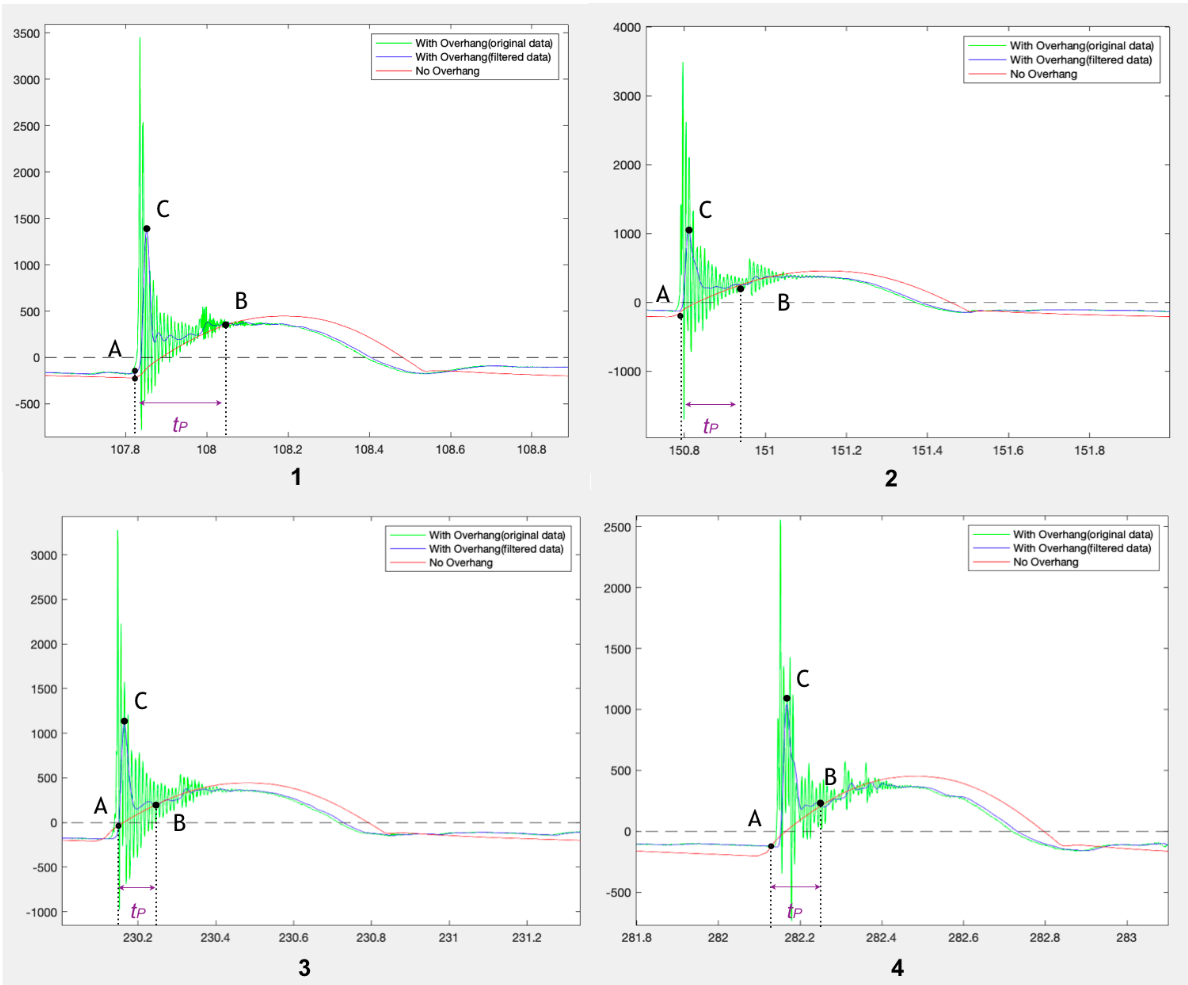

Figure 5.20: Typical moments of impact pressure

are still not fully developed and there is no intersection on left side of peak pressure point. Left end of the impulsive peak period is the point where difference between the vertical ordinates is the smallest. Impulsive impact period is longer at the beginning and decreases to a certain range as time went on. At wave 3, impulsive peak period t_p is relatively small and area of unfiltered pressure that is smaller than zero is relatively large. Wave 4 is one of the most common and ideal waves. After low-pass filtering, violent vibrations are removed and smoother curve is observed. The value of pressure impulse is not affected by low-pass filtering.

2) Low-pass filtering smooths Pressure-Time curve. Intersections of P-T curves with and without overhang are influenced directly by filtering frequency. Thus impact period and impact impulse is also changed;

3) Error of intersection selection. Circular statement is added in Matlab and batch data undergoes loop processing. Beginning point and ending point of different impacts are defined to be in an estimated range to reduce program workload. Error may occur during this process because the estimated range does not fit some certain impacts, as is shown in Figure 5.17 (c).

5.5. De-dimensionalization of pressure impulse

Calculated pressure impulse is dimensional while in theoretical model, pressure impulse is non-dimensional. In order to make dimensional pressure impulse in physical experiment and non-dimensional pressure impulse in theoretical model comparable, it is necessary to de-dimensionalize pressure impulse calculated in section 5.4.2. According to Wood & Peregrine (2000),

$$P = P^D/\rho U W \tag{5.2}$$

in which,
P: non-dimensional pressure impulse;
P^D: dimensional pressure impulse;
ρ: liquid density. Clean water is used in the experiment, ρ=1000kg^3;
U: velocity of water impact;
W: length scale.

Liquid density ρ, length of the overhang W and wave velocity U at impact should be known.

5.5.1. Wave impact velocity calculation

For vertical structure with overhang, impact occurs when the upward moving wave profile hits the bottom of the overhang. At this moment, vertical wave velocity at the overhang bottom causes wave impact and for vertical structure, horizontal wave velocity is estimated to be zero. So vertical velocity a moment before the impact is studied here. There are two methods to obtain impact wave velocity:

1) Theoretical calculation: linear wave theory;

2) Experimental measurement: Wood & Peregrine (2000) proposed several equipment to measure velocity at impact experimentally: (1) High velocity camera; (2) PIV (particle image velocimetry), which is capable of measuring an instantaneous velocity field. In our experiment, wave gauges are installed along the wave flume to measure height of wave surface. Wave velocity can be calculated according to change of water level.

Linear wave theory (Airy wave theory):

Incoming wave produced by wave generator is progressive and regular wave. Incoming wave height H_i = 0.06m, wave period T = 1.316s and water depth h = 0.60m. Wave parameters are calculated using linear wave theory and calculation process is shown in **Appendix.D**. Since impact velocity is the velocity exerted on the bottom of horizontal overhang, vertical particle velocity is applied instead of vertical wave velocity.

Vertical particle velocity:

$$w = \omega a \frac{\sinh k(h+z)}{\sinh kh} cos\theta \tag{5.3}$$

in which,
h (m): water depth;
z (m): wave surface elevation, which is y in this master thesis;
a (m): wave amplitude, a=$\frac{H}{2}$;

k : wave number, k=$\frac{2\pi}{L}$ = 2.552;
ω (rad/s): angular velocity, ω =$\frac{2\pi}{T}$ = 4.774 rad/s;
θ (degree): $\theta = \omega t - kx$;

It is known that incident wave height H_i = 0.06m, wave period T = 1.316s and water depth h = 0.60m. Waves are reflected by the vertical structure, so impact waves are standing waves, which are combination of incoming waves and reflected waves. Thus for impact waves, amplitude can be calculated:

$$a_{impact} = H_{impact}/2 = H_i * 2/2 = 0.06m \tag{5.4}$$

Impact occurs at the moment when wave surface touches the overhang bottom. Height of overhang bottom is 0.6m, which equals to water depth. Thus when wave impact occurs, (h+z) = h+0 = 0.6m and θ at impact is 0. Vertical particle velocity at impact is then:

$$w = \omega a_{impact} = 4.774 * 0.06 * 1 * 1 = 0.286m/s \tag{5.5}$$

Through linear wave theory, vertical particle velocity is determined to be velocity of wave impact U = w = 0.286 m/s.

Impact velocity calculated using linear wave theory is symbolled by **Lin.V** (in Table 5.5).
Experimental measurement:

Since wave gauge 8 measuring water surface height is installed 3.5cm away from the vertical wall, vertical velocity at wave gauge 8 can be calculated and taken as wave impact velocity. For regular waves, data is measured under two experimental conditions – (1) vertical structure with overhang (*rA60s*); (2) vertical structure without overhang (*rA60*). Linear wave theory is applied in tested situation and vertical wave velocity can be calculated as the time derivative of water level. Vertical wave velocity under these two cases are presented in Figure 5.21.

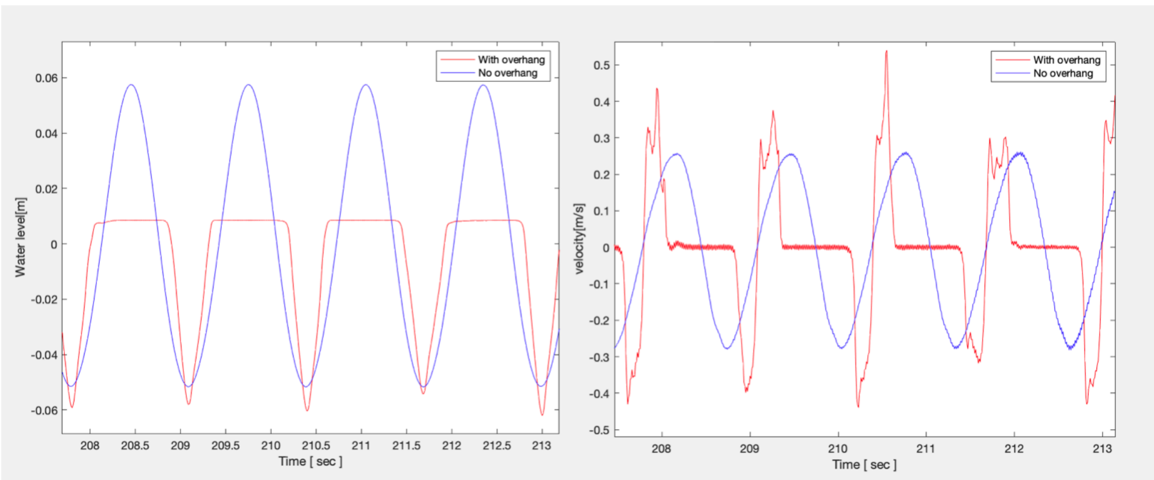

a) Wave surface height b) Vertical wave velocity

Figure 5.21: Water level and vertical wave velocity measurement from wave gauge 8 (with and without overhang)

Moment of impact occurrence (beginning moment of impulsive impact) is defined in section 5.4.1 (point A in Figure 5.15). Moments of impact occurrence are selected and shown (moment A) in Figure 5.22.

During each wave impact, velocities at four typical and representative moments are defined and selected:

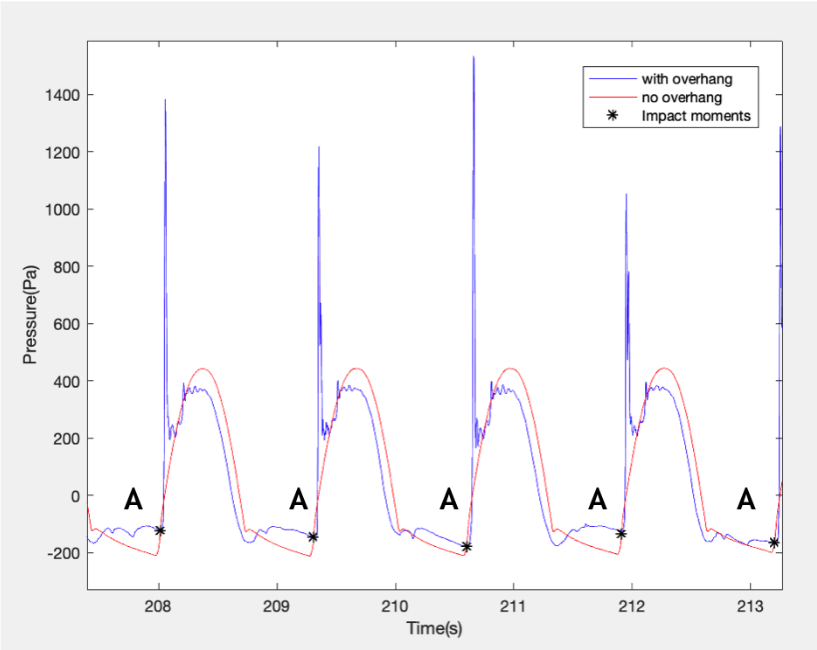

Figure 5.22: Moment (A) of impact occurrence during each wave impact

Vertical structure with overhang:
(1) **IM.S Velocity:** Velocity at the moment right before the occurrence of impact;
(2) **M.S Velocity:** Maximum velocity during each wave period;

Vertical structure with no overhang:
(3) **IM.Velocity:** Velocity at the moment right before the occurrence of impact;
(4) **M.Velocity:** Maximum velocity during each wave period.

Theoretically, since sampling frequency of wave gauge is 100Hz, vertical velocity calculated 0.01s right before the occurrence of wave impact (moment A in Figure 5.22) is determined to be the impact velocity. Typical velocities are marked in Figure 5.23.

One interesting phenomenon is that when same regular waves are produced, maximum velocity measured with overhang is larger than that measured without overhang. This is because the presence of overhang decreases the space where waves can develop. Thus when same volume of water comes, water level increases more violently and vertical wave velocity also increases. Average velocity of 180 waves are listed in Table 5.5.

Table 5.5: Typical velocities during wave impacts

Case	Overhang	Symbol	Velocity (m/s)
(1)	Yes	Lin.	0.286
(2)	Yes	IM.S	0.1692
(3)	Yes	M.S	0.3918
(4)	No	IM.	0.2118
(5)	No	M.	0.2694

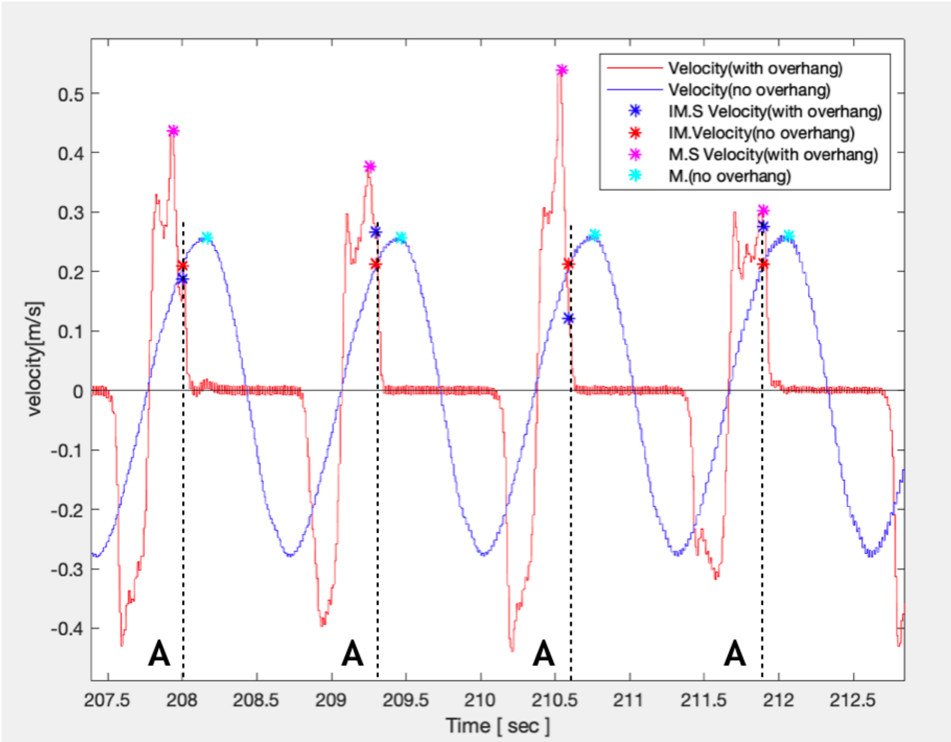

Figure 5.23: Typical velocities during wave impacts (Moment A: moment of impact occurrence during each wave impact)

5.5.2. De-dimensionalization calculation

It is already known that fresh water density is $\rho=10^3$ kg/m^3. Length scale W and impact velocity U should be determined in equation (5.2).

Length scale W

In research of Wood & Peregrine (2000), wave impact is caused by the presence of vertical structure and water depth h is taken as the length scale. It can be observed that water depth is relatively shallow, which is smaller than 0.3m in all tests. Also, impact pressure impulse still has considerable value at the flume bottom.

However, in our experiment, wave impact is caused by the presence of horizontal overhang. Water depth is 0.6m, which is relatively greater compared to wave height(H_i = 0.06m). Both physical result and model result have proven that wave impulse decreases to almost zero at the flume bottom. Thus it is unreasonable to take water depth as the length scale here and instead, length of overhang should be the length scale (W = 0.1m).

Impact velocity U

Five typical velocities are calculated as possible impact velocities in section 5.5.1 from both linear wave theory and experimental measurement, which can be substituted in Equation 5.2 for non-dimensionalization.

Non-dimensionalization result

It is already known that fresh water density is $\rho=10^3$ kg/m^3, length scale W = 0.1 m. There are five alternatives to impact velocity. Variables can be substituted in equation (5.2) and result is shown in Figure 5.24.

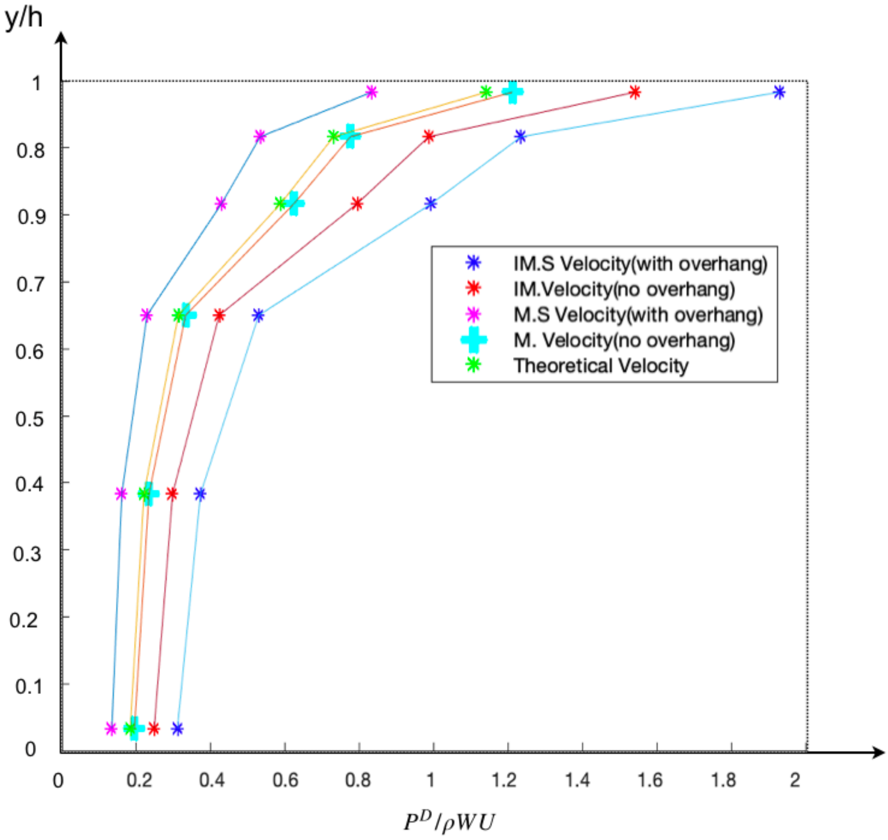

Figure 5.24: Non-dimensional pressure-impulse along the vertical structure (Calculated using different velocities)

6

Theoretical model validation and Discussion

Chapter 6 compares theoretical model result with physical model result and makes a choice of variables in these two models.

Pressure impulse distribution on wall is theoretically modelled in Chapter 3. Test data is processed and experimental pressure impulse distribution on vertical wall is calculated in Chapter 5. Results of theoretical and physical models are presented in Figure 6.1.

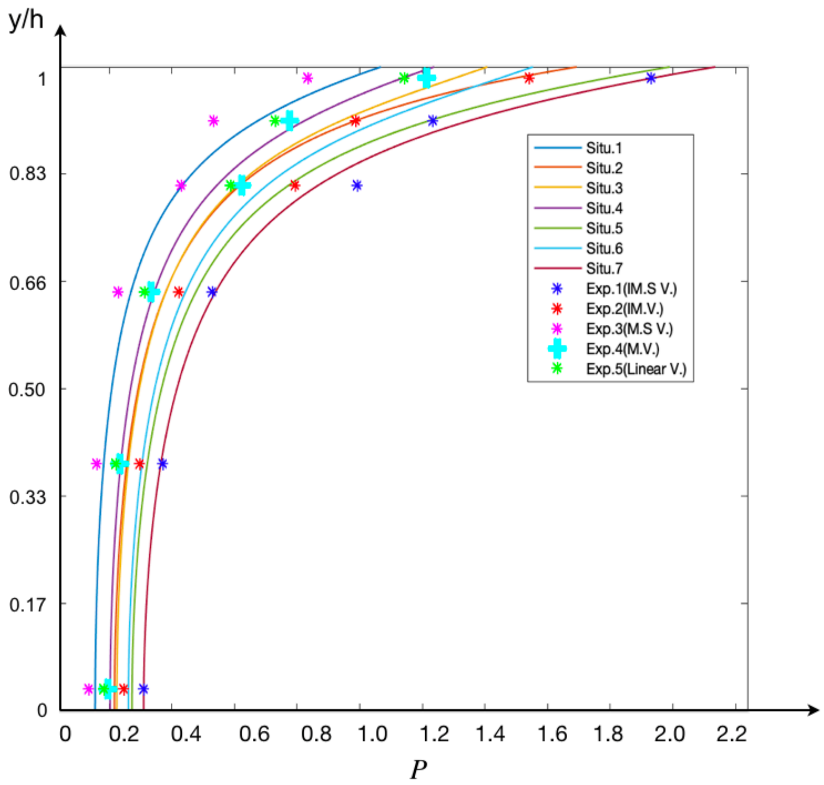

Figure 6.1: Pressure impulse (P) distribution along the vertical structure from physical model and theoretical model (lines: situation 1-7 in Table 3-1; scattered dots: experimental results calculated from different impact velocities in section 5.5.1)

6.1. Variable determination in physical model and theoretical model

In Figure 6.1, lines represent result of theoretical model and scattered dots represent results of physical model. Results of two models are in the same range of values, which indicates the theoretical model is reasonable. Theoretical model and physical model both have their variables, which will be discussed below:

(a). Physical model: impact velocity U;

(b). Theoretical model: air pocket position and air pocket size.

6.1.1. Determination of impact velocity U in physical model

As has been addressed in section 5.5.1, there are 5 possible values for impact velocity U. Actually, IM.S Velocity and IM. Velocity (cases 2 and case 4 in Table 5.5) is selected right before (0.01s) the moment of impact occurrence. However, selection of impact moment (Figure 5.22) may not be accurate considering filter delay, random error of data processing and so on. Thus it is not fully accurate to first find out the moment right before wave impact and then output vertical wave velocity accordingly.

It can be observed from Figure 5.23 that M.S. velocity (cases 3 in Table 5.5) also occurs closely before the impact moment. Vertical velocity (with overhang) first increases to maximum and then decreases sharply because the wave surface rises to touch the overhang bottom and the up-rising trend is stopped. Besides, maximum velocity measured with overhang is larger than that measured without overhang. This is because the presence of overhang decreases the space where waves can develop. Thus when same volume of water comes, water level increases faster and accordingly, vertical wave velocity also increases sharply. Thus, it can be inferred that the collision between horizontal overhang and uprising wave is a violent and dynamic process, during which linear wave theory is no longer applicable. Since M.S. velocity is calculated as the time derivative of water level (linear wave theory), it is not reasonable to take M.S. velocity as impact velocity U.

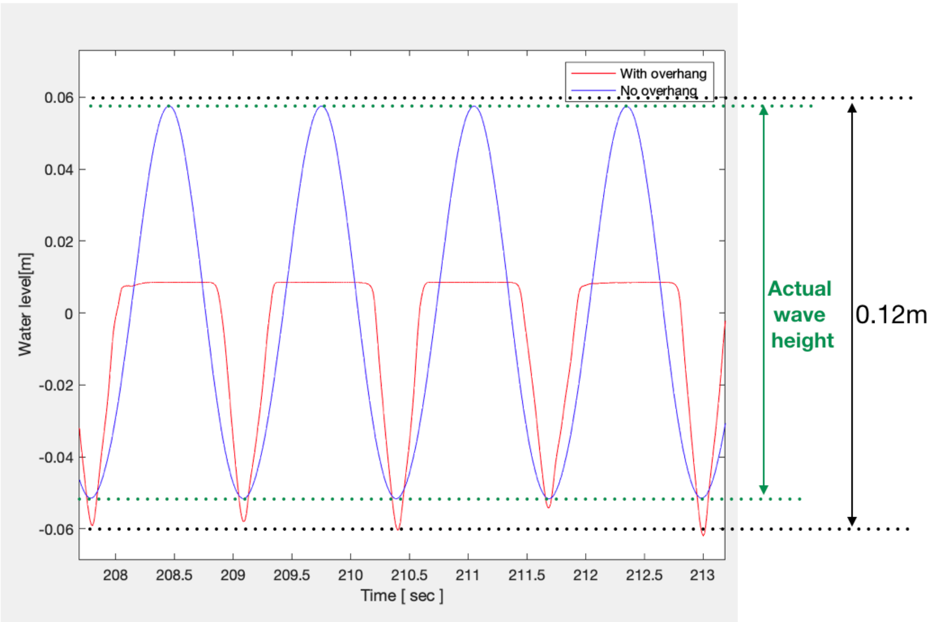

Figure 6.2: Water wave height measured by Wave Gauge 8

Thus Lin. velocity and M. velocity (case 1 and case 5 in Table 5.5) are both reasonable to be take as the impact velocity. It can also be found that the value of Lin. velocity(0.286m/s) and M. velocity(0.2694m/s) is close to each other.

In addition, M. velocity is more recommended because is it closer to reality. Theoretically, since impact waves compose of incoming waves and reflected waves, amplitude of impact waves is taken to be 0.12m (Equation 5.4). However, water level measurement from wave gauge 8 shows the actual impact wave height is smaller than 0.12m (Figure 6.2). This is the reason why Lin. velocity is larger than M. velocity.

Therefore, maximum velocity measured with vertical structure (M. velocity, case 5 in Table 5.5) is taken to be impact velocity: U = 0.2694m/s. If measurement of water surface elevation is not available, impact velocity can also be calculated as vertical particle velocity using linear wave theory although certain errors may be introduced.

Pressure impulse (P) distribution along the vertical structure from physical model is calculated and result is shown in Figure 6.3 and Table 6.1.

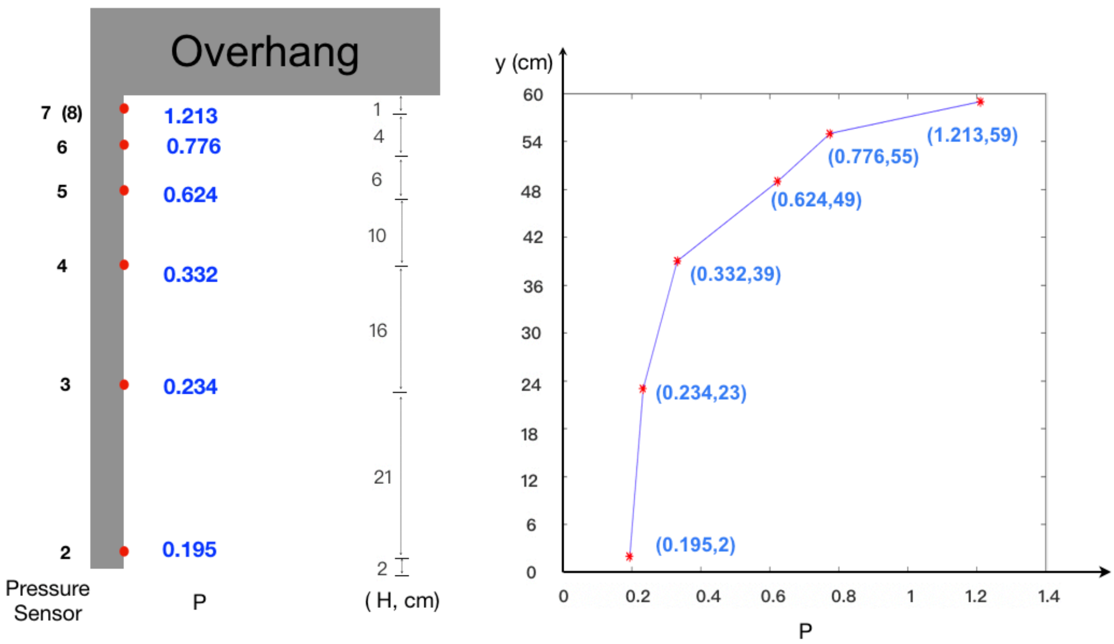

Figure 6.3: Non-dimensional impact impulse (filtered) distribution along the vertical structure measured in physical experiment (W=0.1m, U=0.2694m/s)

Table 6.1: Non-dimensional impact impulse at different pressure sensors (W=0.1m, U=0.2694m/s)

Pressure sensor	Height (cm)	Impact impulse
2	2	0.1949
3	23	0.2337
4	39	0.3323
5	49	0.6240
6	55	0.7757
7	59	1.1957
8	59	1.2297

6.1.2. Discussion of air position and air size in theoretical model

In theoretical model, there are two variables – air pocket position and air pocket size. 7 situations of air presence are modelled in section 3.3 (Table 3.1). In physical experiment, it is observed that when wave impact occurs (Figure 5.8), a certain volume of air is present below the bottom of horizontal overhang. Situations (1), (5), (6) and (7) in Table 3.1 differ a lot from actual situation because in situation (1), no air is considered and in situation (5), (6) and (7), size of air is relatively large. Thus these four situations are not discussed. Results of situation (2)–(4) and physical experiment are present in Figure 6.4. Experiment result matches well with theoretical model results and fits the best with situation 4 – air pocket size is $\frac{1}{3}$ of the overhang length and lies at the free end of the horizontal overhang. Thus it can be concluded that theoretical model simulates the mechanism of air effect on wave impacts under rA60s properly. Also, the rationality of the theoretical model has been verified.
(**Note:** For situations mentioned, check Table 3.1 and Table 5.5.)

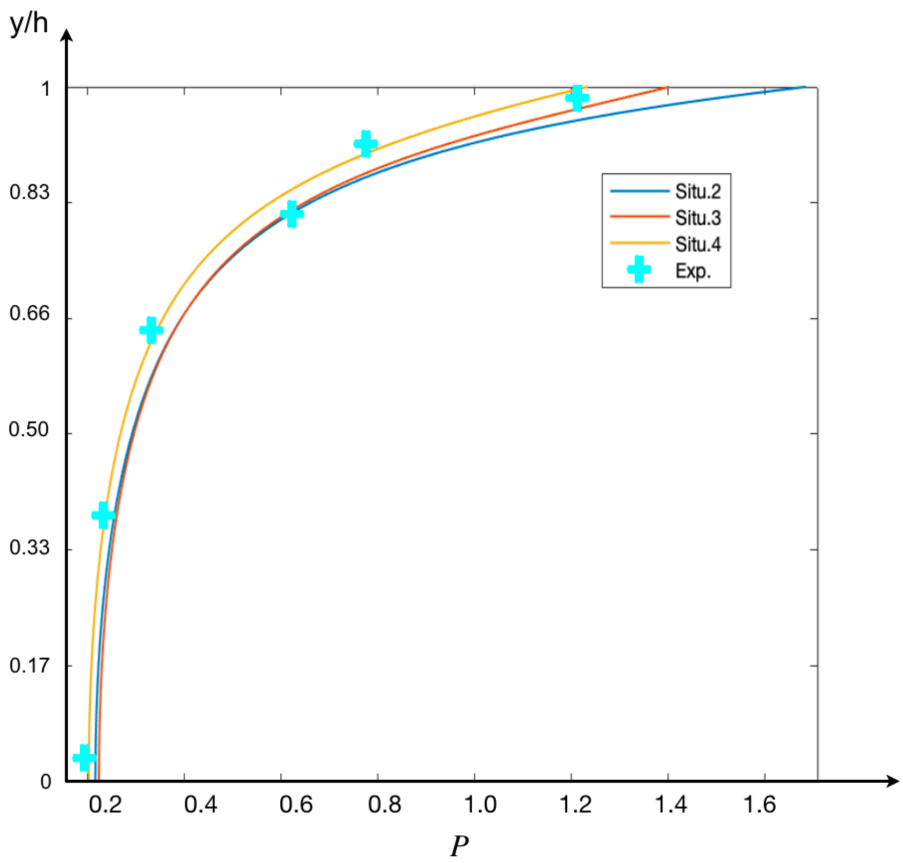

Figure 6.4: Non-dimensional impact impulse distribution along the vertical structure

Besides, air pocket size in situation (2)-(4) is $\frac{1}{3}$ of overhang length and the only difference between situation (2)-(4) is air position. Since results of situation (2)-(4) all show a great consistency with experiment result, it is reasonable to assume that air pocket size is $\frac{1}{3}$ of overhang length in further model study and check or improve it with more experiment data. There are two variables (air pocket size and air pocket position) but only on set of control experiment. Thus for representative nor persuasive conclusions, more experimental data is required. Also, it is better to determine air pocket position and air pocket size through observing experimental phenomena.

7
Conclusions and recommendations

This chapter concludes the work developed throughout this thesis, providing answers to the main research question and three research sub-questions. In addition, recommendations for future studies are briefly presented.

7.1. Conclusions of research questions

Regular waves are study focus in this master thesis. The main research question is addressed answering first 3 sub-questions:

Sub-question 1: How does the entrapped air change during the process of wave impacts?

Sub-question 1 is addressed in Chapter 4 and Chapter 5. Chapter 4 (section 4.2.1) briefly describes air development under regular waves and irregular waves with images. Chapter 5 (section 5.2) directly displays air content under different wave pressures and analyses air development during one wave impact in detail. Air pocket is first entrapped by wave water and splits into several parts with water wave movement. Small air pockets breaks into air bubbles under wave impacts and get mixed with water. Most air bubbles are washed away from the vertical structure by reflected waves, finally float up and escape into the atmosphere. Very few air bubbles may also hide under the overhang bottom.

Sub-question 2: How is the wave loading influenced by the presence of horizontal overhang?

An experiment is analysed with 2 cases – with and without horizontal overhang. Measurement data is processed and compared in Chapter 5. For vertical structures without overhang, regular waves do not induce wave impacts. For structures loaded under non-breaking regular waves(regular waves rA60s), when the wave touches the bottom of the overhang, wave impulse occurs and peak impulse on the vertical structure is observed, with a bending moment occurs on the vertical structure. Regular trigonometric function distribution of pressure changes to irregular distribution with two peak pressures during each wave impact.

Sub-question 3: How is the wave loading influenced by the presence of air pocket?

Theoretical model is set up accounting for air influence and is validated by physical experiment result in chapter 3. Air participating in the impact is simplified to be a whole air pocket. Air influence is simulated as bounce back effect and is mainly affected by two variables: (1) air pocket size, (2) air pocket position. It can be concluded that with the increase of air pocket size and decrease of distance between air pocket and the structure, impact pressure-impulse loaded on hydraulic structure is increased.

In chapter 4 and chapter 5, air influence is described according to the recorded video and test data in experiment. During each wave impact, peak pressure occurs when least air is entrapped, which is consistent with Bagnold (1939). For different wave impacts, the less the air is entrapped under the horizontal overhang, the larger the impulsive peak pressure would be.

In chapter 5, test data is processed. Pressure and pressure impulse distribution along the vertical structure is calculated. The maximum impulsive pressure, as well as the maximum pressure impulse, occurs at the highest point of the vertical structure and impact pressure decreases with the increase of water depth, which means influence of wave impact and air entrapment decreases away from the water surface. It is found that wave impact impulse (P^D) is rather constant in different wave impacts. Value of impact impulse is almost unchanged after low-filtering. Thus it can be concluded that low-pass filtering does not influence the value of of impact impulse.

Theoretical model and test model are correlated by comparing non-dimensional pressure impulse distribution along the vertical wall. For de-dimensionalization of tested pressure impulse, the overhang length is taken to be length scale and the peak velocity measured under rA60 is selected to be impact velocity. Result of theoretical model in chapter 3 fits well with physical experiment, which validates theoretical model under case rA60s. It is reasonable to assume that air size is $\frac{1}{3}$ of overhang length in further model study while air pocket position is undetermined.

After all the three sub-questions are considered, the main research question can be answered:

> *Research question: How are the impulsive wave loads on vertical structures with overhangs influenced by air?*

Air leakages along with pressure increase and maximum pressure is reached when least air is entrapped. Thus pressure impulse is also increased. For quantitative description, theoretical model is set up accounting for air influence and is validated by physical experiment result under rA60s.

7.2. Recommendations for further study

(1) Poor quality of wave images:

Importance of air size and air position is highlighted. However, since the reflection of the glass sink and poor light beneath the horizontal overhang, quality of wave videos are of poor quality and air is hard to identify. More light should be given to the bottom of the horizontal overhang so that movement of air could be observed more clearly. Coordinate grids is suggested to be drawn on the overhang bottom so that air position and air size can be determined more precisely. Also, transparent and solid overhang can be applied in next experiments and videos can be recorded above the overhang. Besides, structure frames obstructing sight should be removed. In this way, air involvement and wave profile can be directly observed and described.

(2) Determination of air presence in theoretical model:

Estimation of air size and position at the moment of wave impact is needed to be more accurate in theoretical model. It is recommended to record high-quality videos above the transparent overhang and select images at impact moments. Thus air size and position can be described from pictures directly. Also, air is assumed to be one air pocket while it may actually be several separate air pockets or air bubbles. Assumptions about air presence can be more varied in future study.

(3) Different assumption of air influence :

In this master thesis, air influence is considered as bounce back effect. Bounce back coefficient β (section 3.3) is introduced. β=1 represents wave impacts with no bounce back effect and β=2 represents wave impacts with bounce back effect. Peregrine & Thais (1996) found that under some conditions, air entrainment increases water compressibility and air cushions the wave impact since the pressure is spread in both space and time. Under different conditions, air influence may be different. Thus, it is also possible the coefficient β is not 1 or 2 but other values, which is worth further study.

(4) Model applicability improvement:

Theoretical model is only validated with one experiment rA60s. It should be compared with more physical experiment with different parameters (wave height, wave velocity, water depth, structure dimension, regular and irregular waves) to validate the theoretical model and improve its applicability.

Bibliography

Allsop, N.W.H. Vicinanza, D. (1996), 'Wave impact loadings on vertical breakwaters: development of new prediction formula', *Proc. 11th Int. Harbour Congress, Anterwerp, Belgium* .

Anand, K. & Sundar, V. (2010), 'Dynamic pressures on curved front seawall models under random waves', *Hydrodynamics, Ser. B* **22**, 538 – 544.

Bagnold, M. R. A. (1939), 'Interim report on wave-pressure research', *Institution of Civil Engineers* **12**, 201–226.

Blackmore, P. & Hewson, P. (1984), 'Experiments on full-scale wave impact pressures', *Coastal Engineering* **8**, 331 – 346.

Bredmose, H. & Peregrine, D. (2009), 'Violent breaking wave impacts. part 2: modelling the effect of air', *J.Fluid Mechanics* **641**, 389–430.

Bullock, G. & Crawford, A. (2001), 'The influence of air and scale on wave impact pressures', *Coastal Engineering* **42**, 291–312.

Bullock, G. & Obhrai, C. (2007), 'Violent breaking wave impacts. part 1: Results from large-scale regular wave tests on vertical and sloping walls', *Coastal Engineering* **54**, 602–617.

Chowdhury, S. & Anand, K. (2017), 'Nonlinear wave interaction with curved front seawalls', *Ocean Engineering* **140**, 84 – 96.

Cooker, M. J. & Peregrine, D. H. (1995), 'Pressure-impulse theory for liquid impact problems', *J. Fluid Mech.* **297**, 193–214.

Cuomo, G. (2007), 'Wave impact on vertical seawalls and caisson breakwaters'.

Cuomo, G. & Allsop, W. (2010), 'Breaking wave loads at vertical seawalls and breakwaters', *Coastal Engineering* **57**, 424 – 439.

Denny, D. & Hewson, P. (1951), 'Further experiments on wave pressures', *J. Inst. Civil Engrs* **35**, 300–345.

Dogan Kisacik, Peter Troch, P. V. B. R. C. (2014), 'Investigation of uplift impact forces on a vertical wall with an overhanging horizontal cantilever slab', *Coastal Engineering* **90**, 12–22.

Goda, Y. (1974), 'New wave pressure formulae for composite breakwater', *Int. Conf. on Coastal Engineering Proceedings* (14), 1702–1720.

Goda, Y. (2000), *Random seas and design of maritime structures*, Advanced Series on Ocean Engineering, Yokohama National University, Japan.

Holthuijsen, L. (2007), *Waves in Oceanic and Coastal Waters*, Cambridge.

Hu, Z. Z. & Mai, T. (2017), 'Investigations of offshore breaking wave impacts on a large offshore structure', *Journal of Fluids and Structures* **75**, 99 – 116.

Kirkgoz, M. (1982), 'Shock pressure of breaking waves on vertical walls', *Journal of the Waterway, Port, Coastal and Ocean Division* **108**, 81–95.

Kirkgoz, M. (1991), 'Impact pressure of breaking waves on vertical and sloping walls', *Ocean Engineering* **18**(1/2), 45–59.

Kisacik, D. & Ozyurt, G. (2017), 'Hydrodynamic conditions in front of a vertical wall with an overhanging horizontal cantilever slab', *Oceanic and Coastal Sea Research* **16**, 978–990.

Kisacik, D. & Troch, P. (2012), 'Experimental study of violent wave impact on a vertical structure with an overhanging horizontal cantilever slab', *Ocean Engineering* **49**, 1–15.

Kortenhaus, A. & Oumeraci, H. (1998), 'Classification of wave loading on monolithic coastal structures', *Coastal Engineering* pp. 867–880.

Moutzouris, C. (1979), *Influence of ambient air pressure on impact pressure caused by breaking waves*, Vol. Internal report no. 10-79, Delft University of Technology, Department of Civil Engineering, Fluid Mechanics Group.

Partenscky, H. & Tounsi, K. (1989), 'Theoretical analysis of shock pressures caused by waves breaking at vertical structures', *Journal of the Waterway, Port, Coastal and Ocean Division* p. 6.

Peregrine, D. (2003), 'Water-wave impact on walls', *Annu. Rev. Fluid Mech.* **35**, 23–43.

Peregrine, D. & Thais, L. (1996), 'The effect of entrained air in violent water wave impacts', *J. Fluid Mech.* **325**, 377–397.

Ramkema, C. (1978), 'A model law for wave impacts on coastal structures', *August, 27-31, September 1-3, 16 th Conf. Coastal Engng, ASCE* .

Rattana Pitikon, W. & Shibayama, T. (2000), 'Verfication and modification of breaker height formulas', *Coastal Engineering* **42**(4), 389–406.

Richert, G. (1968), 'Experimental investigation of shock pressures against breakwaters', *Conf. Coastal Engng, ASCE* **11th**, 954–973.

Rouville, M.A., B. P. & Petry, R. (1938), 'Current state of international studies on the forces due to the blades', *Ann. Ponts Chauss es* **108**(2), 5–113.

Song, B. & Zhang, C. (2018), 'Boundary element study of wave impact on a vertical wall with air entrapment', *Engineering Analysis with Boundary Elements* **90**, 26 – 38.

Turek, D. B. (2004), 'Design of efficient digital interpolation filters for integer upsampling', **Master thesis**.

Weggel, J. & Maxwell, W. (1970), 'Numerical model for wave pressure distributions', *Waterways, Harbour and Coastal Eng. Division* **ASCE August**(WW3).

Wikipedia (2018*a*), 'Wikipedia', https://en.wikipedia.org/wiki/Chebyshev_filter.

Wikipedia (2018*b*), 'Wikipedia', https://en.wikipedia.org/wiki/Butterworth_filter.

Wood, D. & Peregrine, D. (1996), 'Wave impact beneath a horizontal surface', *Coastal Engineering* pp. 2573 – 2583.

Wood, D. & Peregrine, D. (2000), 'Wave impact on a wall using pressure-impulse theory i: Trapped air', *Coastal Engineering* **126**(4), 182–190.

List of Figures

List of Tables

A

Low Pass Filtering Scheme

A.1. Frequency spectrum

Two methods are applied to draw signal frequency spectrum:
1) Pwelch function;
2) Detrend+FFT (Fast Fourier Transform).

Method 1: Pwelch function

Welch PSD estimate of signal with frequency in Hertz (Welch's power spectral density estimate) is applied in Matlab to study frequency spectrum of signals.

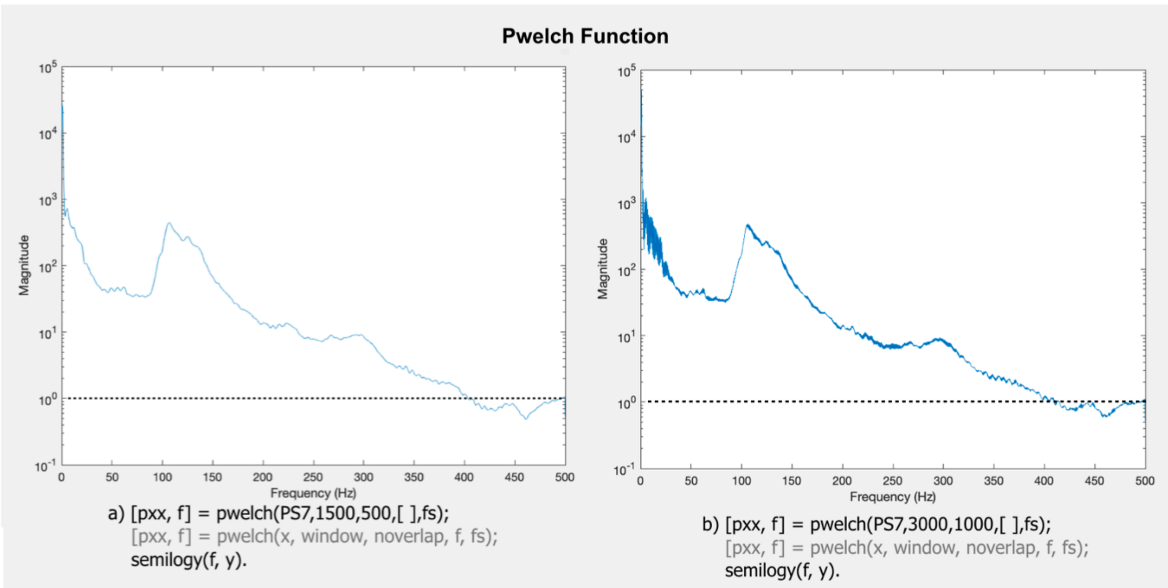

Figure A.1: Frequency spectrum (Pwelch Function)

Parameters in Pwelch function *[pxx, f]=pwelch(x, window, noverlap, f,* f_s*)* are explained:

x: Input signal;

Window: Window, specified as a row or column vector or an integer. The length N of the window indicates the length of the segment data for each process. The larger the length, the higher the power spectral resolution (more accurate), but the variance is larger (large noise and curve vibrates violently);

the smaller the length, the smaller the result variance (smooth curve). But the power spectral resolution is lower and the result is not very accurate. Since the sampling frequency is 1000Hz and the wave period is 1.3s, window length is determined to be 1500, which is long enough to include a whole wave period and not too long to induce smooth curve;

Noverlap: Noverlap refers to the length of the overlap between the adjacent two segments of data. For a signal, frequency domain resolution is much higher when there is overlap than there is no overlap. Typical overlap values vary between 33% to 50%. 33% is chosen here;

f: Frequencies, specified as a row or column vector with at least two elements. The frequencies are in cycles per unit time;

f_s: Sampling rate, 1000Hz.

As can be seen in Figure B.1, when the window length is increased from 1500 (case a) to 3000 (case b), general distribution trend of power-frequency graph stays unchanged while variance of the graph is increased. Two ranges of frequency possess relatively large magnitude – (1) 0Hz – 40 Hz and (2) 100Hz – 150 HZ. As a result, we can propose **2 assumptions about filter frequency**:

1) Frequencies range from 0Hz to 40Hz are mainly wave pressure frequencies that we should keep. Remaining frequencies should be filtered, especially main noise frequencies from 100Hz–150Hz;

2) Frequencies range from 100Hz to 150Hz are important frequencies that we should keep. Remaining frequencies should be filtered.

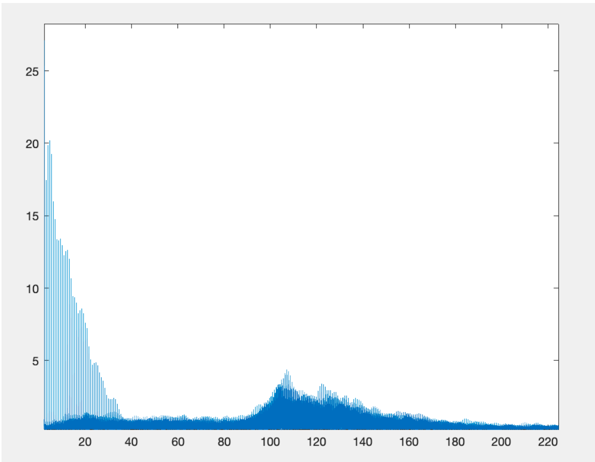

Figure A.2: Frequency spectrum (detrend + FFT function)

Method 2: Detrend + FFT transform

Fast Fourier transform *fft(X)* computes the discrete Fourier transform (DFT) of X using a fast Fourier transform (FFT) algorithm. First, *detrend* function is applied to remove the mean value or linear trend from measured pressure. Next, FFT is applied and Power-Frequency graph of tested data is drawn. Result is shown in Figure B.2.

As can be seen, frequencies distributing in 2 main ranges have relatively larger magnitude. Result of FFT transform is consistent with that from Pwelch function and rationalizes the 2 assumptions made above.

A.2. Filter type selection

Since lower frequencies should be kept, low pass filter is applied. Three low pass filters (Chebyshev filter Butterworth filter and low-pass filter) are applied and compared. Chebyshev filter and Butterworth filter are the most commonly used low pass filters (IIR filters) nowadays. Low-pass filter is also applied. Results will be compared and filter producing better results will be selected.

1) Chebyshev filter

According to Wikipedia (2018*a*) and Turek (2004), Chebyshev filters minimize the error between idealized and actual filter within filtering range. Also, Chebyshev filters have shorter response time. There are 2 types:

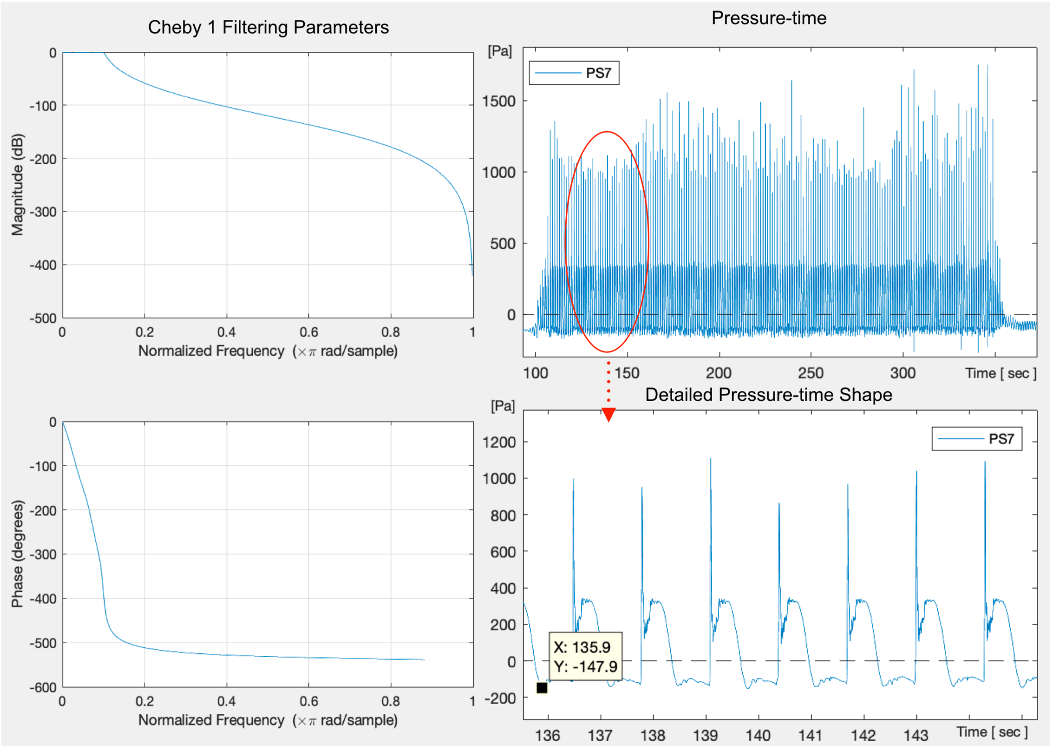

Figure A.3: Fltered result of Cheby I (bandpass = 0Hz – 40Hz)

a) Chebyshev Type-I filter: more passband ripple and faster frequency cut-off speed, suitable for situation requiring a fast attenuation and allowing for ripples in the passband;

Results of Chebyshev I filter is shown in Figure A.3 and Figure A.4. Results of Chebyshev. Bandpass is defined to be 0Hz – 40Hz. After being filtered, pressure–time curve becomes smoother while maximum peak pressures drop sharply from over 7000Pa to less than 2000Pa. One thing to notice is that before filtering, irregularly large peak pressures appear during the period of 277.8s to 350s. After filtering, the whole Pressure–time graph becomes regular along the whole testing period. So it is reasonable to deduce that the irregular large peak pressures are caused by vibration accumulation of pressure sensors and the structure.

In Figure A.4, bandpass is determined to be 100Hz–150Hz. Pressure–time curve within this frequency range becomes different from typical impulsive wave impact graph but more like free damping of structural vibration. So we can conclude that frequencies range from 100Hz–150Hz is vibration frequencies of the structure and experimental equipment that should be filtered.

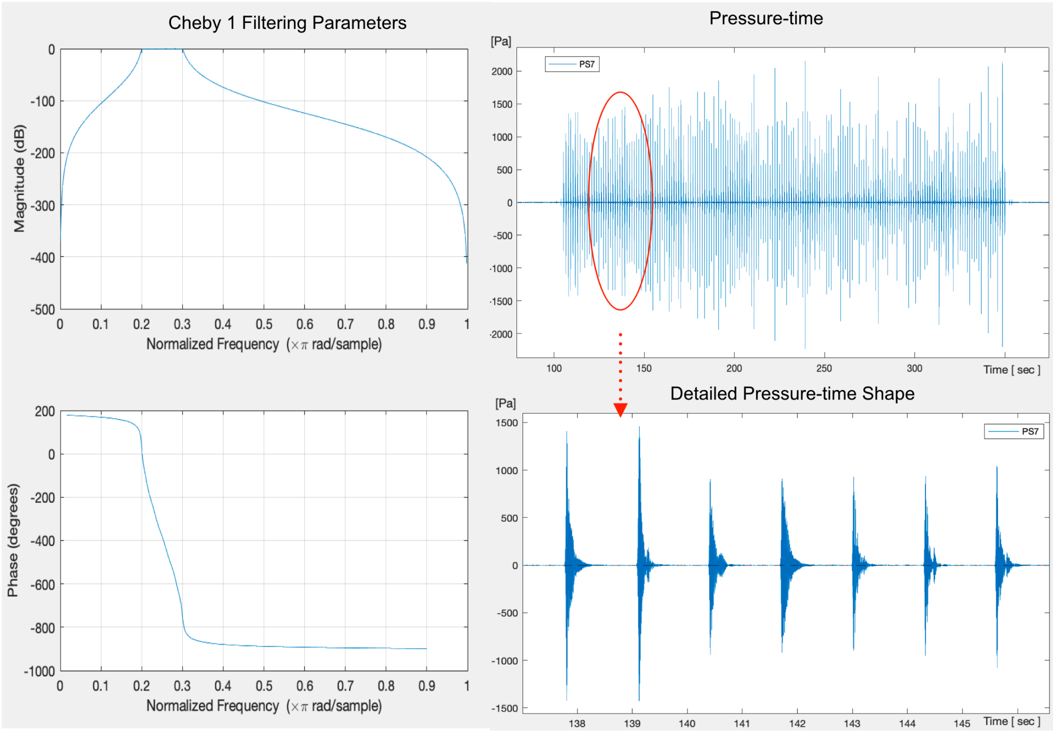

Figure A.4: Filtered result of Cheby I (bandpass = 100Hz – 150Hz)

b) Chebyshev Type-II filter: more stopband ripple, suitable for requirement of fast attenuation without allowing amplitude fluctuations in the passband.

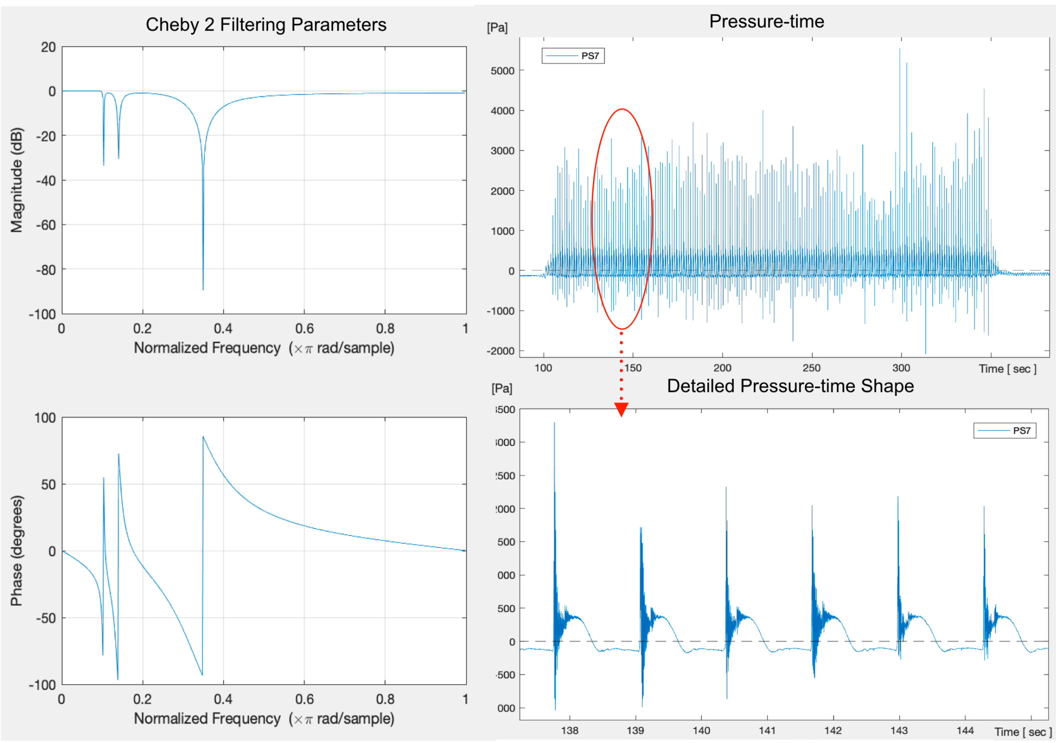

Figure A.5: Filtered result of Cheby II (bandpass = 0Hz – 40Hz)

Chebyshev Type-II filter is applied and bandpass is determined to be 0Hz–40Hz. Result is shown in Figure A.5. Compared to Chebyshev Type-I filter, result of Chebyshev Type-II filter loses large part of peak pressure and the curve still retains much vibrations. Thus Chebyshev Type-I filter is superior.

2) Butterworth filter

According to Wikipedia (2018*b*), Butterworth filter has a flat frequency response in passband, thus Butterworth filter is referred to as a maximally flat magnitude filter. The Butterworth and Chebyshev Type II filters have flat passbands and wide transition bands. The Chebyshev Type I and elliptic filters roll off faster but have passband ripple. The frequency input to the Chebyshev Type II design function sets the beginning of the stopband rather than the end of the passband.

Image processing result of Butterworth filter is relatively ideal compared to that of Chebyshev Type II filter.

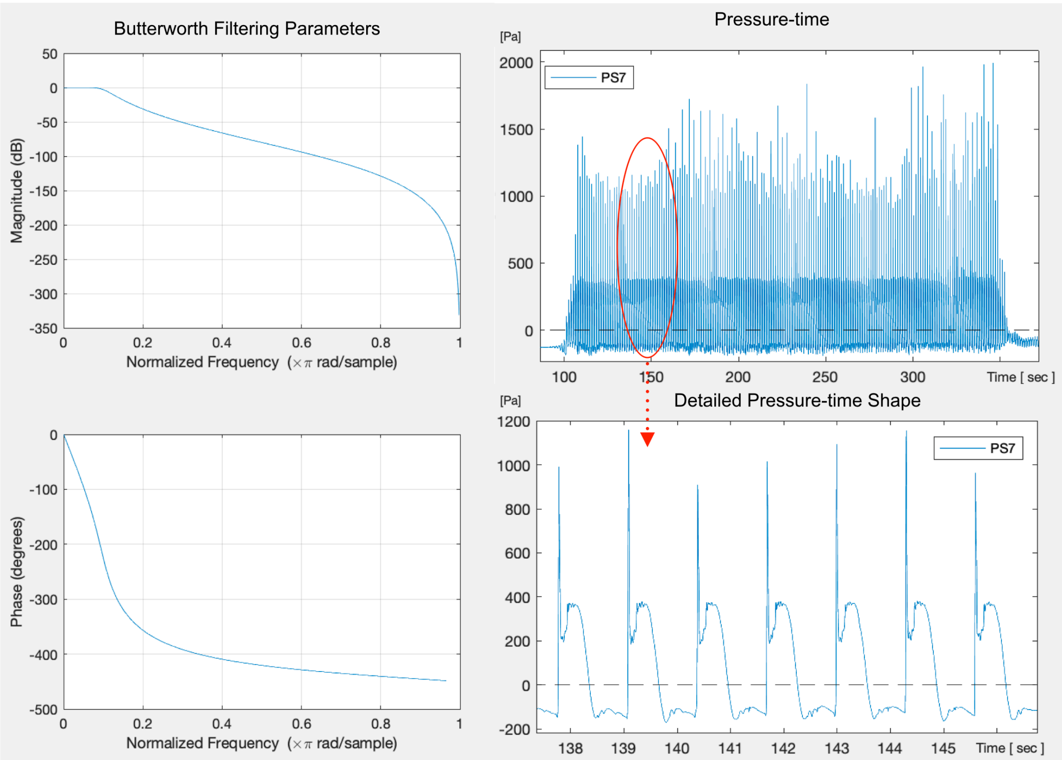

Figure A.6: Flitered result of Butterworth (bandpass = 0Hz – 40Hz)

3) Low pass function in Matlab

Low pass function in Matlab *y = lowpass(x,fpass,fs)* specifies that x is sampled at a rate of fs hertz. fpass is the passband frequency of the filter in hertz.

Result of low-pass filter is not ideal since there are many pressure values smaller than hydrostatic pressure in pressure sensor 7, as is shown in Figure A.7.

In conclusion, Butterworth filter is determined for data processing. Smoother curve could be achieved using Butterworth filter under the same filtering range.

A.3. Filtering frequency range determination

As is analyzed above, 2 ranges of frequencies are significant with relatively large magnitude:
1) 0Hz-40Hz: frequency of wave impact pressure, which should be kept;

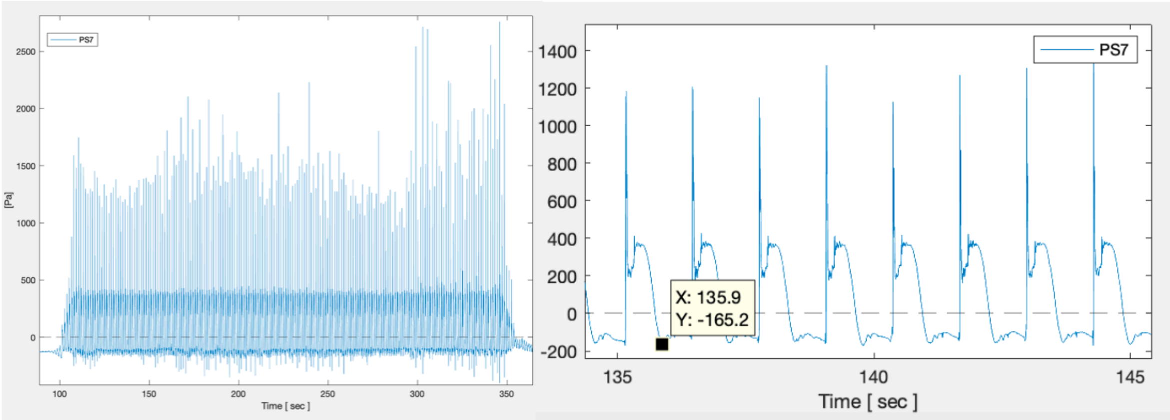

Figure A.7: Filtered result of low-pass function (bandpass = 0Hz – 40Hz)

2) 100Hz-150Hz: frequency of noise, like structural vibration, which should be filtered.

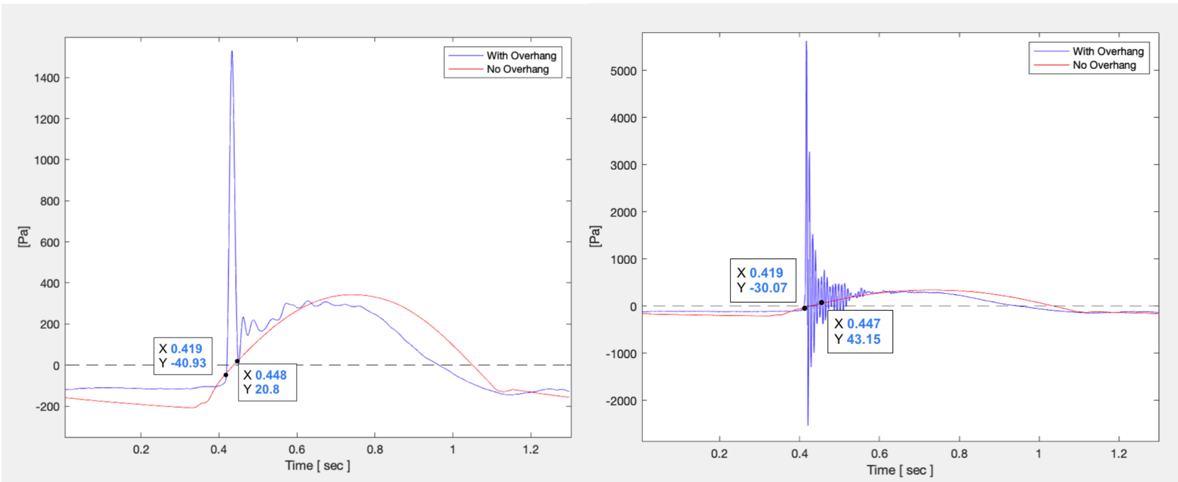

Filtering frequency range: bandpass [0,40] Hz
Average Impulse: 22.779 Pa*s

Filtering frequency range: bandstop [50,100] Hz
Average Impulse: 11.6383 Pa*s

Figure A.8: Filtered result of Butterworth (bandpass = 0Hz – 40Hz)

When bandpass is set to be 0Hz–40Hz, smooth curve is achieved while peak pressures undergo serious loss, which may cause loss of wave pressures. When filtering frequencies range from 100Hz to 150Hz (bandstop), relatively large peak pressures are maintained while pressure-time curve vibrates violently. We should strike a balance in filtering frequency determination.

Three definitions are made here:
Strict filtering (SF): When only wave pressure frequencies (about 0Hz–40Hz) are reserved;
Rough filtering (RF): When only noise frequencies (about 100Hz–150Hz) are filtered;
No filtering (NF): Original data is reserved and no filtering is applied.

The most significant research variable is pressure impulse P. Method to calculate wave impact impulse can be checked in Chapter 5. Since graphs not filtered vibrate violently, wave impact period under RF and NF situation are consistent with SF situation. To simplify the analyzing process, average Pressure-Time curve is drawn and studied.

When signals with frequencies of 0Hz–40Hz are passed (strict filtering), the average wave impact impulse is 22.779 Pa*s. When signals with frequencies of 100Hz–150Hz are filtered (rough filtering), the average wave impact impulse is 18.96 Pa*s, which is a bit smaller than 22.779 Pa*s. When signals are not filtered, the average wave impact impulse is 11.638 Pa*s, which is only about one half of 22.779 Pa*s. Much noise maintains and vibrations influence the result. As can be seen in Table A.1, filtering frequency range influences wave pressure impulse largely and directly. When strict filtering is applied, smoother curve will be achieved and pressure impulse calculated can even be twice as large as that of no filtering.

Table A.1: Filtering frequency influence on impact period and impact impulse

Reserved frequency range (Hz)	Impact period (s)	Impact impulse (Pa*s)
[0-20]	0.424-0.475	25.603
[0-100]&[150-100]	0.424-0.475	10.453
NF	0.424-0.475	13.748
[0-30]	0.418-0.458	24.051
[0-100]&[150-100]	0.418-0.458	22.254
NF	0.418-0.458	19.371
[0-40]	0.419-0.447	22.779
[0-100]&[150-100]	0.419-0.447	18.962
NF	0.419-0.447	11.638
[0-50]	0.418-0.635	32.5096
[0-100]&[150-100]	0.418-0.635	29.444
NF	0.418-0.635	26.166

Thus, strict filtering range is selected since larger pressure impulse is calculated, which can ensure more safety in structural design. Signals with frequencies ranging from 0Hz-40Hz are maintained.

B

Representative moments description

The 6 selected wave impacts have some common characteristics, which are described below:

a). Moment of the maximum primary peak pressure (A):

1) Bottom view: Entrapped air is first pressed out by the uprising wave surface. After that, the impulsive peak pressure occurs while the least air is still under horizontal overhang;

2) Side view: Wave surface rises above the lower right corner of the structure and water splashes quite violently.

As can be seen, phenomenon observed coincides with the conclusion of Bagnold (1939): Greatest pressures occur when least air is entrapped.

b). Moment of reflected peak pressure (B):

(Moment B in Figure B.1, B.2, B.4, B.5 and B.6)

1) Bottom view: Moment B is right after moment A and air is still being pressed out in form of small bubbles;

2) Side view: Wave surface rises above the lower right corner of the structure and water flower begins to drop back to water surface.

c). Moment after the reflected peak pressure (C):

(Moment C in Figure B.1, B.2, B.3 and B.4)

1) Bottom view: Large percent of air is already pressed out and large amount of bubbles are present in water;

2) Side view: Reflected wave is developed and peak of the reflected wave has already moved a certain distance away from the right end of the overhang, which means the reflected wave has left the overhang for seconds. Water surface is more gentle.

1) Maximum peak pressure 2139.61 Pa, t=345.937 s

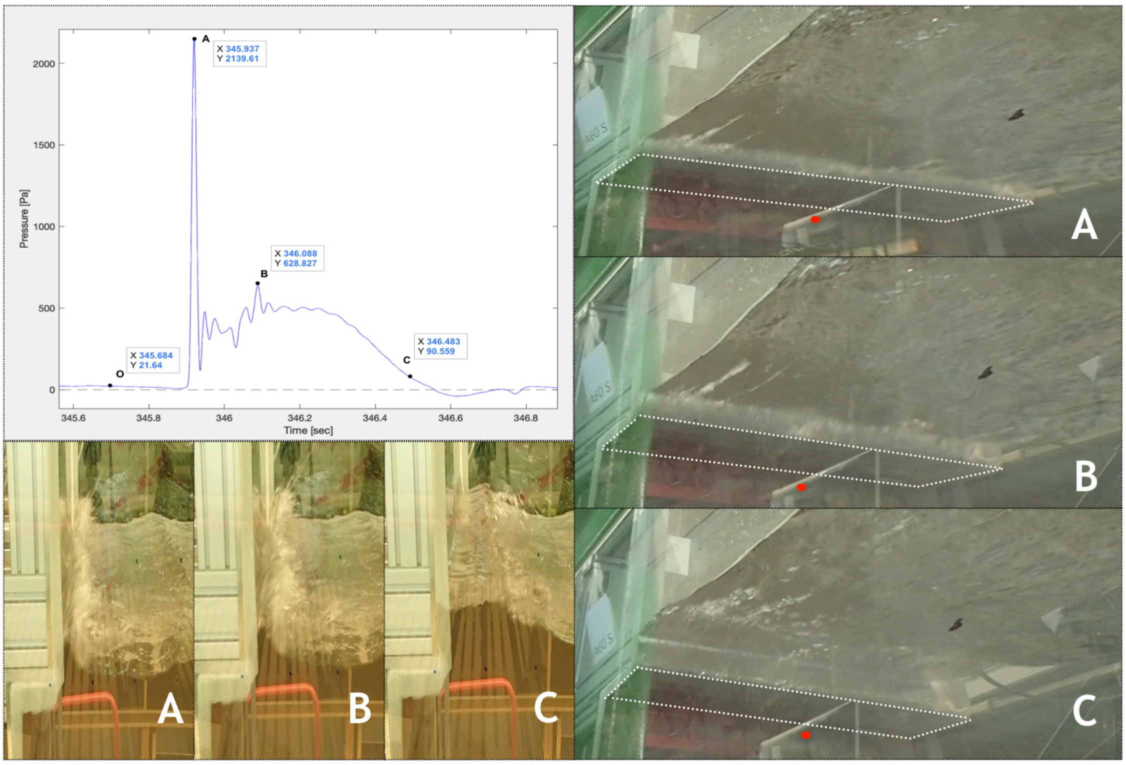

Figure B.1: Detail of peak pressure 1 (Pressure sensor:7, Peak pressure = 2139.61 Pa, t = 345.937s)

2) Maximum peak pressure 2130.58 Pa, t = 340.729 s

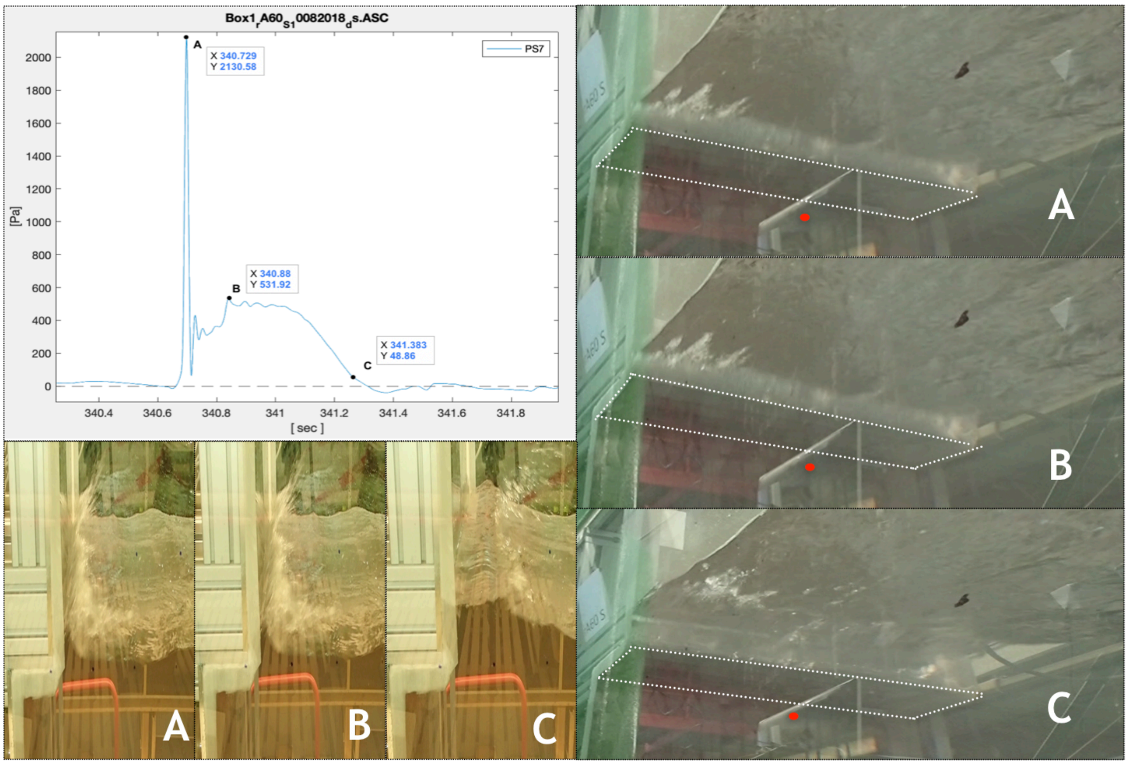

Figure B.2: Detail of peak pressure 2 (Pressure sensor:7, Peak pressure = 2130.58 Pa, t = 340.729 s)

3) Maximum peak pressure 1375.03 Pa, t = 293.927 s

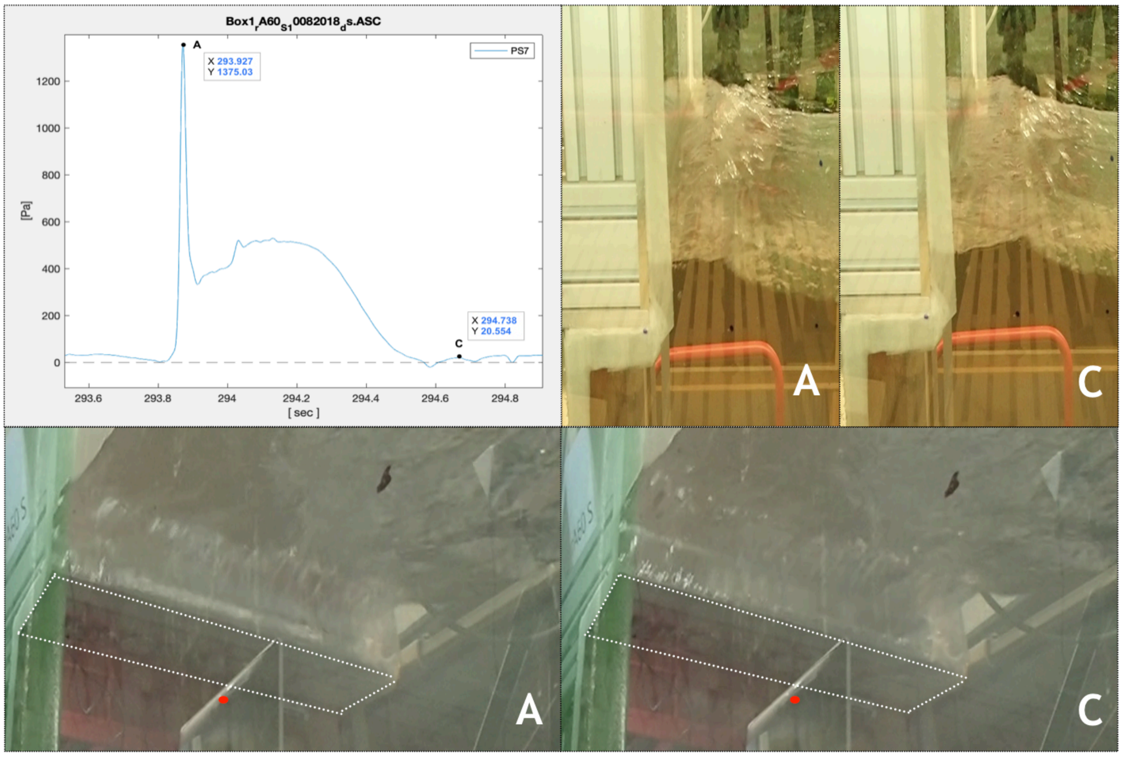

Figure B.3: Detail of peak pressure 3 (Pressure sensor:7, Peak pressure = 1375.03 Pa, t = 293.927 s)

4) Maximum peak pressure 1047.69 Pa, t = 288.726 s

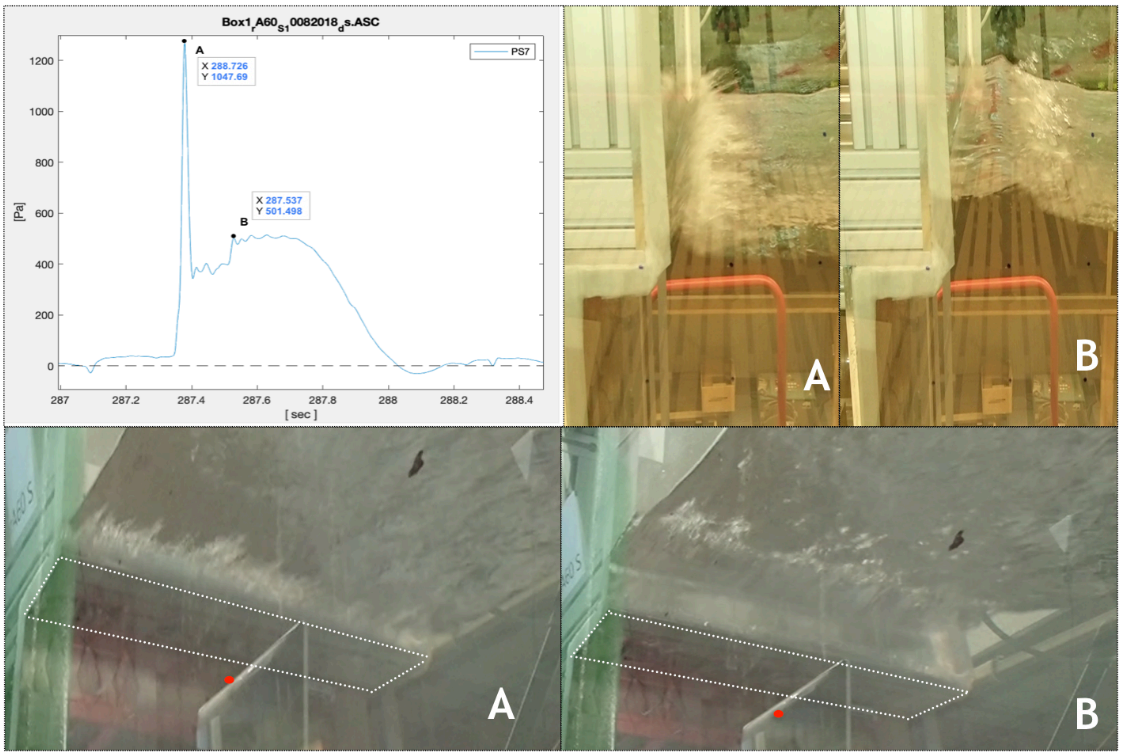

Figure B.4: Detail of peak pressure 4 (Pressure sensor:7, Peak pressure = 1047.69 Pa, t = 288.726 s)

5) Maximum peak pressure 987.27 Pa, t = 300.432 s

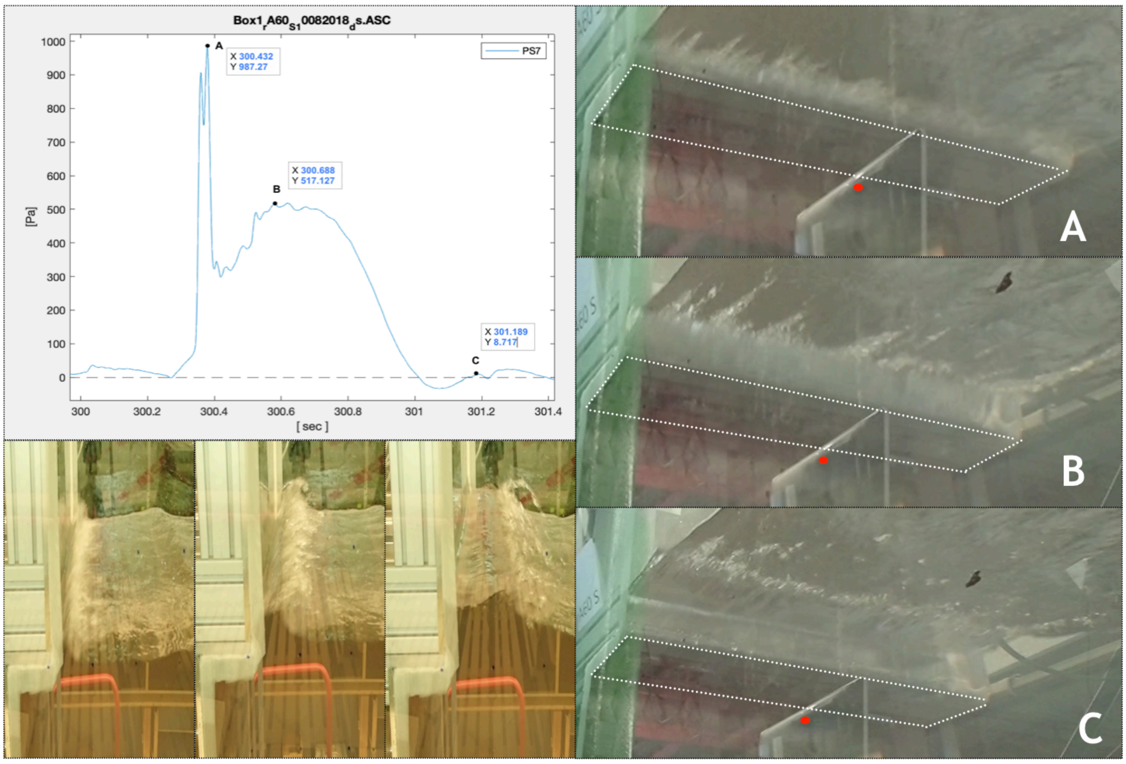

Figure B.5: Detail of peak pressure 5 (Pressure sensor:7, Peak pressure = 987.27 Pa, t = 300.432 s)

6) Maximum peak pressure 986.06 Pa, t = 245.827 s

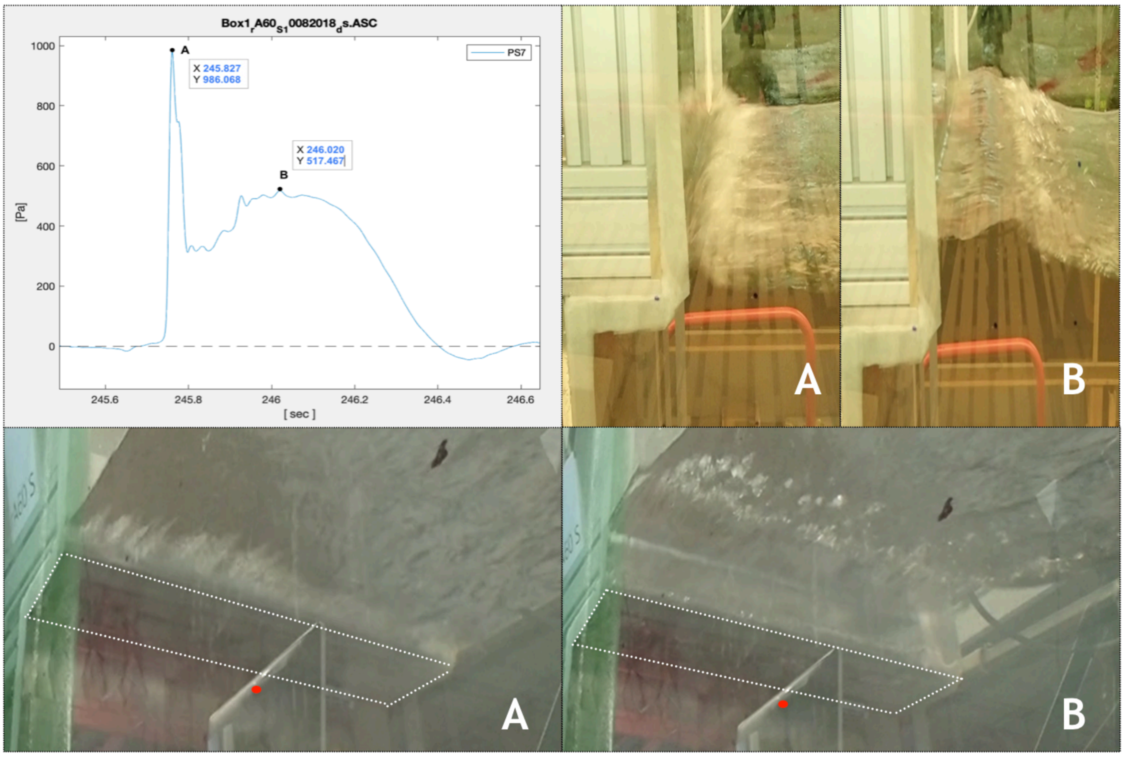

Figure B.6: Detail of peak pressure 6 (Pressure sensor:7, Peak pressure = 986.06 Pa, t = 245.827 s)

C

Wave impact impulse

C.1. Wave impact impulse calculation

Impact impulses are calculated by pressure integration. Positions of pressure sensors can be checked in Figure 4.6 and method for calculating wave impact can be checked in section 2.3. 9 pressure sensors are installed and accordingly, 9 sets of data are analyzed. For each set of data, the analysis range is taken to be 111s–345.4s and 178 waves are included. Both value of impact impulse (filtered unfiltered data) and ratio between filter impulse and unfiltered impulse are presented.

Graph (a), left part of each figure, shows value of impact impulse. Red line shows impact impulse calculated upon originally-calculated date and blue line represents impact impulse after low-pass filtering. Graph (b), right part of each figure, shows the ratio between filtered impact impulse and unfiltered impact impulse. For all the 9 pressure sensors, the ratio is around 1 with some vibrations, which means filtered impact impulse almost equals to unfiltered impact impulse for different impacts. Thus it can be concluded that low-pass-filtering has ignorable influence on the value of impact impulse.

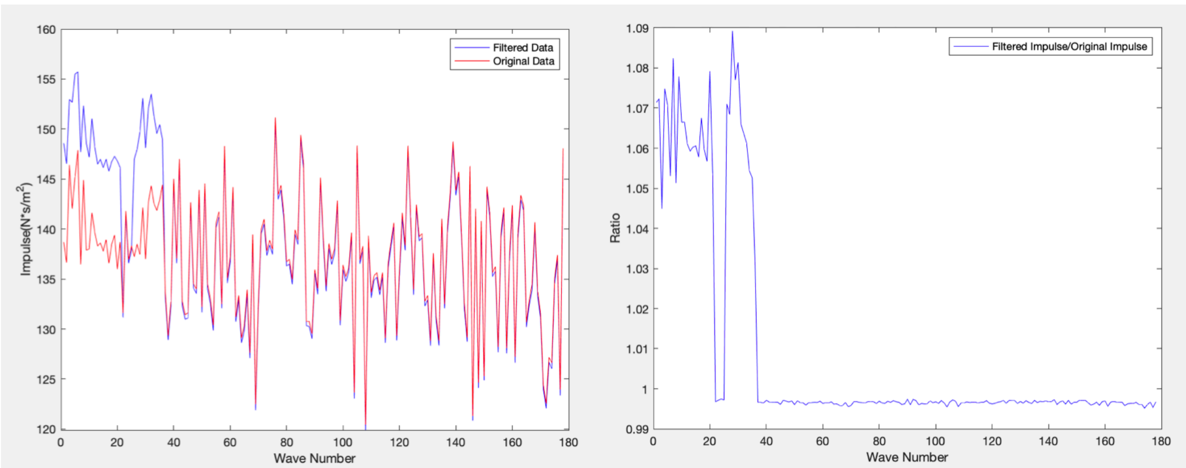

(a) Pressure impulse under filtered and unfiltered situation

(b) Ratio $\frac{P^t_{10,filtered}}{P^t_{10,unfiltered}}$

Figure C.1: Impact impulse under filtered and unfiltered cases – pressure sensor 10

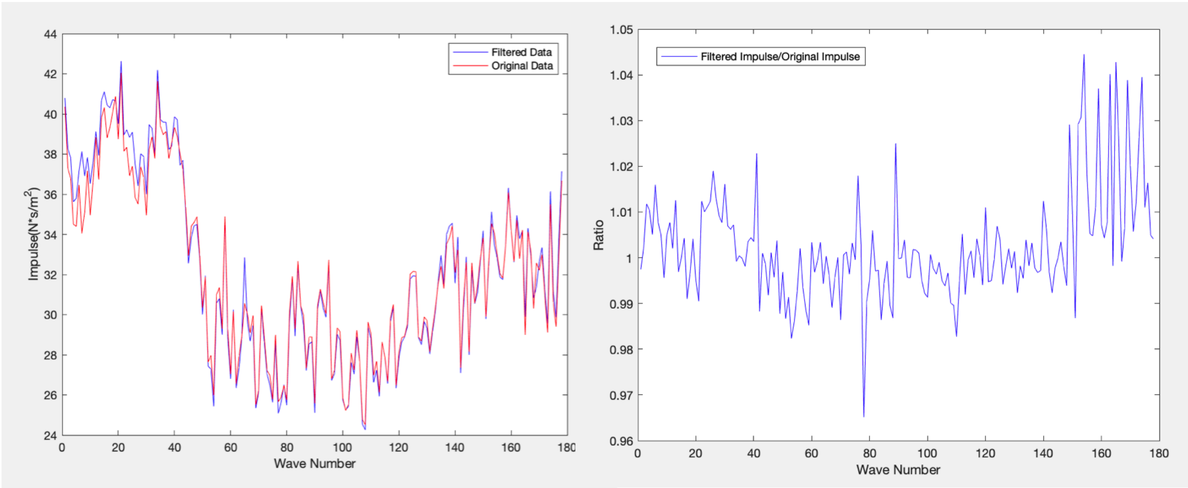

(a) Pressure impulse under filtered and unfiltered situation

(b) Ratio $\frac{P^t_{8,filtered}}{P^t_{8,unfiltered}}$

Figure C.2: Impact impulse under filtered and unfiltered cases – pressure sensor 8

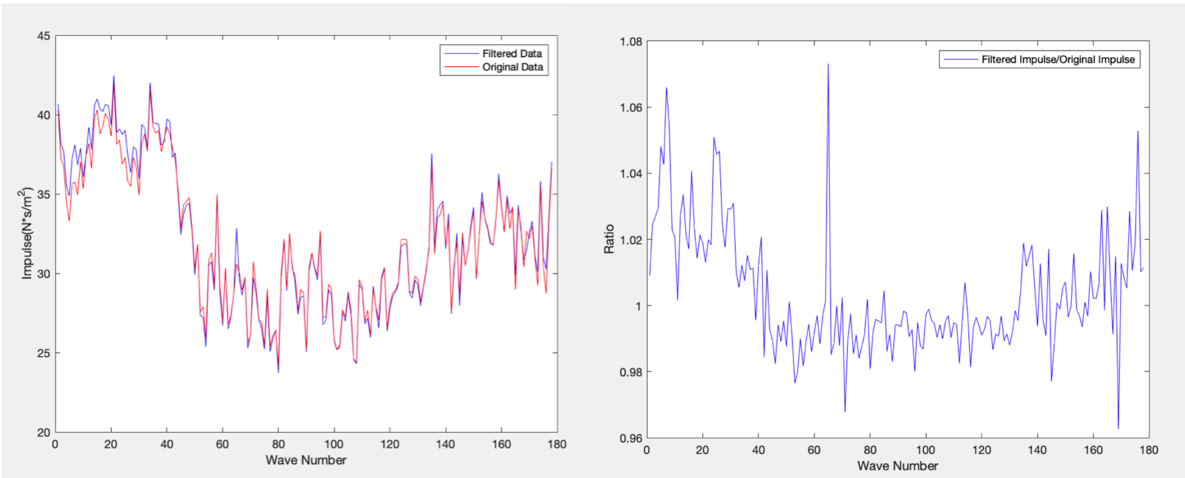

(a) Pressure impulse under filtered and unfiltered situation

(b) Ratio $\frac{P^t_{7,filtered}}{P^t_{7,unfiltered}}$

Figure C.3: Impact impulse under filtered and unfiltered cases – pressure sensor 7

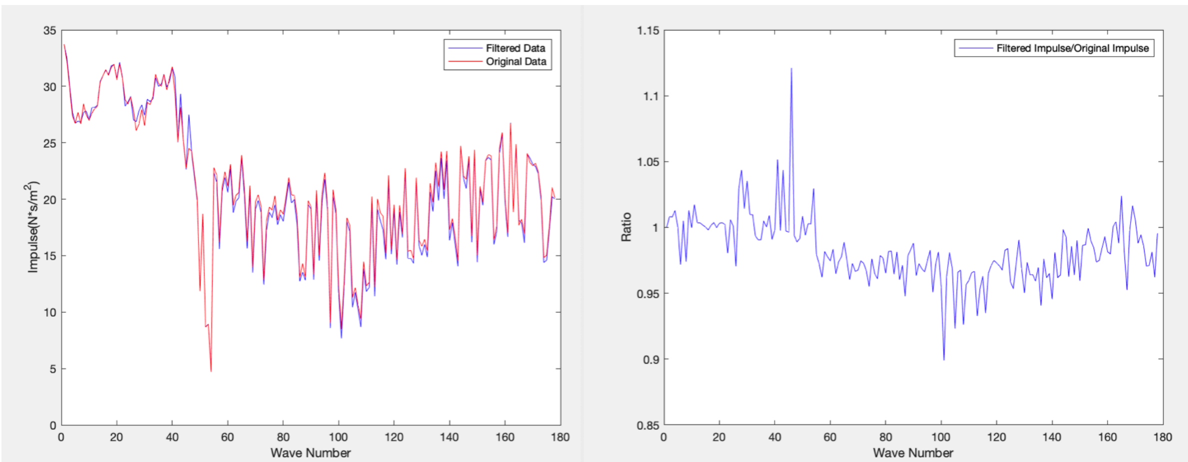

(a) Pressure impulse under filtered and unfiltered situation

(b) Ratio $\frac{P^t_{6,filtered}}{P^t_{6,unfiltered}}$

Figure C.4: Impact impulse under filtered and unfiltered cases – pressure sensor 6

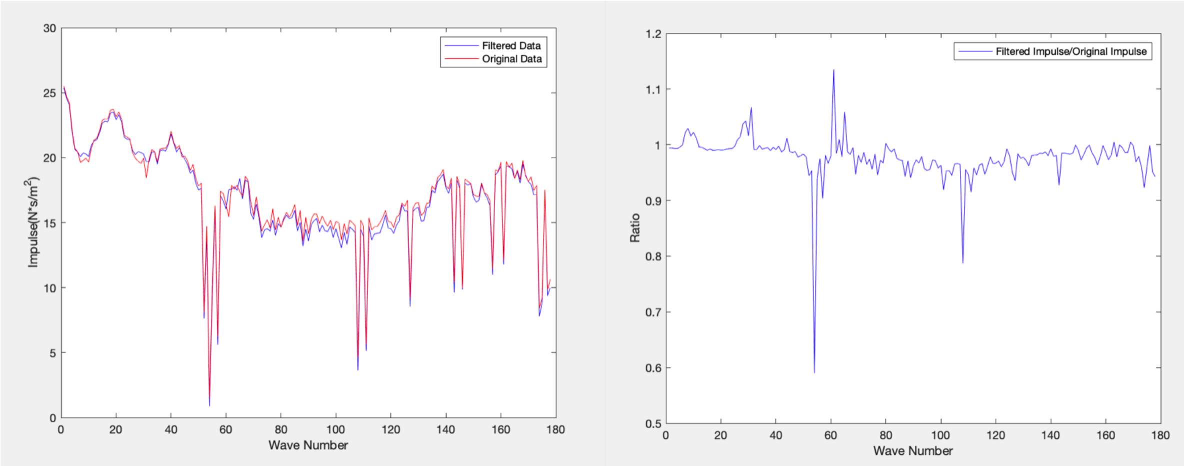

(a) Pressure impulse under filtered and unfiltered situation

(b) Ratio $\frac{P^{I}_{5,filtered}}{P^{I}_{5,unfiltered}}$

Figure C.5: Impact impulse under filtered and unfiltered cases – pressure sensor 5

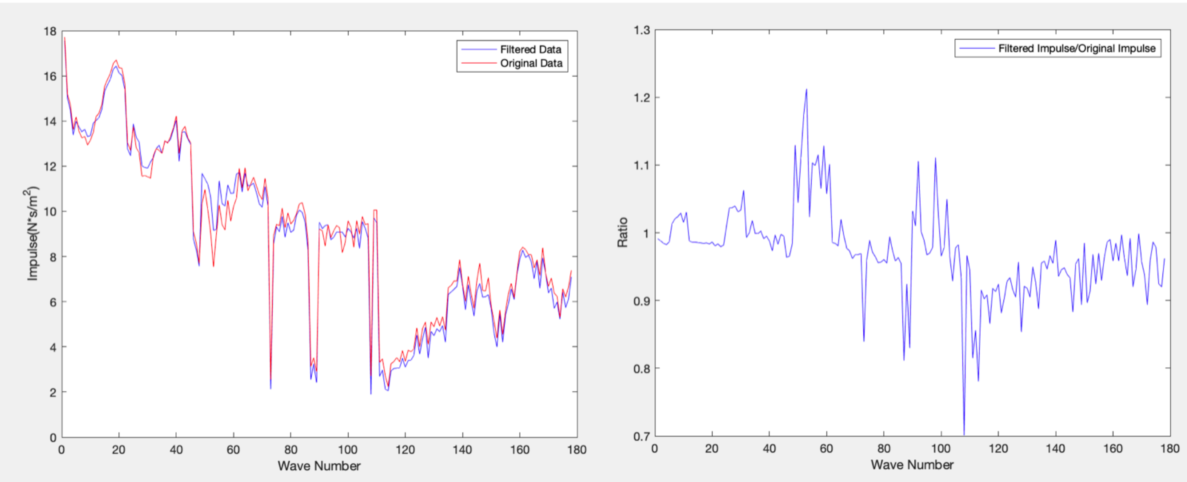

(a) Pressure impulse under filtered and unfiltered situation

(b) Ratio $\frac{P^{I}_{4,filtered}}{P^{I}_{4,unfiltered}}$

Figure C.6: Impact impulse under filtered and unfiltered cases – pressure sensor 4

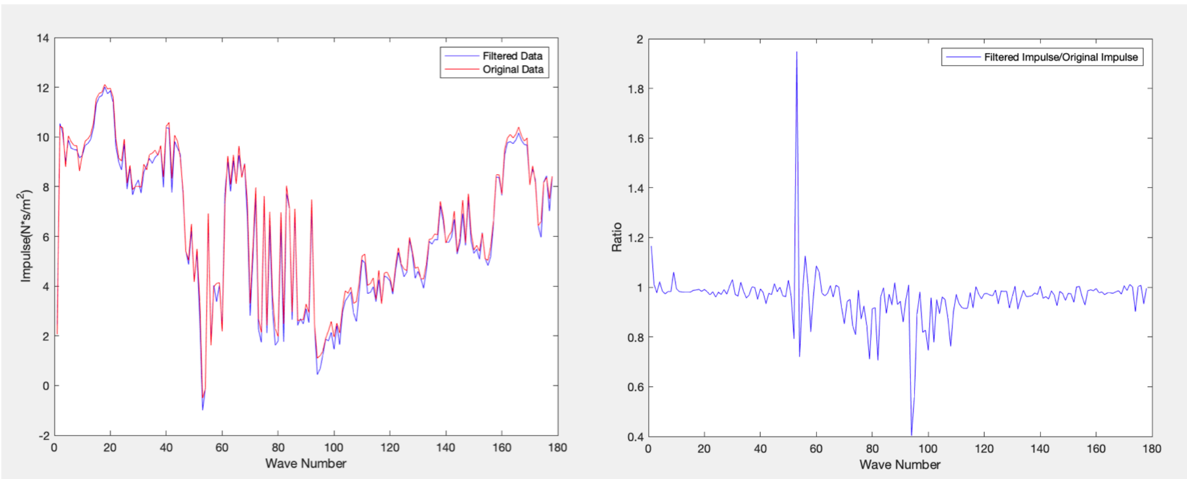

(a) Pressure impulse under filtered and unfiltered situation

(b) Ratio $\frac{P^{I}_{3,filtered}}{P^{I}_{3,unfiltered}}$

Figure C.7: Impact impulse under filtered and unfiltered cases – pressure sensor 3

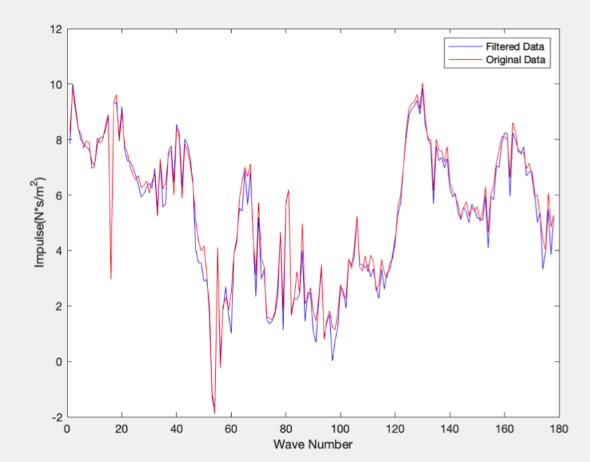

(a) Pressure impulse under filtered and unfiltered situation

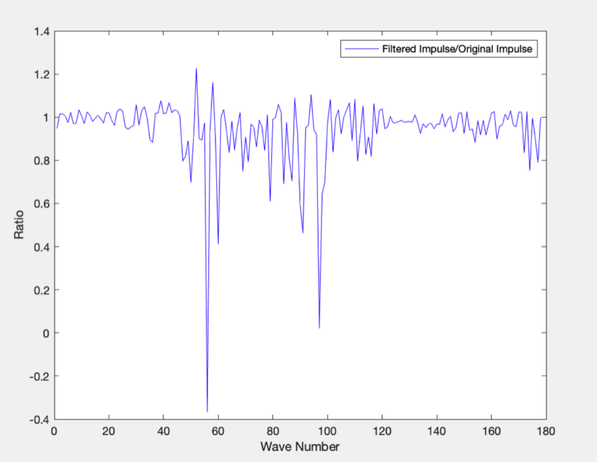

(b) Ratio $\frac{P^t_{2,filtered}}{P^t_{2,unfiltered}}$

Figure C.8: Impact impulse under filtered and unfiltered cases – pressure sensor 2

D

Regular wave parameters calculation

For incoming wave *rA60*, it is already known that wave height H_i = 0.06 m, wave period T = 1.316s, water depth h = 0.60m. Wave parameters can be calculated using linear wave theory.

Wave celerity:

$$c = \frac{gT}{2\pi} tanh(\frac{2\pi h}{L}) \tag{D.1}$$

Group velocity:

$$c_g = nc = \frac{1}{2}[1 + \frac{2kh}{\sinh 2kh}] * c \tag{D.2}$$

Horizontal particle velocity:

$$u = \omega a \frac{\cosh k(h+z)}{\sinh kh} sin\theta \tag{D.3}$$

Vertical particle velocity:

$$w = \omega a \frac{\sinh k(h+z)}{\sinh kh} cos\theta \tag{D.4}$$

in which,
c (m/s): wave celerity/ phase velocity, the propagation speed of the surface wave profile;
c_g (m/s): group velocity, the phase speed of the envelope of the surface elevations;
L (m): wave length;
T (s): wave period;
h (m): water depth;
a (m): wave amplitude, a=$\frac{H}{2}$;
u (m/s): the horizontal component of water particle velocity;
k : wave number, k=$\frac{2\pi}{L}$;
ω (rad/s): angular velocity, $\omega = \frac{2\pi}{T}$;
θ (degree): $\theta = \omega t - kx$;

It is known that wave height H_i = 0.06m, wave period T = 1.316s, water depth h = 0.60m. According to iterative calculation, wave celebrity C = 1.871 m/s, wave length L = 2.462 m, wave number k = 2.552, group velocity c_g= 1.204 m/s. Since $\frac{1}{20} < \frac{d}{L} = \frac{0.6}{2.462}$ = 0.2437 < $\frac{1}{2}$, relative depth characteristic in the laboratory flume is transitional water depth. Since water impact occurs at the moment when wave surface touches the overhang, so h+z = 0.6m.

Waves are reflected by the vertical structure, so impact waves are standing waves, which are combination of incoming waves and reflected waves. Thus for impact waves, amplitude can be calculated:

$$a_{impact} = H_{impact}/2 = H_i * 2/2 = 0.06m \tag{D.5}$$

Thus horizontal particle velocity u = 0.3146 m/s, vertical particle velocity w = 0.286 m/s. Through linear wave theory calculation, vertical particle velocity is determined to be velocity of wave impact U = w = 0.286 m/s.